Diss. ETH No. 21007

Host cell factors that affect UUKV infection identified by two genome-wide siRNA screens

A dissertation submitted to
ETH ZURICH

for the degree of
Doctor of Sciences

presented by
ROGER MEIER
Master of Science in Biology, Human Biology
University of Zurich, Switzerland

born March 29th, 1978
citizen of Dintikon AG, Switzerland

accepted on the recommendation of

Prof. Dr. Ari Helenius, examiner
Prof. Dr. Hubert Hilbi, co-examiner
Dr. Michèle Bouloy, co-examiner

2013

Summary

Bunyaviruses are considered as agents of emerging diseases. Many bunyaviruses are pathogens in humans and cause severe health problems such as fatal hepatitis, hemorrhagic fever, and encephalitis. No treatments or vaccines are currently approved by the Food and Drug Administration (FDA) for human use. Furthermore, bunyaviruses cause diverse diseases in livestock all over the world and diminish global agricultural productivity.

We recently found that Uukuniemi virus (UUKV) and other phleboviruses, that belong to the bunyaviruses, use DC-SIGN mediated endocytosis to enter immature dendritic cells (DCs) and cells ectopically expressing DC-SIGN. We also showed that UUKV belongs to the late penetrating viruses colocalizing with Rab7a and LAMP1 positive vacuoles [1, 2].

In this study we aimed at gaining more insights into UUKV entry - i.e. binding, internalization, fusion, penetration, and expression of viral nucleoprotein N - and at elucidating which host factors are involved in these steps. For this purpose, we performed two image based genome-wide siRNA screens in HeLa cells stably expressing DC-SIGN using Qiagen's un-pooled and Dharmacon's pooled genome-wide siRNA libraries.

Our screen analysis revealed 521 (Qiagen) and 294 (Dharmacon) inhibitory and enhancer hits. A comparison of hit lists of both screens revealed 21 common hits (4% (Qiagen) and 7% (Dharmacon) of total hits). This number matches the overlap of previously published infection screens performed with other viruses. The weak comparability of the hit lists of different siRNA virus infection screens is a major concern in the research field [3, 4].

To improve the analysis of our screens we performed off-target analysis consisting of 1.) a transcriptome correction and 2.) an assessment of siRNA seed effects on UUKV infection. It has been shown, that siRNAs can act like microRNAs (miRNAs).

1.) The transcriptome of HeLa-DC-SIGN cells was determined by a microarray approach using Agilent Humane Gene Expression chips. We identified a total of 13'421 transcripts in four independent transcriptome analyses.

Comparing hit lists with the identified transcripts in HeLa-DC-SIGN cell line, we identified 30% of preliminary hits as non-expressed genes, hence as false-positives, in both screens. The two screens revealed 477 inhibitory and 63 enhancer hits after transcriptome correction.

2.) The seed analysis for the Qiagen screen revealed 50% of the transcriptome corrected hits to be targeted by at least one siRNA that most probably acted like a miRNA and inhibited UUKV infection. In total 20% of "inhibiting hit siRNAs" were predicted to act like miRNAs. To confirm this prediction, we tested if mimic miRNAs (miRs) that had the same seed as predicted seeds inhibited UUKV infection. All miRs, except one, showed the predicted inhibitory effect.

The seed effect in the Dharmacon screen was clearly less dominant compared to the Qiagen screen. However, we also noted that the inhibition of the infection in the on-target analysis was in general weaker in the Dharmacon screen than in the Qiagen screen. This indicated that the depletion efficiency of the siRNAs in the Dharmacon screen was less efficient than in the Qiagen screen possibly leading to false-negative hits.

The results of our off-target analysis showed the importance of correcting siRNA screening data against the transcriptome and seed effects. We propose that transcriptome and seed correction should be included in data analysis protocols of siRNA projects. In addition, we suggest that false-positive hits caused by siRNA seed off-target effects in the Qiagen screen and the presumably high number of false-negative hits in the Dharmacon screen are the main reasons for the low number of common hits in the screens.

Amongst the miRs that inhibited UUKV infection, we found that miR-142-3p inhibited UUKV fusion or a pre-fusion event. To identify genes that are regulated by the miR-142-3p, we performed microarray analysis in HeLa-DC-SIGN cells. The gene expression analysis revealed VAMP3 and several other genes to be regulated by the the miR-142-3p. VAMP3 was identified as an inhibitory hit in both screens. We confirmed the role of VAMP3 in UUKV infection using VAMP3-inactivating tetanus toxin. Colocalization studies led us to suggest that VAMP3 may play a role in UUKV infection by interfering with the maturation or function of late endosomes (LE). This is consistent with UUKV being a late penetrating virus. Given that VAMP3 is required for the generation of amphisomes and considering that Rab7a and Lamp1 localize to both LE and amphisomes, we suggest a working model in which UUKV fusion takes place in amphisomes.

Zusammenfassung

Bunyaviren zählen zu den Erregern sich ausbreitender und neuer Infektionskrankheiten. Einige Bunyaviren sind menschliche Pathogene und verursachen schwere Krankheiten wie Hepatitis, hämorrhagisches Fieber und Enzephalitis. Zurzeit stehen keine von der "Food and Drug Administration" (FDA) genehmigten Impf- oder Behandlungsmethoden zur Verfügung. Zudem verursachen Bunyaviren weltweit verschiedene Infektionskrankheiten in Viehbeständen und reduzieren den globalen landwirtschaftlichen Ertrag.

Kürzlich konnten wir zeigen, dass gewisse Bunyaviren, wie z.B. das Uukuniemi Virus (UUKV), über DC-SIGN vermittelte Endocytose in dendritsche Zellen und Zellen, die ektopisch DC-SIGN exprimieren, gelangen. Zudem zeigten wir, dass UUKV zu den spät penetrierenden Viren gehört und mit Rab7a und LAMP1 positiven Vakuolen kolokalisiert [1, 2].

Ziel dieser Arbeit war es, den Eintrittsweg von UUKV in seine Wirtszellen besser zu verstehen - d.h. die Bindung, Fusion, Penetration und Expression des viralen Nukleoprotein N in der Wirtszelle. Dabei sollte ein umfassendes Bild der am Eintrittsweg beteiligten Wirtsproteine gewonnen werden. Um dieses Ziel zu erreichen, haben wir zwei siRNA Screens gegen das menschliche Genom durchgeführt. Dabei haben wir die nicht gepoolte Qiagen und die gepoolte Dharmacon siRNA Bibliotheken benutzt.

In der Analyse der Screens wurden 521 (Qiagen) bzw. 294 Hits (Dharmacon) identifiziert, welche die Infektion der Wirtszellen mit dem UUKV verminderten oder verstärkten. Ein Vergleich der in den beiden Screens identifizierten Hits ergab eine Übereinstimmung von 21 Hits (4% (Qiagen) und 7% (Dharmacon) aller identifizierten Hits), wobei alle die Infektion mit dem UUKV verminderten. Der Umfang dieser Übereinstimmung ist mit demjenigen von verschiedenen publizierten siRNA Infektion Screens, die mit anderen Viren durchgeführt wurden, vergleichbar. Diese geringe, wenn auch signifikante Übereinstimmung der identifizierten Hits ist ein bisher ungelöstes Problem im Rahmen von siRNA Infektion Screens [3, 4].

Um die Analyse unserer beiden Screens zu verbessern, haben wir zwei

Fehleranalysen durchgeführt, bestehend aus 1.) einer Korrektur gegen das Transkriptom und 2.) einer Beurteilung von Effekten der seed-Sequenzen von siRNAs auf die UUKV Infektion, da gezeigt wurde, dass siRNAs wie microRNAs (miRNAs) wirken können.

1.) Das Transkriptom von HeLa Zellen, die dauerhaft DC-SIGN exprimierten (HeLa-DC-SIGN), wurde mittels Microarray Analyse bestimmt. Insgesamt wurden 13'421 Transkripte in vier unabhängigen Microarray Analysen identifiziert. Ein Vergleich des Transkriptoms der Hela-DC-SIGN Zellen mit den in den zwei Screens identifizierten Hits ergab, dass 30% der Hits im Transkriptom nicht vorhanden waren, d.h. als falsch positive Hits zu werten waren.

2.) Die Analyse von Effekten der seed-Sequenzen von siRNAs auf die UUKV Infektion im Qiagen Screen ergab, dass 50% der Transkriptom korrigierten Hits von mindestens einer siRNA reguliert wurden, die mit grosser Wahrscheinlichkeit wie eine miRNA funktionierte und so die Infektion mit dem UUKV verminderte. Für insgesamt 20% aller siRNAs, die einen inhibierenden Effekt auf die Infektion mit dem UUKV zeigten, wurde vorhergesagt, dass sie wie eine miRNA wirkten. Um dies zu überprüfen, haben wir die Wirkung von mimic miRNAs (miRs) mit seed-Sequenzen von siRNAs auf die Infektion mit dem UUKV überprüft. Alle bis auf eine miR zeigten den vorhergesagten inhibierenden Effekt.

Der durch die seed-Sequenz vermittelte Effekt zeigte im Dharmacon Screen eine deutlich geringere Ausprägung als im Qiagen Screen. Es war jedoch zu beobachten, dass die Inhibition der Infektion in der on-target Analyse im Dharmacon Screen gesamthaft geringer war als im Qiagen Screen. Dies wies darauf hin, dass die siRNAs im Dharmacon Screen ihre Zielgene weniger effizient herunterregulierten als im Qiagen Screen, weshalb im Dharmacon Screen von mehr falsch negativen Hits auszugehen ist.

Die Resultate unserer off-target Analyse lassen die Wichtigkeit erkennen, Resultate aus siRNA Screens gegen das Transkriptom und gegen Effekte von seed-Sequenzen zu korrigieren. Daher schlagen wir vor, die Korrektur gegen das Transkriptom und gegen Effekte von seed-Sequenzen als festen Bestandteil in die Datenanalyse von siRNA Projekten aufzunehmen. Ferner erwägen wir, dass falsch positive Hits, die durch off-target Effekte von seed-Sequenzen der siRNAs im Qiagen Screen verursacht wurden, und die anzunehmende grosse Anzahl von falsch negativen Hits im Dharmacon Screen für die geringe Anzahl gemeinsamer Hits der beiden Screens verantwortlich sind.

Von den miRs, welche die Infektion mit dem UUKV verminderten, führte die miR-142-3p zu einer Inhibition der UUKV Fusion selbst oder eines Pro-

zesses vor der Fusion. Um Gene zu identifizieren, die von der miR-142-3p reguliert werden, wurde eine Microarray Analyse in HeLa-DC-SIGN Zellen durchgeführt. VAMP3 und einige weitere Gene wurden in dieser Genexpressionsanalyse als von der miR-142-3p reguliert identifiziert. VAMP3 wurde auch in beiden Screens als Hit, der zu einer Verminderung der Infektion führte, identifiziert. Die Rolle von VAMP3 bei der Infektion durch UUKV konnte mittels Tetanus Toxin, das VAMP3 inaktiviert, bestätigt werden. Untersuchungen zur Kolokalisation von UUKV und VAMP3 führten zur Hypothese, dass VAMP3 eine Rolle bei der Infektion mit UUKV spielt, indem VAMP3 mit der Reifung oder der Funktion von späten Endosomen interagiert. Diese Hypothese steht in Übereinstimmung mit dem Befund, dass UUKV zu den spät penetrierenden Viren zählt. Angesichts der Tatsachen, dass VAMP3 in die Bildung von Amphisomen involviert ist und Rab7a sowie Lamp1 sowohl in späten Endosomen als auch in Amphisomen zu finden sind, schlagen wir als Arbeitsmodell vor, dass die Fusion von UUKV in Amphisomen stattfindet.

Contents

Chapter 1

Introduction

Viruses are obligate intracellular parasites. They exploit cellular factors to propagate. As a crucial early step in their life cycle, viruses need to be transported from the extracellular space to the interior of their host cells, where replication of the viral genome occurs. To reach these sites many viruses take advantage of the diverse endocytic pathways of their host cells. Endocyotsis is a constitutively occurring mechanisms for macromolecular uptake by invagination and pinching-off of pieces of the plasma membrane (PM). Through endocytosis, cells internalize cargo such as nutrients, extracellular matrix, and hormones and transport them enclosed in membrane vesicles to their final destinations. Viruses mimic these natural cargo and bind to receptors on the surface of host cells. One or several endocytic processes are then activated that transport viruses to their site of replication, either the cytoplasm or the nucleus.

Endocytic pathways that viruses use to reach their replication sites are promising targets for interference with viral infection. For this purpose, it is crucial to investigate the molecular basis of these early host-pathogen interactions. Recently, a new approach emerged to study the role of host cell proteins in virus infection: the use of RNA interference (RNAi).

RNAi is based on a cellular mechanism that specifically down-regulates the expression of proteins on the messenger (mRNA) level. Down-regulation is caused by either mRNA degradation or specific inhibition of translation. Only those mRNAs are affected whose sequences show specific homology to small, double-stranded RNAs (dsRNA) [5].

Together with the breakthrough findings of the Human Genome Project that achieved full-sequencing of the human genome in 2001, and pivotal technological progress in laboratory automation and data analysis, it became feasible to screen thousands of host cell genes according to their impact on virus infection [6].

In this project we developed and performed a high-throughput RNAi screening strategy to identify the cellular factors required for infectious entry of Uukuniemi virus (UUKV). UUKV is a model virus of the virus family *Bunyaviridae*. The family contains species that cause severe and fatal diseases in human and livestock; moreover, many are a global threat to agricultural productivity. Despite their emerging importance as pathogens, not much is known about the viral mechanisms used to enter and infect host cells. Recent studies report that clathrin-mediated endocytosis (CME) is the major entry pathway for some viruses of the *Bunyaviridae* family.

In the following sections I introduce three major topics: Firstly, I present the current state of research on the *Bunyaviridae* family; secondly, I focus on major endocytic routes such as CME that serve as portals into their host cells for many viruses; finally, I describe in detail RNA interference and the technical basis of the screening strategy that we used in this project to search for cellular factors that affect UUKV entry.

1.1 *Bunyaviridae*

The virus family of *Bunyaviridae* contains more than 350 viruses that encompass five genera, *Orthobunyavirus*, *Hantavirus*, *Nairovirus*, *Phlebovirus*, and *Tospovirus*. *Bunyaviridae* infect animals with the exception of *Tospoviruses* that are plant pathogens. Most viruses of the *Bunyaviridae* family are transmitted by arthropods such as mosquitoes, ticks, and sandflies, and thus belong to the *ar*thropod-*bo*rne viruses (arboviruses). Hantaviruses, however, are rodent-borne and are transmitted by rodent bites or by direct contact with the excreta of infected rodents. Medically relevant *Bunyaviridae* are spread all over the world. They include many serious human pathogens, such as Crimean-Congo hemorrhagic fever (CCHFV), La Crosse virus (LACV), Rift Valley fever virus (RVFV), and Sin Nombre virus (SNV). Bunyavirus-related human diseases include viral hemorrhagic fever, hanta virus pulmonary syndrome, fatal hepatitis, encephalitis, and acute febrile illness. In addition, bunyaviruses are considered as agents of emerging diseases. An example of this is the new hantavirus isolated from Yosemite National Park in California in summer 2012, associated with a fatality rate of 30% in humans, or the recently identified Huaiyangshan virus (SFTSV) in China that showed a fatality rate of 15% in humans [7, 8, 9, 10, 11]. CCHFV and RVFV expanded from parts of Africa over the whole continent towards Southern Europe and Asia within the last eight decades [12, 13]. No treatments or vaccines are currently approved by the Food and Drug Administration (FDA) for human use. Bunyaviruses cause diverse diseases in livestock all over the

world and diminish global agricultural productivity.

1.1.1 Bunyavirus Structure

Bunyaviruses are spherically-shaped, enveloped viruses with a diameter of about 100 nm. Their genome consists of three negative stranded RNA segments that replicate in the cytosol and encode four structural proteins: the nucleocapsid protein N (25 kDa), two glycoproteins Gn and Gc (70 kDa and 64 kDa), and the RNA-dependent RNA polymerase (RdRp) L (200 kDa). The two transmembrane glycoproteins (GPs), Gn and Gc, are integral membrane proteins and form spike-like projections of 8-10 nm. The GPs have been reported to form both homodimers and heterodimers [14, 15]. As bunyaviruses do not have a matrix protein it is thought that the GPs determine integrity, shape, and structure of virus particles.

1.1.2 Organization and Regulation of Viral Genes and Genome Replication

The viral genome consists of three negative-sense, single-stranded RNA segments termed small (S), medium (M), and large (L) [16]. The S segment of all bunyaviruses encodes the N protein. The primary role of N is to encapsidate viral RNA replication products to form ribonucleoprotein (RNP) complexes. Most members of the genera *Orthobunyavirus*, *Tospovirus* and *Phlebovirus* also encode a nonstructural protein (NS_s). The main role of NS_s is modulation of the host-cell antiviral response [17].

The M segment of all bunyaviruses encode the precursor protein p110. It is post-translationally processed into the GPs in the ER. GPs perform critical roles in mediating virus assembly, formation of the virus particle, and attachment to new target cells [17]. Most members of *Orthobunyavirus*, *Tospovirus* and *Phlebovirus* also encode NS_m. For *Orthobunyavirus* it is suggest that NS_m plays a role in virus assembly [18, 19] . For *Tospovirus* NS_m is involved in the inter-cell virus transmission within infected plants [20]. For *Phlebovirus* the NS_m is non-essential, but has been suggested to play a role in the regulation of apoptosis [21].

For all bunyaviruses the L segment encodes the RdRp L protein. No additional proteins are encoded by the L segment.

The 3'- and 5'- terminal non-translated regions (NTRs) of the virus segments contain complementary sequences that are highly conserved between different genera. Base pairing of the terminal nucleotides builds stable panhandle hairpin structures [22, 23, 24]. The RNA segments form complexes

with N and L proteins that constitute the S, M, and L RNPs. RNPs are important for transcriptional initiation, viral RNA (vRNA) synthesis, and genome packaging.

Viral protein synthesis and genome replication occur in the host cytoplasm. Primary transcription of the negative-sense vRNA [vRNA (-)] to messenger RNA [mRNA (+)] is initiated by interaction of the virion-associated L protein and the three viral RNPs [25]. mRNA synthesis is primed by a cap-snatching mechanism, a transcription initiation process during which a nucleotide fragment (10 to 20 nt) is cleaved from the 5' end of host mRNAs serving as primers. Primers are cleaved by the endonuclease activity of L. Besides L, N is also an essential component for vRNA transcription. N unwinds and dissociates the RNA panhandle and remains attached to the 5' terminus of the RNA. This enables cleaved primers to bind to the vRNA and the transcription of vRNA to mRNAs by L [24]. Furthermore, for Hantaviruses it was shown that N also plays an important role for translational initiation by mimicking the cellular cap-binding complex, eukaryotic initiation factor (eIF) 4F [26]. Bar and colleagues showed that translation is spatially linked to transcription, a mechanism that is well known for prokaryotic systems [27].

Genome replication requires L to switch from primed mRNA synthesis to primer-independent transcription. The mechanism behind this switch is not known. It is suggested that N participates in the initiation of genome replication by acting as an RNA chaperone. It transiently and continuously unfolds the RNA to form more stable structures [24].

1.1.3 Virus Assembly and Release

For virus assembly, RNPs as well as Gn and Gc, must move to the same intracellular location. Bunyavirus particles bud from the Golgi apparatus [17]. After p110 processing into mature Gn and Gc, both form heterodimers in the endoplasmic reticulum (ER) and enter the secretory pathway, triggered by a signal located in the cytoplasmic tail of Gn [28, 29]. In parallel to accumulating GPs within the Golgi, the RNPs line up on the cytoplasmic side of the Golgi [30]. For initiation of budding, a direct interaction between RNPs and GPs has been suggested for UUKV, and co-immunoprecipitation studies have confirmed an interaction between the N protein and the Gn/Gc proteins. Overby et al. showed that the information necessary for packaging of RNPs into UUKV virus-like particle is located within the Gn cytoplasmic tail [31]. Budded viruses are transported in secretory vesicles to the PM, where membrane fusion occurs, and viruses are released.

1.1.4 Uukuniemi Virus (UUKV)

UUKV belongs to the *Phlebovirus* genus of the family of *Bunyaviridae* like RVFV. UUKV was first isolated from ticks in Uukuniemi, Finland, in 1959 [32]. Since then, UUKV has served as a model bunyavirus to study fundamental questions such as structure, organization, and regulation of viral genes, genome replication, assembly, and virus entry [16, 33, 34, 35].

1.1.5 Host Cell Entry of Bunyaviruses

For propagation, viruses have to be transported from the extracellular space to the intracellular site of replication. The virus entry process comprises several tightly controlled, consecutive steps. First, the virus binds to receptors on the cell surface followed either by direct penetration through the PM or by uptake via one of several existing endocytic pathways (see section 1.2). Upon endocytic internalization, viruses are trafficked in vesicles, sorted to different intracellular compartments, and finally reach the cytosol or nucleus by penetrating the limiting membrane of the organelles. This step occurs in early endosomes (EEs), late endosomes (LEs), or lysosomes (LYS) if viruses are internalized for example by CME or caveolae/raft-dependent endocytosis. Viruses entering by macropinocytosis are released from macropinosomes, and some viruses penetrate from the endoplasmic reticulum (see figure 1.2) [36, 37, 38, 39].

Little is known about host proteins that are essential for bunyavirus entry. For Hantaviruses, New York 1 (NY-1), and SNV, β3-integrin is suggested as a cellular receptor [40]. Protein Kinase C epsilon (PKCε) seems to be involved in RVFV infection [41]. Simon et al. showed that CCHFV entry, replication, assembly, and egress are microtubule-dependent. [42]. For UUKV and some other bunyaviruses, we found that DC-SIGN (dendritic cell specific intercellular adhesion molecule-3-grabbing non-integrin), a c-type lectin mainly expressed on the surface of dermal dendritic cells (DCs), serves as an entry receptor.

Due to the DC's presence in the anatomical site of the initial infection, DCs are among the first host cells to encounter the virus. As an endocytic receptor in dermal DCs, we suggested that DC-SIGN plays a critical role in the initial transmission after bites by arthropods infected with bunyaviruses (see figure 1.1) [1, 2].

CME (see 1.2.1) is proposed to be the entry pathway for the bunyaviruses hantaan virus (HV, *Hantavirus*), oropouche virus (OV, *Orthobunyavirus*), CCHFV (*Nairovirus*), and LACV (*Orthobunyavirus*) [43, 44, 45, 46].

In DCs and cells expressing DC-SIGN, we observed that many of UUKV

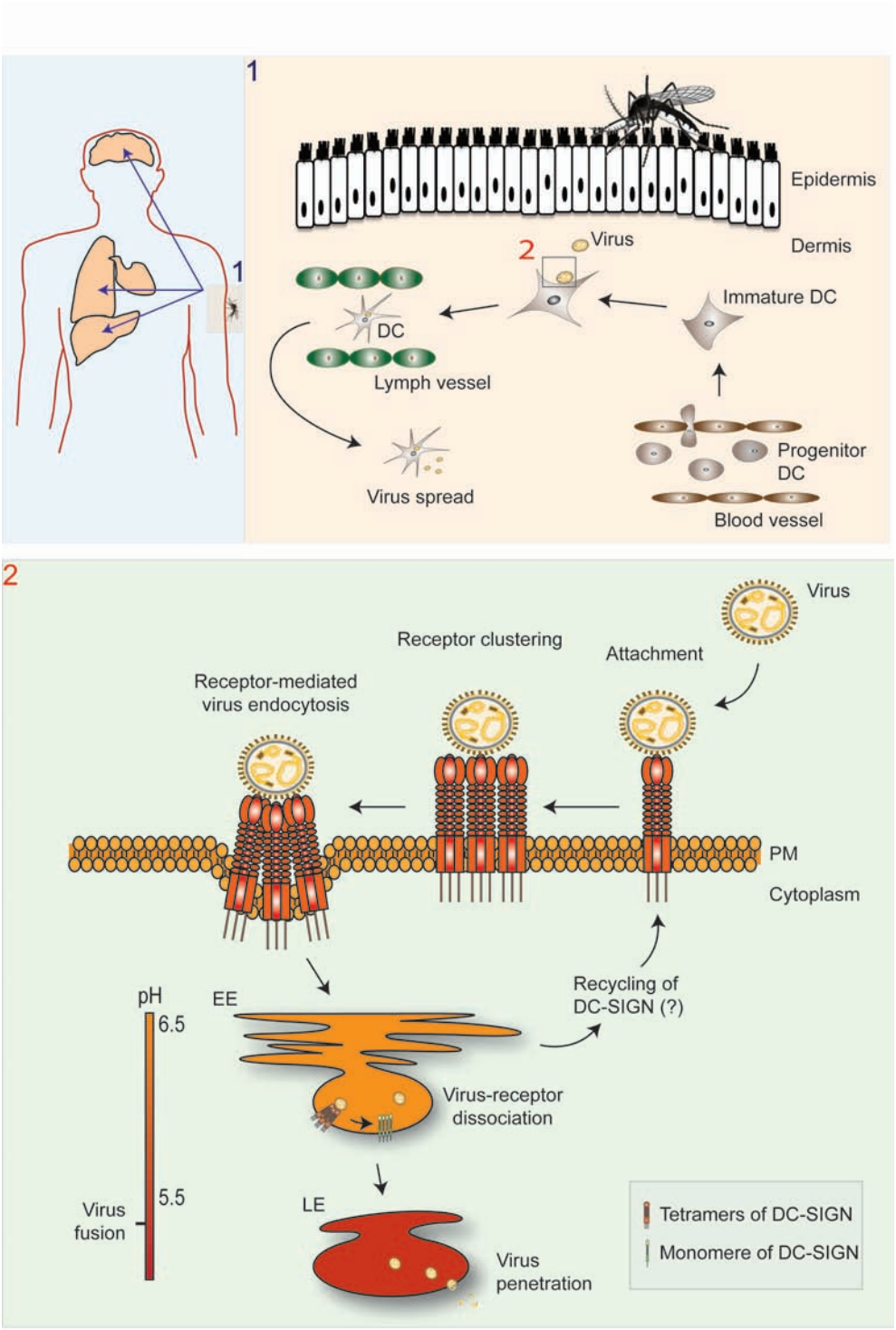

Figure 1.1 Transmission and host cell entry of Phleboviruses 1.) Phleboviruses are introduced into the human skin through an infected arthropod bite. Due to their presence in the anatomical site of the initial infection, dermal DCs are amongst the first host cells to encounter the virus. It supports the view that bunyaviruses use DCs to spread throughout the human host. 2.) DC-SIGN is a c-type lectin expressed on the surface of DCs. It binds the virus and serves as a receptor. Binding of virus to the receptor induces a receptor-clustering followed by receptor mediated endocytosis. After internalization, the virus dissociates from DC-SIGN in EEs and is further processed to LEs where virus penetration may occur. *Abbreviation*: DCs, Dermal dentritic cells; EE, early endosome; LE, late endosome; PM, plasma membrane; Figure adapted from [2].

particles on the cell surface were in clathrin-coated pits (CCPs). In addition, we observed viruses in clathrin-coated vesicles (CCVs). We identified CME as the main pathway of DC-SIGN-mediated entry [1]. In contrast, in cells that do not express DC-SIGN, we observed only few UUKV particles in CCPs and CCVs. Instead, the majority were located in noncoated indentations at the PM and after endocytosis in noncoated, small cytoplasmic vesicles. Therefore, in cells that do not express DC-SIGN, we proposed that UUKV use a clathrin-independent pathway for infectious entry [33].

After internalization, we observed that UUKV entered Rab5a-positive (Rab5a, member RAS oncogene family) EE and, subsequently, Rab7a-positive (Rab7, member RAS oncogen family) and LAMP1-positive (lysosomal-associated membrane protein 1) LE. Acid-activated penetration, occurring 20-40 min after internalization, required maturation of EE into LE. In addition, we determined the pH threshold of 5.4 as optimal for UUKV membrane fusion [33].

We thus proposed that late endosomal compartments are the location of virus penetration and that UUKV is a late-penetrating virus [33].

1.2 Principles of Endocytosis

The term endocytosis summarizes processes that are employed by cells to internalize soluble cargo or PM-bound cargo from the extracellular space (e.g. fluids, solutes, macromolecules, nutrients, and particles) in membrane-enclosed vesicles to the cell interior. Endocytosis includes phagocytosis, CME, the caveolae/raft-mediated pathway, Interleukin-2 receptor (IL-2)-, clathrin-independent carrier (CLIC)/glycosylphosphatidyl-inositol (GPI)-anchored protein-enriched early endosomal compartment (GEEC)-, flotillin-pathways, as well as macropinocytosis. The distinct endocytic pathways are defined by their differential dependencies on certain lipids and proteins, including clathrin, caveolin-1, flotillin-1, GRAF1, kinases, small G proteins, actin, and dynamin [37, 47, 48] (table 1.1). Viruses can exploit endocytosis pathways to enter their host cells. Vaccinia virus for example uses macropinocytosis, whereas for some bunyaviruses CME was reported to be the predominant internalization pathway (see figure 1.2 & table 1.1). Currently, the best characterized endocytic mechanism is the clathrin-mediated route.

Table 1.1 Cellular endocytic pathways

Endosomal pathway	Involved cellular factors	Viruses	Other cargo	References
Clathrin-mediated	Actin, amphiphysin, AP2, Arf6, clathrin heavy/light chain, dynamin-2, Eps15, epsin, FCHo1/2, Rab5, Rab7, SNX9, synaptojanin, etc.	BDV, CCHFV, CPV, DV, HAdV2/5, HRV2, HV, IAV, JUNV, LACV, MHV, OV, PICV, SFV, SFV *fus-1*, UUKV, VSV	Anthrax toxin, GPCRs, RTKs, transferrin receptor	[49, 50, 51, 52, 53, 54, 55, 56, 57, 58, 59, 60]
Caveolae pathway	Actin, caveolin-1, cavin-1-4, dynamin-2, EHD2, microtubules, PKC, Src, cholesterol	Mouse polyomavirus, SV40	CTxB, GPI-linked proteins	[61, 62, 63, 64]
IL-2 pathway	Actin, dynamin-2, PAK1/2, Rab5, Rab7, RhoA, Rac1	-	FCεRI, Kir3.4, IL2Rβ, γc-cytokine receptor	
CLIC/GEEC	Arf1, ARHGAP10, Cdc42, GRAF1, Rab5, PI(3)K	-	CTxB, Fluids, GPI-linked proteins	[65, 66, 67]
Flotillin pathway	Actin, Flotillin1 and 2, Fyn, Rab5, PI(3)K	-	CTxB, CD59, proteoglycans	[68]
Macropinocytosis	Actin, HDAC6, PAK1, PI3K, Rac1, Ras, Src	EBOV, HAdV3, HAdV35, HHV8, HSV1, IAV, VV (MVs and EVs)	Fluids, large particles	[69, 70]

Abbreviations: AP2, adaptor protein 2; Arf1/6, ADP-ribosylation factor 6; ARHGAP10, Rho GTPase activating protein 10; BDV, borna disease virus; CCHFV, crimean congo hemorrhagic fever virus; Cdc42, cell division cycle 42; CPV, canine parvovirus; CTxB, cholera toxin subunit B; DV, dengue virus; Eps15, epidermal growth factor receptor pathway substrate 15; EVs, vaccinia extracellular viruses; FCεRI, fragment crystallizable εreceptor I; Fyn, oncogen related to SRC, FGR, YES; GPCR, G protein-coupled receptor; GPI, glycosylphosphatidyl-inositol; GRAF1, Rho GTPase activating protein 26; HAdV2/3/5/35, human adenovirus 2/3/5/35; HDAC6, histone deacetylase 6; HHV8, human herpes virus 8; HRV2, rhinovirus serotype 2; HSV1, herpes simplex virus 1; HV, hantaan virus; IAV, influenza A virus; IL2Rβ, interleukin-2 receptor β; JUNV, Junin virus; Kir3.4, potassium inwardly-rectifying channel, subfamliy J, member 5; LACV, la crosse virus; MHV, mouse hepatitis virus; MVs, vaccinia mature viruses; PAK1/2, p21 protein (Cdc42/Rac)-activated kinase 1/2; PI3K, phosphoinositide-3-kinase; OV, oropouche virus; PICV, pinchindé virus; PKC, protein kinase C; RhoA, ras homolog gene family, member A; Rac1, ras-related C3 botulinum toxin substrate 1; Ras, rat sarcoma; RTK, receptor tyrosine kinase; SFV, Semliki Forest virus; SFV *fus*-1, Semliki Forest virus mutant with a lower pH-threshold for penetration; SNX9, sorting nexin-9; FCHo1/2, F-Bar domain-containing Fer/Cip4 homology domain-only protein 1/2; Src, v-src sarcoma (Schmidt-Ruppin A-2) viral oncogene homolog (avian); SV40, simian virus 40; UUKV, Uukuniemi virus; VV, vaccinia virus; VSV, vesicular stomatitis virus; -, not known. Compiled from [37, 47, 48].

1.2.1 Clathrin-Mediated Endocytosis

CME mediates the uptake of cargo into cells via CCVs. The formation of CCV occurs in several steps: nucleation, cargo selection, coat assembly, scission, and uncoating.

1.2.1.1 Nucleation

Nucleation involves the formation of membrane invaginations called CCPs. It is regulated by phosphoinositides (PIs) and PIs-binding adaptors that have multiple interaction sites. Phosphatidylinositol-4,5-bisphosphate (PtdIns(4,5)P_2) and adaptor protein complex 2 (AP2) play pivotal roles during nucleation. PtdIns(4,5)P_2 is a low abundance phospholipid that is specifically enriched at PM sites of CCP format. It recruits AP2 to the PM [71, 72]. AP2 is a heterotetrameric protein consisting of two large subunits, α and β2, a medium-size subunit, μ2, and a small subunit, σ2 [73]. AP2 contains four PtdIns(4,5)P_2 recognition sites, one each on the α subunit and β2 subunit and two on the C-terminus of the μ2 subunit [49, 50, 74, 51].

1.2.1.2 Cargo selection

Receptors for endocytosis show a more or less stringent specificity towards their cargo. It is mediated in a selection process that involves AP2 and takes place after phosphorylation of the μ2 subunit of AP2 by adaptor-associated kinase 1 (AKK1) [75]. Phosphorylation induces a conformational change that stabilizes the interaction between PtdIns(4,5)P_2 and AP2. Stabilization of this interaction is due to additional binding between PtdIns(4,5)P_2 and its recognition site on AP2 μ2 that becomes accessible due to conformational change. In addition, phosphorylation of AP2 facilitates the interaction between the receptor to the bound cargo. The interaction takes place between the endocytic motifs in the cytosolic domain of cargo proteins such as transmembrane receptors and their recognition sites of AP2 [74]. The endocytic motif Yxxϕ (where ϕ is a hydrophobic amino acid (I, L, M, F, or V) and x is an arbitrary residue) is recognized by the subunit μ2 of AP2 [76]. The σ2 subunit and the α subunit of AP2 recognize the endocytic motif [ED]xxxL[LI] (where brackets indicate either of the depicted amino acids, while "x" denotes an arbitrary residue) [53, 56].

1.2.1.3 Coat assembly

Coat assembly involves the recruitment of clathrin triskelions to the site of AP2 concentration at the PM. The clathrin triskelion consists of three

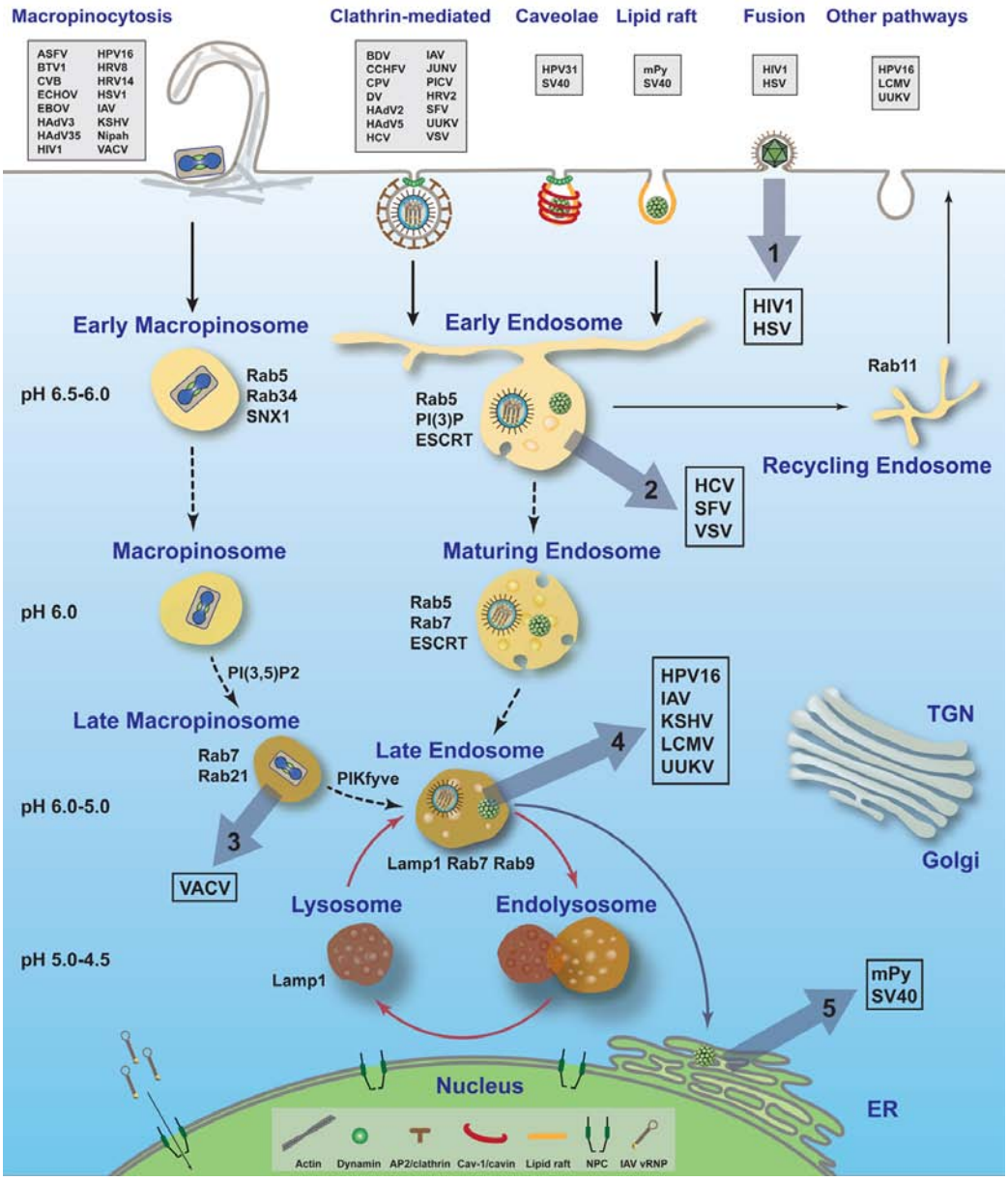

Figure 1.2 Virus entry – from internalization to penetration. Summary of the endocytoic pathways that viruses exploit, the main organelles to which viruses traffic, and their penetration sites indicated by arrows 1 to 5. In addition the figure shows key cellular factors involved in the maturation of endocytotic vesicles. *Abbreviation*: Adeno2, human adenovrius 2, Adeno3, human adenovirus 3; Adeno5, human adenovirus 5; Adeno35, human adenovirus 35; BDV, borna disease virus; BTV-1, blue tongue virus 1; CCHFV, crimean congo hemorrhagic fever virus; CPV, canine parvovirus; HCMV, human cytomegalovirus; HCV, hepatitis C virus; HIV-1, human immunodeficiency virus 1; HPV-16, human papillomavirus 16; HRV8, human rhinovirus serotype 8; HRV14, human rhinovirus serotype 14; HSV-1; herpes simplex virus 1; HSV, herpes simplex virus; IAV, influenza A virus; JUNV, Junin virus; KSHV, kapok's sarcoma-associated herpesvirus; LCMV, lymphocytic choriomeningitis virus; mPy, mouse polyoma virus; PICV, pinchindé virus; SFV, Semliki Forest virus; SV40, simian virus 40; UUKV, Uukuniemi virus; VV, vaccinia virus; VSV, vesicular stomatitis virus; Figure by courtesy of Yohei Yamauchi (Yamauchi and Helenius, in review).

clathrin heavy chains and three light chains interacting at their C-termini. The heavy chains build the structural backbone of the clathrin coat. The light chains regulate the formation and disassembly of the coat. Clathrin triskelions are recruited by the β2 subunits of AP2 that bind clathrin via the clathrin-binding consensus sequences (L[L,I][D,E,N][L,F][D,E]) [73, 77].

1.2.1.4 Scission

Clathrin-coated vesicle scission depends on the large GTPase dynamin. Dynamin is recruited by BAR domain-containing proteins such as amphiphysin, endophilin, and sorting nexin 9 (SNX9) [78, 79]. The BAR domain of these proteins is capable of sensing membrane curvature. Thus, these proteins accumulate at the CCP neck and bud. Dynamin is recruited by an interaction of its proline-rich domain with the SRC homology 3 (SH3) domains of BAR proteins. The precise mechanism of how dynamin mediates vesicle scission is not clear, but the protein undergoes a GTP hydrolysis-dependent conformational change that promots the scission step [80].

1.2.1.5 Uncoating

Uncoating of the nascent vesicles is mediated by the ATPase heat shock cognate 70 (HSC70) protein as well as the co-chaperone auxilin/cyclin-G-associated kinase (GAK) [58, 60]. Auxilin/GAK binds to the terminal domains and ankles of clathrin triskelia and recruits HSC70 initiating the disassembly of clathrin-coated vesicles [52, 54, 55, 57, 60]. Furthermore, auxilin/GAK has been shown to bind dynamin, so that both proteins might be recruited simultaneously to the closing neck of CCVs and concertedly support the scission process [81]. Moreover, the phosphatase synaptojanin is recruited to the CCV. It hydrolyzes PtdIns(4,5)P_2 that results in dissociation of AP2 [82]. Uncoated vesicles finally fuse with the limiting membrane of EEs to release their cargo into the interior of endosomal vesicles.

1.2.2 Clathrin-Independent Endocytosis Pathways

The best-understood non-clathrin-mediated endocytosis pathways are caveolae/lipid raft-dependent endocytosis and macropinocytosis.

1.2.2.1 Caveolae/Lipid Raft-Dependent Endocytosis

Caveolae/lipid raft-dependent endocytosis is a subgroup of lipid raft-dependent endocytosis processes. Lipid rafts are PM domains that are enriched in sphingolipids and cholesterol. The main structural protein of caveolae is caveolin-1

[61, 63]. In contrast to the clathrin coat, caveolins are integral membrane proteins. Most of the caveolae are immobile, serving as signaling platforms and PM reservoirs. Immobile caveolae can be activated through external and internal stimuli to undergo internalization and to carry cargo from the PM to EEs. This endocytic process requires dynamic, local actin rearrangements, as well as phosphorylation events.

Dynamin-2 is important for the fission of caveolae from the PM. Recently, Eps-15 homology domain-containing protein 2 (EHD2) has been found to colocalize with caveolin-1 and it was found that EHD2 plays a key role in controlling the switch between immobile caveolae and mobile caveolar carriers [62, 64]. Reported cargo for caveolae/lipid raft-dependent endocytosis are cholera toxin subunit b (CTxB), simian virus 40 (SV40), and mouse polyoma virus [83].

Other lipid raft-associated endocytic pathways are the CLIC/GEEC pathway, the interleukin-2 receptor (IL2R) pathway, the flotillin pathway, and a postulated Arf6 pathway.

The CLIC/GEEC route is characterized by the requirement of Arf1, GRAF1, ARHGAP10, and cdc42 [65, 66, 67]. GPI-anchored proteins and fluid phase enter the cell via tubular invagination at the cell surface into GEEC compartements. After internalization via GEECs, GPI-anchored proteins are proposed to fuse with EEs [84].

The IL2R pathway depends on dynamin-2 and is regulated by the small GTPases RhoA and Rac1. IL2Rβ FCεRI, Kir3.4 γc-cytokine receptor are cargo of the IL2R pathway [47].

Flotillin1/2 proteins form oligomers in distinct membrane micro-domains and have been shown to colocalize in endosomal structures with fluid phase markers, GPI-linked proteins, and CTxB. No colocalization was observed between flotillin-1 and caveolin-1 or clathrin. Therefore, flotillin-1 has been suggested to control a clathrin- and caveolae-independent endocytic pathway [68].

1.2.2.2 Macropinocytosis

Macropinocytosis is a transient endocytic process that depends on actin cytoskeletal reorganization, Na^+/H^+ exchangers, Rho GTPases (Rac1 or Cdc42), p21-activated kinase 1 (Pak1), PI(3)K, and protein kinase C (PKC). Macropinocytosis is triggered by growth factors, integrin substrates, and phosphatidylserine (PS)-containing cell debris that induce actin cytoskeletal reorganization resulting in PM protrusions. Depending on the cell type, the PM protrusions resemble lamellopodial ruffles, circular ruffles, filopodial protrusions, or blebs [69]. During entry, these protrusions collapse into

large, uncoated vesicles called macropinosomes, which contain the internalized cargo. Cargo for macropinocytosis are fluids, vaccinia virus extracellular virions (EVs), and vaccinia virus mature virions (MVs) [70, 85].

1.3 Endosomal Maturation

The endocytic system is a complex vesicular network that consists, in a simplified picture, of two main parts, the recycling circuit and the degradative system. The recycling circuit comprises of the PM, EE, and recycling endosomes (RE). The degradation system consists of LE and LYS. LEs link LYS and EEs by a unidirectional feeder pathway that transports endocytosed fluids and selected components of the membrane and their ligands from the recycling circuit into the degradative system [86]. Fluid transitions occur between the PM and the EE, between the EE and the RE, between the EE and the LE, and between the LE and the LY. Each transition state contains a complex maturation program involving Rab switches, PI conversion, endosomal acidification, and endosomal motility (see table 1.2) [37, 48, 86, 87, 88, 89].

1.3.1 Early Endosomes

EE are the main sorting station in the endocytic pathway. EEs receive their cargo from different endocytotic pathways including CME, caveolar-, and CLIC/GEEC pathways. While some of the cargo is sorted into recycling endosomes and recycled back to the PM, other cargo is further processed into the degradation system.

A key component of EEs is Rab5. Together with its effectors it regulates the conversion to LEs (see table 1.2).

EEs are weakly acidic (pH 6.8 - 6.1) and contain a low Ca^{2+} concentration [86].

1.3.2 Late Endosomes and Lysosomes

LEs are derived from the vacuolar domains of EEs. Rab5 on EE recruits Rab7 resulting in hybrid Rab5/Rab7 endosomes that further matures into LEs. Two possible models on LE formation exist. The first model suggests that Rab5 gets converted to its inactive form after recruiting Rab7 and subsequently dissociates together with its effectors [90]. The second model suggests a fission event that separates the parts of the hybrid endosome containing the nascent Rab7 domain from the rest [91]. The newly formed LEs continue further maturation which is temporally and spatially mainly controlled by

Rab7 and its interactions with various effector proteins. The LE maturation involves exchange of membrane components, movement to the perinuclear area, acidification, a switch in the tethering complexes for fusion, a switch in microtubule-mediated motors, and a change in morphology (see table 1.2). Mature LE finally fuse with LYS where cargo is degraded.

1.3.3 The Rab Switch

The GTPases Rab5 and Rab7 are key regulators of the endocytic pathway and the replacement of Rab5 with Rab7 is an essential step in LE formation. Rab5 itself, its guanine-nucleotide exchange factors (GEFs), GTPase-activating proteins (GAPs), Guanosine diphosphate (GDP)-dissociation inhibitors (GDIs), and GDI displacement factors (GDFs), as well as Rab5 effectors, determine the functions of EEs. Similar, Rab7 and its effector factors are the key mediators for LE and LYS.

Rab5 is activated by its GEF Rabex-5 [92]. The GEF activity of Rabex-5 is attained by the Rab5 effector Rabaptin-5. Through interactions between Rabex-5, Rabaptin-5, and Rab5 a complex is formed that establishes a positive feedback loop, in which Rab5-GTP recruits additional Rab5 to EE [93].

Rab5 removal requires inhibition of the positive feedback loop and GAP activity. The so called "cutoff switch" model suggests that Rab5-GTP is converted after recruiting of Rab7 to its inactive Rab5-GDP and thereby Rab5 is removed [90].

SAND1/Mon1 [Mon1A Mon1 homolog A (yeast)] and CCZ1 [CCZ1 vacuolar protein trafficking and biogenesis associated homlog (S. cervisiae)] play a key role in the conversion of Rab5 to Rab7 [94]. It has been suggested that the SAND1/Mon1-CCZ1 complex is recruited by to binding Rab5-GTP and phosphoinositol-3-phosphate. The, SAND1/Mon1 subunit of the complex displaces Rabex5, and the SAND1/Mon1-CCZ1 supports Rab7 association and Rab5 dissociation [94, 95].

1.3.4 The Phosphoinositide Switch

Like the Rab GTPase switch, the PI conversion is an essential part of endosomal maturation. PIs recruit important effector proteins with PI-binding domains such as FYVE (preferred target PtdIns(3)P), PH (PIs, quite diverse, some specific), and PX (preferred target PtdIns(3)P) [96].

PtdIns(3)P and PtdIns(3,5)P(2) are the equivalent to Rab5 and Rab7. In EEs, PtdIns(3)P is the predominant species of PIs and in LEs PtdIns(3,5)P(2), respectively [97].

PtdIns(3)P is generated by Rab5 and its effector VPS34/p150, a phosphatidylinositol 3-kinase (PI(3)K) complex. PtdIns(3,5)P(2) is generated by the phosphatidylinositol 3-phosphate 5-kinase (PIKfyve) [98]. PIKfyve binds to PtdIns(3)P by its PI-binding domain FYVE.

1.3.5 The Formation of Intralumenal Vesicles

The formation of intraluminal vesicles (ILVs) is one of the most important processes in LE biogenesis. It is critical for several events, including sorting of cargo into the degenerative pathway and inactivation of receptor signalling.

The biogenesis of ILVs is coordinated by the ESCRT (endosomal sorting complex required for transport) complexes (ESCRT-0, -I, -II, -III). The ESCRT machinery is present in EEs and sorts ubiquitinated cargo that should go in the degradative pathway. Ubiquitinated cargo is recognized by components of the ESCRT through their various Ub-binding domains [87, 99].

1.3.6 Acidification

The lumen of endocytic organelles and LYS is acidic. Acidification and its regulation is an additional key component of endosomal maturation. EEs have a pH in the 6.8-6.1 range, LEs in the 6.0-4.8 range, and in LYS the pH can drop to values around 4.5 [86]. The low pH is important for sorting and routing of cargo, for membrane trafficking, and it provides an optimal environment for hydrolytic reactions.

The pH difference in extracellular space and EE enables receptors to bind their ligands in one compartment and to dissociate in the other. Thus, the decreasing pH in the endocytic pathway directs incoming cargo to their location within the pathway. In addition, for many enveloped viruses, the decrease in endosomal pH triggers conformational changes in viral GPs required to initiate fusion [37, 48].

Table 1.2 Steps in endosome maturation.

Endosome maturation	Function & implicated factors	Ref
Switch of Rab subsets	Rab5 and its effectors (GAPVD1, Rabex5, Rabaptin5, VPS34/p150, EEA1, Rabenosyn5, APPL1, APPL2, VPS11) are exchanged for Rab7 and its effectors (RILP, ORP1L, FYCO1, VPS41, VPS39); Rab4 and Rab11 are removed; Rab9 is added	[89, 93, 100, 101]
Switch of PI	PtdIns(3)P is phosphorylated to PtdIns(3,5)P_2	[102]
ILVs formation	Sorting of ubiquitinated cargo into degradation pathway by ESCRT complex (ubiquitin ligases (Cbl), ESCRT-0 (Hrs), ESCRT-1 (Tsg101), ESCRT-II, and ESCRT-III) via intraluminal vesicles.	[87, 99]
Acidification	pH range of 6.8-6.0 in EEs drops to pH range 6.0-5.0 in LEs and pH range of 5.0-4.5 in LYS (vATPases, Na^+/K^+ ATPase, ClCs, Ca^{2+})	[103]
Changes in lumenal ionic environment	Increase in H^+, Cl^-, K^+, decrease in Na^+ and Ca^{2+}	[104]
Coatomer requirement	Formation of MVB (COP1, Arf1)	[105, 106]
Switch in tethering complexes for fusion	Homotypic and heterotypic fusion between LEs and between LEs and LYS (CORVET is replace by HOPS complex)	[107]
Acquiring of lysosomal components	Gain of lysosomal hydrolases and membrane proteins for degradation, previously sorted proteins into degradation pathway,	[107]
Switch in MT-mediated motors	Kinesins are exchanged for dynein and dynactin (RILP, LIC1/2, Rab7)	[108]
Change in size and morphology	Tubular extensions of EE are lost; endosomes become a round or oval shape and grow in size	
Change in temperature sensitivity	LE formation and their fusion with LYS is inhibited at temperatures below 19°C-20°C	

Abbreviations: APPL, adaptor protein-phosphotyrosine interaction-PH domain and leucine zipper containing 1; Arf1, ADP-ribosylation factor; CCV, clathrin coated vesicle; ClC, chloride channels; COP1, clathrin-ordered protein 1; CORVET, class C core vacuole/endosome tetherin; EE, early endosome; EEA1, early endosome antigen 1; ESCRT, endosomal sorting complex required for transport; FYCO1, FYVE and coiled-coil domain containing 1; GAPVD1, GTPase-activating protein and VPS9 domain-containing protein 1; ILVs, intraluminal vesicles; LE, late endosomes; LYS, lysosomes; MT, microtubules; MVB, multivesicular bodies; ORP1L, oxysterol binding protein-like 1; PI, phosphoinositides; PtdIns(3)P, phosphatidylinositol-3-phosphate; PtdIns(4,5)P_2, phosphatidylinositol-4,5-bisphosphate; RILP, Rab interacting lysosomal protein; vATPase, vacuolar H^+ ATPase; VPS34, phosphatidylinositol (PI) 3-OH kinase; VPS[X], vacuole protein sorting [X] (where [X] = 11, 34, 39, 41). Table modified from [37].

1.4 RNA interference (RNAi)

RNA interference (RNAi) is a cellular mechanism to regulate gene expression in eukaryotic organisms such as plants, worms, fungi, and mammals. Gene regulation is mediated by the RNA-induced silencing complex (RISC) that represses messenger RNA (mRNA) translation or facilitates the deadenylation of mRNA and their subsequent degradation. Small double stranded 19-31 base pairs-long ribonucleic acids (small RNAs) play a key role in RNAi. Based on their biogenesis and their mode of action in RNAi, small RNAs are classified into ten different classes [109]. Two main classes are the short interfering RNAs (siRNAs) and the microRNAs (miRNAs).

1.4.1 siRNA and miRNA Silencing Pathways

The small RNA silencing pathways of siRNA and miRNA can be divided into three steps: 1.) biogenesis of small RNAs, 2.) formation of RISC, 3.) silencing of target mRNA expression (see figure 1.3).

1.4.1.1 Biogenesis

SiRNA and miRNA biogenesis relies on the endonucleolytic processing of double stranded (ds)RNA precursors by enzymes of the RNase family termed Drosha and Dicer. Both can process miRNA, while siRNA is specifically generated by Dicer [109, 110, 111]. In case of siRNA biogenesis, dsRNA precursors derive from exogenous dsRNA, e.g. from viruses or artificial introduction. MiRNAs are generated from precursor dsRNAs (so called pre-miRNAs) that derive from endogenous transcripts (called pri-miRNAs).

Cleavage of dsRNAs by Drosha and Dicer yields products with characteristic termini, i.e. a monophosphate group at the $5'$ ends, and a two-nucleotide overhang at the $3'$ ends [110].

Dicer processes dsRNA substrates to 21-25 nucleotides long small interfering (si)RNAs or micro (mi)RNAs. Dicer enzymes contain a DEXD/H ATPase domain, a DUF283 domain, a PAZ (Piwi-Argonaute-Zwille) domain, two tandem RNaseIII domains (RNaseIIIa and RNaseIIIb), and a dsRNA-binding domain (dsRBD) [110, 112]. PAZ and the RNaseIIIa domain are connected via a connector helix. The PAZ domain binds the $3'$ dinucleotide of the dsRNA. The RNaseIII domains cleaves RNA phosphodiester bonds.

The function of the DUF283 domain and the DEXD/H-box are not fully understood. The DEXD/H-box domain is present in diverse groups of proteins involved in the ATP-dependent binding and remodeling of nucleic acids.

However, mammalian Dicer proteins bind dsRNA in an ATP-independent manner [110].

The structure of Dicer in *Giardia intestinalis* (*G. intestinalis*) revealed a distance of 65Å between the PAZ domain and the RNaseIIIa domain. This corresponds to the length of the 25-nucleotide small RNAs that *G. intestinalis* Dicer produces [110]. The structure of *G. intestinalis* Dicer suggests that the length of the non-conserved connector of the PAZ and the RNaseIIIa domain determines the size of the product.

Drosha is a nuclear RNaseIII protein that cuts pri-miRNA resulting in pre-miRNAs. It contains a proline-, an arginine-, and a serine-rich region at the N terminus, followed by two RNaseIII domains and a dsRBD (double-stranded RNA binding domain). Together with the DGCR8 protein, Drosha forms the "microprocessor" complex that enables specific cleavage of pri-miRNA. In detail, DGCR8 binds the pri-miRNA molecule and spatially aligns Drosha to cleave the RNA.

1.4.1.2 Formation of RISC

The RISC is responsible for the final silencing process. The core of a RISC complex consists of an Argonaute (Ago) family member protein and the guide strand of a small RNA. The formation of the RISC is mediated by the RISC-loading complex, consisting in humans of three proteins, Dicer, TRBP (TAR (HIV-1) RNA binding protein), and Ago2. The RISC-loading complex recruits the guide strand to Ago2 generating the functional RISC. This step is common for all small interfering RNAs [112] [113]. The thermodynamic properties at the 5′ ends of siRNAs and miRNAs determines the identity of the guide and passenger strand. The guide strand is defined as the strand whose 5′ end is less tightly paired to its complement. This is usually the case for the 5′ end of the antisense strand [114, 115].

Ago proteins are characterized by four domains: N-terminal domain, PAZ domain, middle domain (MID), and PIWI domain [113]. The PAZ domain binds to the 3′ end of single-stranded RNA (ssRNA). The MID domain binds the phosphate group at the 5′ end of the guide strand. The remainder of the guide strand aligns with the positively charged surface of the Ago protein domains [112]. Depending on the source of the small RNAs, RISCs are termed miRISCs or siRISCs.

1.4.1.3 The Silencing Process of mRNA Expression

RISC mediates different modes of mRNA expression silencing depending on the source of the guide strand. SiRISC mediates the degradation of the target

mRNA. MiRISC either inhibits translation of target mRNA or facilitates its deadenylation and subsequent degradation.

1.4.1.4 Post-transcriptional Silencing by siRNAs

The guide strand of an siRNA directs siRISC to the target mRNA by binding to a homolog sequence in the mRNA. The guide strand of an siRNA recognizes a perfectly complementary sequence in mRNAs, leading to Ago-catalyzed mRNA cleavage. The degradation of the target is induced by the PIWI domain of the Ago protein. The PIWI domain possess the endonucleeolytic activity.

1.4.1.5 Post-transcriptional Silencing by miRNAs

The guide strand of a miRNA directs miRISC to the target mRNA by imperfectly binding to a complementary sequence in the 3' untranslated region of the target mRNA. The latter is recognized by its sequence homology in the nucleotide positions 2 to 7 or 8 of the 5' end of the guide strand – the so called seed region. For miRISC, three different modes of action are known: inhibition of either translation initiation or a step thereafter, or mRNA deadenylation followed by degradation.

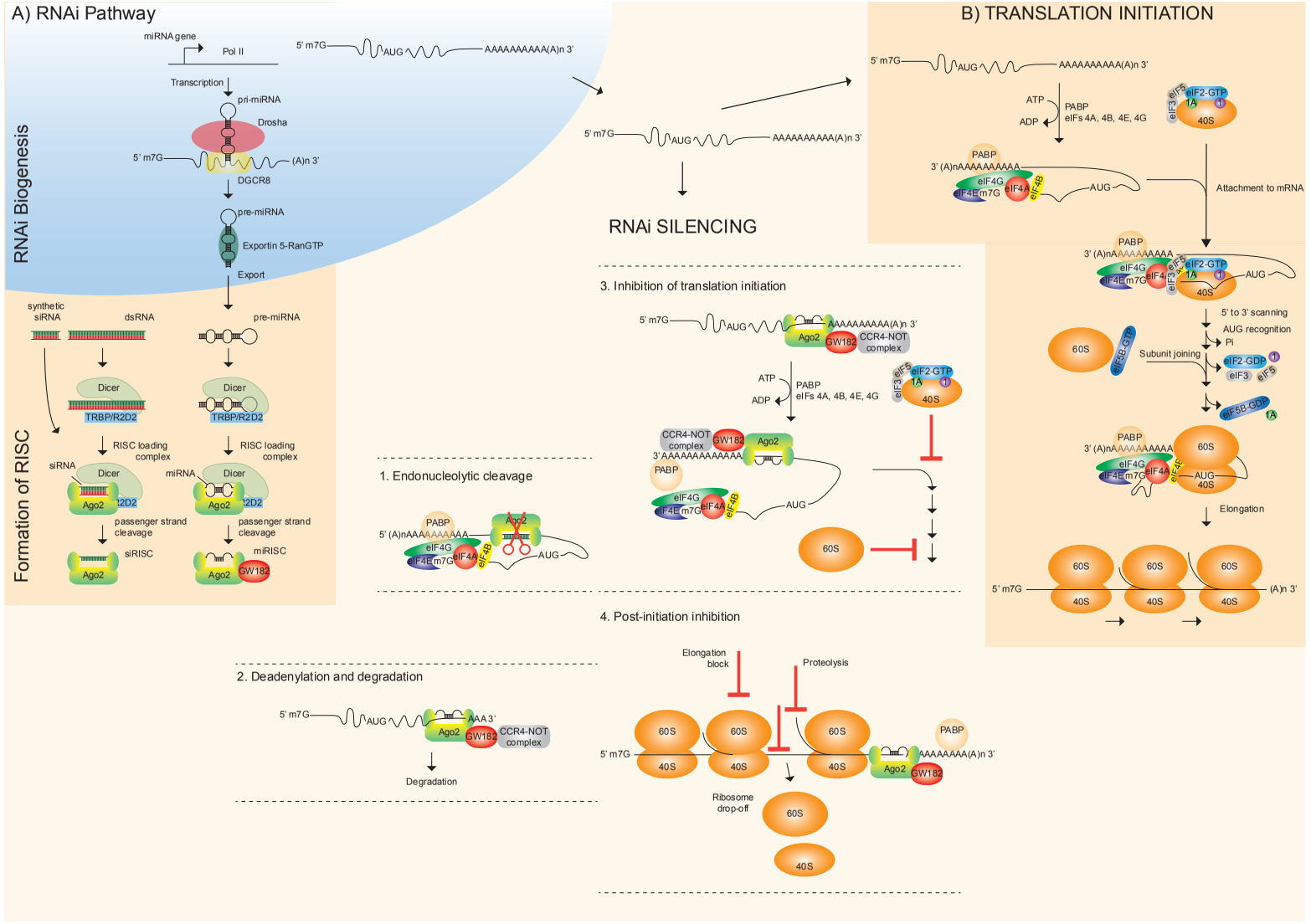

Figure 1.3 see figure legend on next page

1.4.2 RNAi – an Effective Tool to Study Gene Functions

The discovery of RNAi provides a powerful tool to systematically and specifically down-regulate cellular proteins, and to quantitatively study the depletion effects on cellular functions [116]. Together with the progress in automation and genome sequencing, high-throughput RNAi screening (HTS) of the whole human genome has become a state-of-the-art tool in functional genomics and related fields. Studies of signal transduction, cancer progression and host cell responses to pathogens have employed RNAi and also in virology, numerous studies have been published using this technology [117, 118, 119, 120, 121, 122, 123, 124, 125, 126, 127, 128, 129].

The general procedure of RNAi screens is to deplete in a population of cells one gene at a time by triggering the RNAi pathway. The depletion of a gene results in a phenotype on a desired screening read-out that is compared to the phenotype of a non-depleted gene control. Thereby, predictions about gene functions concerning the read-out can be made.

To trigger the RNAi pathway, three main HTS screening strategies have been devised:

Figure 1.3. Principle of the RNAi pathway and translation initiation in humans A) RNAi biogenesis, RISC formation, and the RNAi silencing mechanism are depicted. Pri-miRNA are transcribed in the nucleus by Polymerase II (Pol II) and further processed by the RNaseIII enzyme Drosha to pre-miRNA. Exportin-5 mediates pre-miRNA export to the cytoplasm where it is cut into miRNAs by Dicer. Dicer, TRBP/R2D2, and Ago2 forms the RISC loading complex and load the guide strand of the miRNA to Ago2. Activated miRISC silences gene expression in four different ways: in cases of a full match of the 21nt with its target mRNA, the mRNA gets cleaved by the endonuclease activity of Ago2 (1.). By incomplete matches only in the seed region, mRNA expression is inhibited by deadenylation and degradation of the mRNA (2.), by inhibiting the recruitment of the 40S and 60S ribosomal subunits to the mRNA (3), or by blocking the elongation step. In human cells, originally derived extracellular dsRNA or injected synthetic RNA are processed like pre-miRNAs or miRNA, respectively. SiRISC inhibits gene expression in the same way as miRISC. B) Principle of translation initiation. The translation initation process takes part when mRNA is not target by a siRNA or miRNA. PABP and eukaryotic initiation factors bind to the poly-A tail and to the 5' prime cap of mRNA, respectively. This enables the 40S ribosomal subunit to bind to the 5' UTR of mRNA and to scan in a 5' to 3' direction for the initiation codon. Recognition of the initiation codon results in a displacement of eIFs and binding of the 60S ribosomal subunit. Thereby, the elongation step is initiated. *Abbreviations*: Ago2, Argonaute 2; CCR4-NOT complex, multi-subunit complex that regulates gene expression in many ways, DGCR8,; dsRNA, double stranded RNA; eIF, eukaryotic initiation factor; GW182, trinucleotide repeat containing 6A; miRNA, microRNA; PABP, poly-A binding protein; Pol II, DNA-directed RNA polymerase II; siRNA, small interfering RNA; 40S, 40S ribosomal subunit ; 60S, ribosomal subunit.

- synthetic siRNAs (pooled or un-pooled library approaches)
- endoribonuclease-prepared siRNA (esiRNAs)
- vector-expressed short hairpin RNAs (shRNAs)

1.4.2.1 Synthetic siRNAs

This strategy uses synthetic siRNAs that target distinct regions of the same gene and are applied either individually or pooled into wells of screening plates. A reverse-transfection step is used consisting of adding transfection reagent to siRNAs, applying cells to each well of the screening plate, and an incubation time for gene depletion.

Such screening protocols usually lead to a depletion efficiency of at least 70% for most siRNAs [130].

For the pooling approach an increase in gene silencing specificity is claimed by vendors. Advantages and disadvantage of pooled versus single siRNAs screening approaches is a highly debated topic [131].

Most vendors offer pooled libraries consisting of pools of three to four different synthetic siRNAs targeting the same gene.

1.4.2.2 EsiRNAs

EsiRNAs are a mixture of many different siRNA oligos sharing the same on-target i.e. their specific cellular mRNA target. EsiRNAs result from *in vitro* cleavage of long dsRNAs with an RNaseIII family enzyme. To generate dsRNAs, first a polymerase chain reaction (PCR) is used in which a cDNA template is amplified and tagged with two bacteriophage-promoter sequences. Then, RNA polymerase is used to generate dsRNAs that is homologous to the target-gene cDNA. Reverse transfection is performed as described in section 1.4.2.1.

An average depletion efficiency of 83.6% and an increased gene silencing specificity is reported compared to single siRNA *in vitro* [132].

1.4.2.3 shRNAs

shRNAs are RNA nucleotide sequences with partial homology that form characteristic hairpins. Due to their secondary structure they mimic pri-miRNAs and thus trigger the RNAi pathway. The expression of shRNA in cells is accomplished by transfection of cells with plasmids or transduction of cells with viral vectors such as adenoviruses and lentiviruses [133]. The shRNA strategy provides methods for longer term silencing, inducible silencing and

a plasmid DNA format that can be replicated for unlimited supply. Also for screening strategies with shRNA, un-pooled and pooled approaches are available.

1.4.3 Challenges in Genome-wide RNAi Screens of Virus Infection

Recently published screens in the field of virology have shown that RNAi HTS is accompanied by many challenges. Three siRNA screens have been published to identify cellular genes required for human immunodeficiency virus (HIV) infection [117, 122, 129]. The screens showed less than 7% shared hits for any pairwise combination [3, 4]. Similarly, maximal 11% hits were shared in pairwise comparisons of three genome-wide studies for influenza virus infection [120, 123, 118, 134].

This low number of common hits between the screens is due to the high abundance of so-called false-positive and false-negative hits. In general, genes are defined as false-positive hits when they are real non-hits but were falsely identified as hits. Accordingly, false-negative hits are the opposite: true hits that could not be identified in the screen.

There are four main challenges that may enhance the numbers of false-positive and/or negative hits:

- Non-optimal experimental kinetics
- Reliability and specificity of siRNA libraries
- Population context-dependent cell-to-cell variability
- Statistical design and analysis of siRNA screens

1.4.3.1 Non-Optimal Experimental Kinetics

The RNAi process selectively depletes mRNA from the cellular transcriptome dependent on parameters that vary from target to target: Different mRNAs show huge variations in intracellular concentrations but also in the time points when depletion reaches its maximum.

In addition, the residual amount of proteins at maximum depletion might still be enough to maintain the protein's cellular function. However, in genome-wide siRNA screens, it is not possible to find an optimal timing for depletion of all mRNAs. Those siRNAs that need more time to effectively deplete their target mRNAs than the experimental protocol allows, might cause too subtle effects on the read-out to be considered as hits. This enhances the number of false-negative hits.

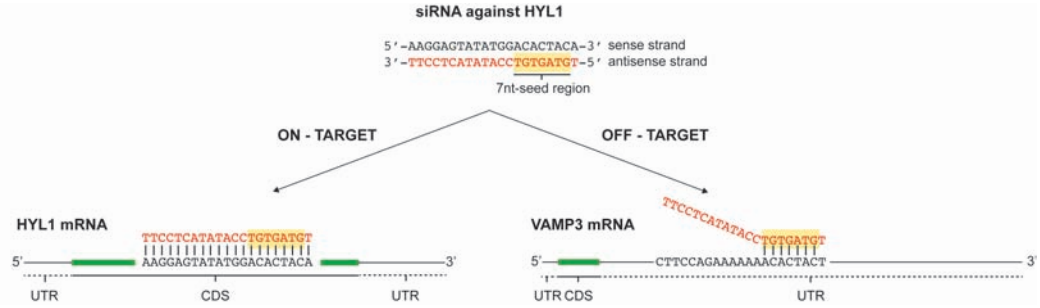

Figure 1.4 siRNA On and Off-targets. The siRNA designed to target HYL1 shows a full match with the CDS of HYL1, but the seed region of the anti-sense strand can also interfere with the 3'UTR of the VAMP3 mRNA. Thus the siRNA can act like an miRNA. *Abbreviations*: CDS, coding sequence; HYL1, hyaluronoglucosaminidase 1; mRNA, messenger RNA; UTR, untranslated region; VAMP3, vesicular associated membrane protein 3

1.4.3.2 Reliability and Specificity of siRNA Libraries

In RNAi experiments, specificity of siRNAs to their targets is crucial. However, siRNAs can act like miRNAs, causing additional downregulation of non-target genes (see figure 1.4). This potentially enhances the number of false-positive hits [135, 136, 137]. Another important issue is the integrity of siRNA libraries. The annotation of the human genome is still ongoing, which requires constant update of an siRNA library [138].

1.4.3.3 Population Context-Dependent Cell-To-Cell Variability

Snijder and colleagues revealed host cell population context dependent differences in virus infection [139]. They showed that the infection of rotavirus is strongly increased in cells that grow in sparsely populated cell areas. This correlated with alterations of the expression levels of surface integrins as the receptors of rotavirus.

In contrast, mouse hepatitis virus (MHV) prefers to infect cells that grow at high local density, similar to where CME is most active, the main endocytic route that MHV uses [139]. These examples show that virus infection can depend on cell density.

SiRNAs on-target and off-target effects can influence cell growth and viability, hence cell density. Therefore, variations in cell infection can be caused by the direct effect of siRNAs but can also be caused indirect by siRNA-induced changes in cell density. To account for this siRNA-mediated change in cell density, the use of so called "checkerboard" plates is suggested [140]. "Checkerboard" plates are control plates with different amounts of cells per well and transfected with a negative control siRNA. Infection indices are calculated for each cell density: $ii_n = ic_n \ / \ tc_n$ (ic_n = number of infected

cells in the nth well; tc_w = total number of cells in the nth well). Based on ii and tc, a regression function is fitted (ii versus tc): $ii_{corr} = f(ii_{raw}, tc)$. This function is then used to correct the raw infection indices of each well of the screen for the individual cell densities of the same wells.

1.4.3.4 Statistical Design and Analysis of siRNA Screens

HTS raises challenges for statistical design and analysis of the screening data. In general, this involves the following challenges: 1.) plate design 2.) normalization 3.) quality control and 4.) selection of hits.

1.) Plate design is a fundamental step in HTS experiments. Proper plate design enables accurate normalization, quality assessment of screening data, and hit selection. Therefore, proper plate design reduces the amount of false-positive and false-negative hits.

A proper plate design is achieved by the fully random distribution of siRNAs throughout each plate. In many commercial siRNA libraries however, siRNAs are pre-dispensed in plates such that the distribution of control siRNAs is limited to the outermost columns. Furthermore, many commercial siRNA libraries are clustered in functional groups.

2.) Normalization in siRNA HTS refers to the process of identifying and removing systematic errors from the data. Normalization is crucial to compare and combine data from different screening conditions such as batches, replicates and / or plates. The systematic errors are mainly caused by technical and biological variations.

Systematic technical variations are screen-to-screen, batch-to-batch, plate-to-plate, well-to-well, image-to-image differences, and illumination problems on the images. Typical examples are different infection indices, different cell numbers, intra-plate variations (e.g. spatial effects such as row, column, and edge effects) and vignetting (reduction of an image's brightness or saturation at the periphery to the image center). Systematic errors can be caused by uneven reagent evaporation, temperature differences within plates, and errors in liquid handling [141].

Proper removal of systematic errors (i.e. not over- or underestimation) is the basis for accurate interpretation of quality control and results. Thus, it is important to normalize data in a proper way. Different normalization methods have been proposed for siRNA HTS. The methods are either control-based or sample-based and account for plate-to-plate and/or within-plate variations. For the calculation formulae and descriptions of the methods see table 1.3 [142, 143, 144].

3.) **Quality control** is the assessment process to remove data with inferior quality. For RNAi HTS, high quality of the data is crucial to reduce the number of false-positive and false-negative hits. A clear distinction between positive and negative controls is an important requirement for good quality [145]. Thus, effective control siRNAs are crucial. Many methods have been proposed to measure data quality such as signal-to-background ratio, signal-to-noise ratio, signal window, assay variability ratio, Z-factor, and strictly standardized mean difference (SSMD). Their calculation formulae and description are depicted in the table 1.4 [143, 146].

4.) **Selection of hits** is the process of selecting those target siRNAs that have a desired difference from a negative reference group. There are two main strategies to select hits: In the first one, ranking and classifying methods grade siRNAs by their effects on the biological phenotype of interest. Hits are selected based on user-defined thresholds of these effects. In another strategy, siRNA are classified whether their specific phenotypes exceed a pre-set level or not. Based on the set-up of a screen, either of them is better. The different hit selection categories and their advantages and disadvantages are depicted in table 1.5.

1.5 Aims of the Project

The goal of this thesis was to investigate early bunyavirus-host cell interactions and entry (binding, internalization, fusion, penetration, and expression of viral N) by performing full-genome-wide siRNA screens to identify host proteins that affect UUKV infection. To this end, it was important to improve the screening technology and minimize false hits. In addition, we aimed at validating and studying the mechanism of action of selected hits from the siRNA screens.

Table 1.3 normalization methods

Normalization method	**Calculation Formula**	**Based on**	**Accounts for plate-to-plate / within-plate variation**	**Description**
Percent activity (PA)	$PA = \frac{x_{\text{siRNA}}}{\bar{c}_{\text{P}}} \times 100$	control	+ / -	Ratio between values of target siRNA and mean of positive controls
Percent inhibition (PI)	$PI = \frac{x_{\text{siRNA}} - \bar{c}_{\text{N}}}{\bar{c}_{\text{P}} - \bar{c}_{\text{N}}} \times 100$	control	+ / -	Ratio between the difference between values of target siRNA and mean of negative controls and the difference between values of means of positive and negative controls
Z score (Z)	$Z = \frac{x_{\text{siRNA}} - \bar{x}_{\text{N}}}{SD_{\text{N}}}$	control or sample	+ / -	Ratio between the difference between values of target siRNA and mean of negative reference and the standard deviation of negative reference
B score	$B_{\text{ijp}} = \frac{r_{\text{ijp}}}{MAD_{\text{p}}}$ $r_{\text{ijp}} = x_{\text{ijp}} - \hat{x}_{\text{ijp}} = x_{\text{ijp}} - (\hat{\mu}_{\text{p}} + \hat{R}_{\text{ip}} + \hat{C}_{\text{jp}})$ $MAD_{\text{p}} = median\{\lvert r_{\text{ijp}} - median(r_{\text{ijp}})\rvert\}$ *principle*: 1. calculate row medians 2. subtract row median from each siRNA meas. in that row 3. record median of row medians as overall effect $\hat{\mu}_{\text{p}}$ 4. subtract $\hat{\mu}_{\text{p}}$ from each row median 5. record new row medians as row effect $\hat{R}_{\text{ip}}$ 6. perform steps 1 to 6 for columns; add median of columns to $\hat{\mu}_{\text{p}}$; record column medians as column effect $\hat{C}_{\text{jp}}$ 7. repeat steps 1 to 6 until no changes occur with row and column effects; Overall-, raw-, and column effects are added to the current at each iteration	sample	+ / +	Iterative method for removing row and column effects. Ratio between residual r_{ijp} of the value for row i and column j on the p^{th} plate and MAD_{p} of p^{th} plate where r_{ijp} is defined as the difference between observed value x_{ijp} and the fitted value $\hat{x}_{\text{ijp}}$ of an siRNA. $\hat{x}_{\text{ijp}}$ is defined as the sum of an overall effect $\hat{\mu}$ of p^{th} plate + i^{th} row effect of p^{th} plate + j^{th} column effect of p^{th} plate

Continued on next page

Table 1.3 Normalization methods – Continued from previous page

Normalization method	Calculation Formula	Based on	Accounts for plate-to-plate / within-plate variation	Description
loess	$S_{\text{fit}} \sim R_{\text{pos}} \times C_{\text{pos}}$ use S_{fit} to calculate $siRNA_{\text{predicted}}$ $siRNA_{\text{adjusted}} = siRNA_{\text{raw}} - siRNA_{\text{predicted}} + \overline{siRNA}_{\text{predicted}}$ *principle*: Polynomial regression fitting is done locally. That is, for the fit at point x, the fit is made using points in a neighborhood of x, weighted by their distance from x. Traditional *tri-cube weight* function is used: $w(x) = (1 - (dist/maxdist)^3)^3$ Normally polynomials of degree 1 or 2 are used.	control or sample	- / +	Local polynomial regression fitting. Adjusts for nonlinear spatial effects.

Robust methods for PA, PI, and Z score are obtained by replacing mean values of $\bar{c}_P$ and $\bar{x}_N$, and SD_{N} through median values and MAD, respectively. *Abbreviations*: meas., measurement; x_{siRNA}, raw meas. on a siRNA; $\bar{c}_P$, mean of the raw meas. of the positive control; $\bar{c}_N$, mean of the raw meas. of the negative (neg.) control; $\bar{x}_N$, mean of the raw meas. of a neg. reference within pth plate; SD_{N}, standard deviation estimated from all meas. of a neg. reference within pth plate; r_{ijp}, residual of the meas. for row i and column j on the p$^{\text{th}}$ plate; MAD_{p}, median absolute deviation of p$^{\text{th}}$ plate; y_{ijp}, observed value for row i and j column on p$^{\text{th}}$ plate; $\hat{y}_{\text{ijp}}$, fitted value for row i and j column on p$^{\text{th}}$ plate; $\hat{\mu}_{\text{p}}$, overall effect of p$^{\text{th}}$ plate; $\hat{R}_{\text{ip}}$ row effect of p$^{\text{th}}$ plate; $\hat{C}_{\text{jp}}$ column effect of pth plate; loess, locally weighted scatterplot smoothing; S_{fit}, fitted value for row position and column position of a plate; R_{pos}, row position on a plate; C_{pos}, column position on a plate; $\overline{siRNA}_{\text{predicted}}$, mean of predicted siRNA values; w, weight; dist, distance; maxdist, maximal distance; table modified from [142, 143, 144].

Table 1.4 Quality control methods and their formula

QC Measure	Calculation Formula	Description
Signal-to-background ratio	$\frac{\bar{c}_P}{\bar{c}_N}$	Interpretation is based on graphics Does not contain any information regarding data variability.
Signal-to-noise ratio	$\frac{\bar{c}_P - \bar{c}_N}{SD_N}$	Interpretation is based on graphics. Takes into account the variability in the negative control but not in the positive control.
Signal window	$\frac{\lvert\bar{c}_P - \bar{c}_N\rvert - 3(SD_P + SD_N)}{SD_N}$	Accounts for data variability in both negative and positive controls. Interpretation is based on graphics.
Assay variability ratio	$\frac{3(SD_P + SD_N)}{\lvert\bar{c}_P - \bar{c}_N\rvert}$	Accounts for data variability in both negative and positive controls. Interpretation is based on graphics. Assay variability ratio = 1-Z-factor
Z-factor	$\frac{\lvert\bar{c}_P - \bar{c}_N\rvert - 3(SD_P + SD_N)}{\lvert\bar{c}_P - \bar{c}_N\rvert}$	Accounts for data variability in both negative and positive controls. Interpretation is based on graphics. No direct probability-based interpretation. Difficult to derive its estimation and confidence interval from a complete statistical basis.
SSMD	$\frac{\bar{c}_P - \bar{c}_N}{\sqrt{SD_P^2 + SD_N^2}}$	Accounts for data variability in both negative and positive controls. Interpretation is based on probability: has a direct relationship with the probability that a draw from the positive control is greater than a draw from the negative control. Simple to derive its estimation and confidence interval from a complete statistical basis.

Abbreviations: QC, quality control; $\bar{c}_P$ and SD_P are sample mean and standard deviation of a positive control, respectively, and $\bar{c}_N$ and SD_N are sample means and standard deviation of a negative reference, respectively. Adapted from [144].

Table 1.5 Hit selection methods

Hit selection methods	**Calculation Formula**	**Hit selection cutoff**	**Advantages**	**Disadvantages**
Fold change (FC)	$FC = \frac{x_{\text{siRNA}}}{\bar{c}_{\text{N}}}$	± k	Easy to calculate	Does not take data variability into account sensitive to outliers
Percent activity (PA)	$PA = \frac{x_{\text{siRNA}}}{\bar{c}_{\text{P}}} \times 100$	± k	Easy to calculate	Does not take data variability into account sensitive to outliers
Percent inhibition (PI)	$PI = \frac{x_{\text{siRNA}} - \bar{c}_{\text{N}}}{\bar{c}_{\text{P}} - \bar{c}_{\text{N}}} \times 100$	± k	Easy to calculate	Does not take data variability into account sensitive to outliers
Quartile method	$IQR = Q_3 - Q_1$	$Hit_{\text{inh}} \leq Q_1 - c \times IQR$ $Hit_{\text{enh}} \geq Q_3 + c \times IQR$	Easy to calculate; Not sensitive to outliers; Data does not need to be symmetrically distributed	Does not take data variability into account
Z score (Z)	$Z = \frac{x_{siRNA} - \bar{x}_{\text{N}}}{SD_{\text{N}}}$	± k	Easy to calculate; Linked to p-values; Takes into account data variability of neg. reference	Sensitive to outliers; Inappropriate if data is not normally distributed

Continued on next page

Table 1.5 Hit selection methods – Continued from previous page

Hit selection methods	Calculation Formula	Hit selection criteria	Advantages	Disadvantages
Z* score (Z*)	$Z^\star = \frac{x_{siRNA} - \tilde{x}_{\mathrm{N}}}{MAD_{\mathrm{N}}}$	± k	Easy to calculate; Not very sensitive to outliers;	Not easily linked to p-values; Inappropriate if data is not normally distributed
B score	$B_{\mathrm{ijp}} = \frac{r_{\mathrm{ijp}}}{MAD_{\mathrm{p}}}$ $r_{\mathrm{ijp}} = y_{\mathrm{ijp}} - \hat{y}_{\mathrm{ijp}} = y_{\mathrm{ijp}} - (\hat{\mu}_{\mathrm{p}} + \hat{R}_{\mathrm{ip}} + \hat{C}_{\mathrm{jp}})$ $MAD_{\mathrm{p}} = median\{\lvert r_{\mathrm{ijp}} - median(r_{\mathrm{ijp}})\rvert\}$ *Principle*: 1. Calculate row medians 2. Subtract row median from each siRNA meas. in that row 3. Record median of row medians as overall effect $\hat{\mu}_{\mathrm{p}}$ 4. Subtract $\hat{\mu}_{\mathrm{p}}$ from each row median 5. Record new row medians as row effect $\hat{R}_{\mathrm{ip}}$ 6. Perform steps 1 to 6 for columns; add median of columns to $\hat{\mu}_{\mathrm{p}}$; record column medians as column effect $\hat{C}_{\mathrm{jp}}$ 7. Repeat steps 1 to 6 until no changes occur with row and column effects; overall-, raw-, and column effects are added to the current at each iteration	± k	Not sensitive to outliers; Adjust for positional effects	Inappropriate if no systematic positional effect is present
t-test	$t = \frac{\bar{d}_i}{\frac{SD_i}{\sqrt{n}}}$	Arbitrary threshold of adjusted p-value for multiple comparison correction	Simple to calculate; Provides p-values	p-values is affected by sample size Inappropriate if data is not normally distributed

Continued on next page

Table 1.5 Hit selection methods – Continued from previous page

Hit selection methods	Calculation Formula	Hit selection criteria	Advantages	Disadvantages
SSMD (β)	$\beta = \frac{x_{siRNA} - \bar{x}_N}{\sqrt{2}SD_N}$ (without replicate) $\beta = \frac{\bar{d}_i}{SD_i}$ (with replicate)	Enhancement effect: Extremely strong $\beta \geq 5$ Very strong $5 > \beta \geq 3$ Strong $3 > \beta \geq 2$ Fairly strong $2 > \beta \geq 1.645$ Moderate $1.28 > \beta \geq 1$ Fairly weak $1 > \beta \geq 0.75$ Weak $0.75 > \beta \geq 0.5$ Very weak $0.5 > \beta \geq 0.25$ Extremely weak $0.25 > \beta > 0$ Inhibition effect: Extremely strong $\beta <$ -5 Very strong -5 $\leq \beta <$ -3 Strong -3 $\leq \beta <$ -2 Fairly strong -2 $\leq \beta <$ -1.645 Moderate -1.28 $\leq \beta <$ -1 Fairly weak -1 $\leq \beta <$ -0.75 Weak -0.75 $\leq \beta <$ -0.5 Very weak -0.5 $\leq \beta <$ -0.25 Extremely weak -0.25 $\leq \beta < 0$	Takes into account data variability of neg. reference; Allows classifying the size of siRNA effect; Independent of sample size; Allows control of false-positive and false-negative rate;	If SD is very small, SSMD value can be very small or very large even if mean difference is small and is not of biological interest (alternative: combine SSMD method with fold change method)
SSMD-based method to assess off-target effects	See [144]	See [144]		
RSA	$P = F(k\|N,m,n) = \sum_{i=0}^{k} \frac{\binom{m}{i}\binom{N-m}{n-i}}{\binom{N}{n}}$	Arbitrary threshold of p-value	Provides p-value; May reduce false-positive owing to off-target	May have limited use for pool-based screens
Rank-product	See [147]	See [147]	Provides p-value; Not sensitive to outliers; May reduce false-positive owing to off-target	Requires many replicates

Continued on next page

Table 1.5 Hit selection methods – Continued from previous page

Hit selection methods	Calculation Formula	Hit selection criteria	Advantages	Disadvantages
Linear mixed-effect models	$Y = siRNA_i + \epsilon_{siRNA}$		Model can be extended to account for confounding effects on the phenotype of interest	Computationally intensive (alternative: stepwise linear modeling (see [148])
Bayesian method	See [149]	See [149]	Provides p-value; Not sensitive to outliers	

Abbreviations: x_{siRNA}, raw measurements (meas.) on a siRNA; $\bar{c}_N$, mean of the raw meas. of the negative (neg.) control; $\bar{c}_P$, mean of the raw meas. of the positive control; IQR, interquartile range; Q_1, first quartile; Q_3, third quartile; $\bar{x}_N$, mean of the raw meas. of a neg. reference; SD, standard deviation estimated from all meas. of a neg. reference; $\tilde{x}_{\mathrm{N}}$, median of the raw meas. of a neg. reference; MAD_{N}, median absolute deviation of a neg. reference; r_{ijp}, residual of the meas. for row i and column j on the p^{th} plate; MAD_{p}, median absolute deviation of p^{th} plate; y_{ijp}, observed value for row i and j column on p^{th} plate; $\hat{y}_{\mathrm{ijp}}$, fitted value for row i and j column on p^{th} plate; $\hat{\mu}_{\mathrm{p}}$, overall effect of p^{th} plate; $\hat{R}_{\mathrm{ip}}$, row effect of p^{th} plate; $\hat{C}_{\mathrm{jp}}$, column effect of p^{th} plate; k, constant; table modified from [142, 143, 144].

Chapter 2

Results

2.1 Genome-wide siRNA Infection Screens

We performed two genome-wide siRNA screens in tissue culture cells to identify cellular factors that affect UUKV infection i.e. virus binding, internalization, fusion, penetration, and expression of the viral N protein.

As depicted in figure 2.1 and described in detail in the following subsections, the screening process consisted of five phases: assay development, pipetting and liquid handling, microscopy and image processing, normalization and quality control, and hit selection and bioinformatic analysis.

The general procedure of the screens was that in a population of cells one gene at a time was depleted using one or four different siRNAs and subsequently, cells were challenged with UUKV. Then, the fraction of infected cells was quantified in an automated readout using indirect immunofluorescence and automated epifluorescent microscopy, followed by image processing and analysis. After normalization and assessment of the quality of screening data, the infection index of a target siRNA was compared to the calculated infection index of a non-targeting control siRNA. These comparisons revealed one of three possible effects of the target siRNA on UUKV infection: an inhibition effect, no effect, or an enhancement effect.

2.1.1 Assay Development

Assay development comprised steps of cell line selection, testing of potential siRNA controls and optimization of infection-, reverse-transfection, and readout protocols. All protocols needed to be upscaled from a "bench-top" to a high-throughput platform (see figure 2.1). In addition, to perform screens with the same virus- and cell line stock, a virus stock was produced for the screen and cells were frozen.

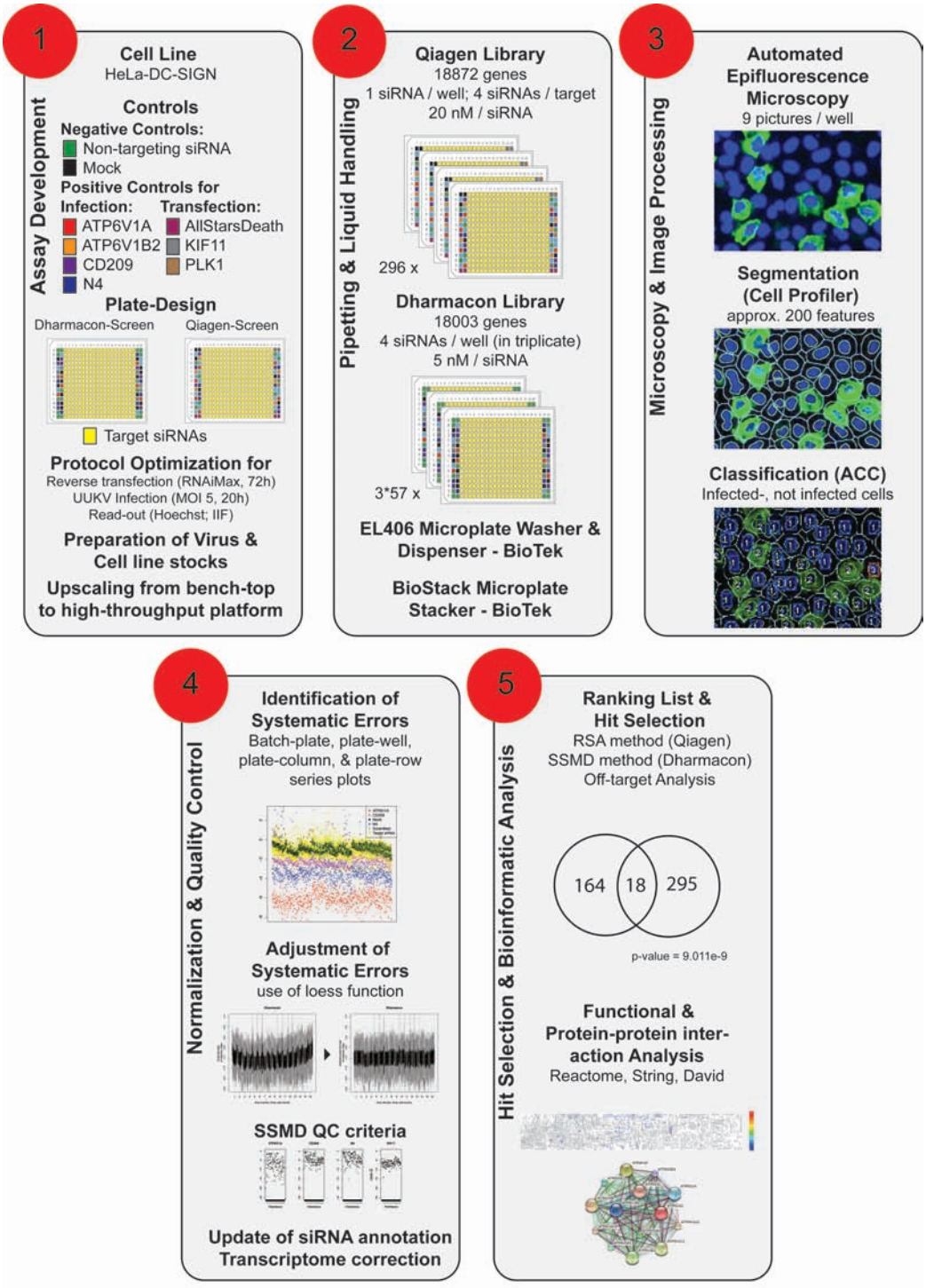

Figure 2.1 Screening workflow in five phases - see figure legend on next page

2.1.1.1 The Cell Line "HeLa-DC-SIGN"

Dermal dendritic cells (DCs) belong to the first cells that encounter a virus after its transmission by a vector. We showed that DC-specific intercellular adhesion molecule 3-grabbing nonintegrin (DC-SIGN), a lectin mainly expressed on the surface of DCs, is a receptor for UUKV and other Phleboviruses [1, 2].

HeLa and raji (B lymphocyte cells) cells showed a poor infection to UUKV particles at moi 10 (HeLa, 10%) and moi 100 (raji, $\leq$1%). In order to render HeLa (cervix epithelial cells) and raji (B lymphocyte cells) cells more susceptible to UUKV infection, we generated cell lines stably expressing DC-SIGN using a Lentivirus approach. HeLa and raij cell lines that stably expressed DC-SIGN (HeLa-DC-SIGN, raji-DC-SIGN) showed a 8-fold (HeLa-DC-SIGN, moi 10) and a 90-fold (raji, moi 100) increase in infection.

To study the first steps after viral transmission we used HeLa-DC-SIGN cells in the genome-wide siRNA screens. The use of human DCs was not possible due to limited availability and their inefficient siRNA transfection.

Figure 2.1 Screening workflow in five phases. **1) Assay development:** Construction of HeLa-DC-SIGN cells, selection and testing of the controls, and the plate design. The reverse transfection-, the infection-, and the read out protocol were optimized and adapted for a high-throughput platform. The read out of the screens was infected cells. It was visualized using indirect immunofluorescence (IIF) against viral nucleoprotein (N) synthesized in the infected cells. **2) Pipepetting and liquid handling:** Genome-wide siRNA libraries from two different vendors, Qiagen and Dharmacon, were used. The Qiagen library consisted of 296 384-well plates, containing 4 different siRNA per target gene pipetted each in a single well in four different plates. The Dharmacon library consisted of 57 384-well plates, containing a pool of 4 different siRNAs targeting the same gene in a single well. Control siRNAs were located in the first and last two columns of each plate. A final siRNA concentration of 20 nM was used for the Qiagen library, 5 nM per pooled siRNA for the Dharmacon library, respectively. For reverse transfection, a mix of 0.1 µl of the transfection reagent RNAiMax and 24.9 µl DMEM was incubated for 1 h, followed by addition of 400 HeLa-DC-SIGN in a volume of 50 µl per well. After incubation at 37 °C for 72 h, cells were washed, infected with 15'000 ffu / well of UUKV (moi 5), and incubated at 37 °C for 1 h. Then, unbound viruses were removed by a washing step and cells were further incubated at 37 °C for 19 h. At 20 h post-infection, cells were fixed and cellular DNA and the viral N were stained using Hoechst and indirect immunofluorescence, respectively. **3) Microscopy and image processing:** Cells were imaged using automated inverted epifluorescent microscopes (MD ImageXpress, Molecular Devices, Wals-Siezenheim, Austria). Pictures were analyzed using Matlab and the open source software Cell Profiler and Advanced Cell Classifier. **4) Normalization and Quality Control:** Screening data were displayed using different series-plots to detect systematic errors. A systematic edge effect in the infection dataset was identified and corrected using a "loess" function. To quantitatively assess the quality of the normalized data the SSMD method based on "very strong control" criteria was applied. SiRNA annotation was up-dated and compared to the transcriptome of HeLa-DC-SIGN cells. **5) Hit selection and bioinformatic analysis:** To determine hits, redundant siRNA activity (RSA) and SSMD combined with fold change methods were used for Qiagen library and Dharmacon, respectively. Hits were analyzed by functional- and protein-protein interaction analysis using different open source software such as Reactome, String, or David.

Also the use of raij-DC-SIGN cells was not possible due to poor siRNA transfection efficiency.

2.1.1.2 siRNA Controls and Plate Layout

To monitor the siRNA transfection efficiency, several siRNA controls were included in each plate. As negative controls, we used non-targeting siRNA (AllStarsNegative (ASN) in the Qiagen screen and scrambled (scr) in the Dharmacon screen) and wells without siRNA (mock). Positive controls were siRNAs against proteins known to be essential for the UUKV life cycle:

- ATPase, H^+ transporting, lysosomal 70 kDa, V1 subunit A1 (ATP6V1A1)
- ATPase, H^+ transporting, lysosomal 56/58 kDa, V1 subunit B2 (ATP6V1B2), but used only in Qiagen)
- DC-SIGN (CD209)
- Viral nucleoprotein (N)

ATP6V1A1 and ATP6V1B2 are essential component of the vesicular proton pump that acidifies the endosomal compartment.

Since N is a viral protein, the siRNA-mediated depletion process occurred right after infection during 20 h, while cellular proteins were depleted over 92 h. Therefore, anti-DC-SIGN, anti-ATP6V1A1, and anti-ATP6V1B2 were the more appropriate positive controls to compare with sample siRNA effects. However, the siRNA against N was an efficient control for the effect on the screen read-out. It showed a strong effect similar to the effects of anti-ATP6V1A1 and anti-ATP6V1B2 siRNA controls. Of note, the Dharmacon siRNA against N showed a cytotoxic effect, in contrast to the Qiagen siRNA.

To monitor transfection, additional positive controls were used against proteins essential for cell viability: siRNA against kinesin family member 11 (Kif11), a kinesin-like motor protein involved in chromosome positioning and other crucial steps during cell mitosis; polo-like kinase 1 (PLK1), a serine/threonine-protein kinase that regulates several important functions in cell cycle, including the regulation of centrosome maturation and spindle assembly; and AllStarsDeath, a positive control siRNA from Qiagen that causes cell death. AllStarsDeath and PLK1 were used only in the Qiagen screen. Cell death were observed starting after 48 h.

2.1.1.3 Adaptation of reverse transfection

We tested the transfection reagents Interferin (Polyplus) and Lipofectamine RNAiMax (Life technologies) for their reverse transfection efficiency and their effect on cell viability at various volumes in presence of the AllStarsDeath siRNA. The best transfection efficiency was reached for both reagents as mentioned in the manuals (see figure 2.2). Thus the quality of the reagents was comparable. Due to a better price offer, we decided to use RNAiMax in the screen. Transfection was finally performed using 0.1 μl/well of a 384 well plate for 72 h (see figure 2.2).

2.1.1.4 Optimizing the Infection Conditions

We considered an infection index range between 15% and 35% for the negative control siRNAs as optimal since it allowed scoring siRNA-mediated inhibitory as well as enhancing effects on UUKV infection with a sufficient dynamic range. Initial tests showed that this range was reached in the negative control wells when 400 HeLa-DC-SIGN cells were plated and infected with 15'000 foci forming units (ffu) of UUKV, corresponding to a moi of 5 (data not shown).

2.1.1.5 Adaptation of Screening Read-Out Protocol

We determined the fraction of infected cells (denoted as infection index). To visualize infected cells, indirect immunofluorescence (IIF) with monoclonal antibodies against the viral N protein was used. N proteins are synthesized in infected cells after UUKV cytoplasm penetration. In addition to quantify the overall number of cells, cellular DNA was stained using Hoechst. To adapt the IIF protocol to a high-throughput platform, we combined the cell permeabilization step with the incubation step of the first antibody. Thus, one step in the "standard" staining protocol was reduced, and the length of the screening protocol was reduced by about 0.5 h per batch.

2.1.2 Pipetting and Liquid Handling

Screens were performed with genome-wide siRNA libraries from two different vendors, Qiagen (Leiden, Germany) and Dharmacon (Thermo Fisher Scientific, Waltham, Massachusetts, US). The Qiagen library was delivered in 296 384-well plates and 4 different siRNAs per gene. Those siRNAs that targeted the same gene were located in different plates at the same well position. The Dharmacon library comprised 57 384-well plates, and each well contained a pool of four different siRNAs targeting the same gene (see figure 2.1).

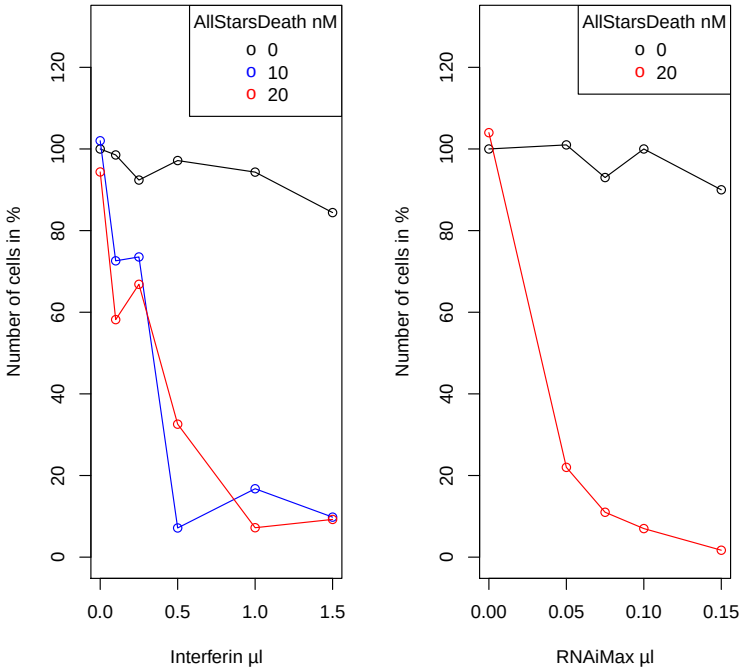

Figure 2.2 Transfection reagent test A) Different reverse transfection conditions were tested in HeLa-DC-SIGN cells using different amounts of the siRNA AllStarsDeath and various volumes of the transfection reagent Interferin. Cell number was 90% decreased compared to control samples (0 nM AllStars Death) if the combinations of 0.5 µl Interferin and 10 nM AllStars Death, 1.5 µl Interferin and 10 nM AllStars Death,1µl Interferin and 20 nM AllStars Death, and 1.5 µl Interferin and 20 nM AllStars Death were used. B) Different reverse transfection conditions were tested in HeLa-DC-SIGN cells using different amount of AllStarsDeath siRNA and various volumes of the transfection reagent Lipofectamine RNAiMax. Cell number was 90% decreased compared to control samples (0 nM AllStars Death) if the combination of 0.1 µl RNAiMax and 20 nM AllStars Death was used.

For the pipetting process, libraries were divided into batches due to the time schedule in the screening protocol. The Dharmacon library was divided into 9 batches each containing 19 plates. The Qiagen library was split into 12 batches consisting of 25 (9x) and 24 plates (4x), respectively. Plates were divided into batches such that no replicate plates (for Dharmacon screen) or none of the 4 different siRNAs targeting the same genes (for Qiagen screen) were in the same batch.

All pipetting steps were performed using "EL406 Microplate Washer & Dispenser" and "BioStack Microplate Stacker" from BioTek (see figure 2.1). HeLa-DC-SIGN cells were dispensed and reverse transfected with the corresponding siRNAs at a final concentration of 20 nM and incubated for 72 h. After washing, 80 μl UUKV suspension was applied to each well and incubated at 37 °C for 1 h. Then, cells were washed to remove unbound viruses and incubated at 37 °C for 19 h. Cells were fixed using 4 % of formaldehyde (FA) and after washing stained.

2.1.3 Microscopy and Image Processing

The detection of stained cellular nuclei and viral N expression, indicating infected cells, was performed using automated inverted epifluorescent microscopes (MD ImageXpress, Molecular Devices, Wals-Siezenheim, Austria). Images were aquired at 10x magnification. After microscopy image processing and analysis followed. Image processing consisted of a segmentation- and cell classification step. Segmentation was used to identify cells in the digital images. It was performed using adapted MATLAB open-source system CellProfiler. CellProfiler allows accurate identification of cells by extracting approximately 200 features from the digital images including area, shape, intensity, and texture ([150]) (see figure 2.1).

The cells were classified as infected, non infected, and apoptotic using the open-source software Advanced Cell Classifier [151]. The performance was determined by measuring cross-validation (CV) accuracy. CV revealed prediction errors of maximal 10% indicating that our classifier correctly predicted more than 90% of new observations (see figure 2.1).

2.1.4 Normalization and Quality Control

High quality data is a prerequisite to determine hits correctly. Therefore, systematic errors within datasets needed to be identified and corrected by normalization procedures (see 1.4.3.4).

2.1.4.1 Normalization

A practical way to identify systematic errors in large datasets is to display the data in different series plots (see figure 2.1). From the screening raw data, median infection indices and their variations were calculated on several levels and dimensions of each screen, i.e. over the whole batch, plate, column, and row. Batch-plate - and plate-well series plots revealed in the Dharmacon screen that the raw data of infection indices varied up to 1.5-fold between batches and up to 3.5-fold between plates. The Qiagen data varied up to 4-fold and up to 15-fold, respectively. The overall median infection index of all siRNAs in the raw datasets was 25% in the Dharmacon screen and 7% in the Qiagen screen, while the median of the negative controls was 34% in the Dharmacon screen and 17% in the Qiagen screen.

Column-well - and row-well plot series were used to display potential within-plate spatial effects in screening data. The plots revealed that the distribution of infection within most of the screening plates was systematically distorted: in the Dharmacon screen, the edge wells had a 1.5- to 2-fold increase in infection compared to mid-plate wells (see figure 2.3; Qiagen screen: 2- to 2.5-fold, see supplementary figure 5.1). Since such a "bowl-shaped" edge effect in the infection datasets was not caused by non-homogenous cell numbers (see supplementary figure 5.2), we assumed as cause uneven thermal and temperature conditions within the plates during infection. To normalize for this effect, we adapted a plate-wise "loess" function (see table 1.3). First, we linearized the sigmoidal distribution of the infection indices by the so-called empirical logit transformation. Figure 2.3 and supplementary figure 5.1 show the logit-transformed data before and after "loess" correction and demonstrate the efficacy of this method to reduce edge effects.

2.1.4.2 Cytotoxicity Criteria

In the next step, we removed all plates for which negative control siRNA treated cells had a median infection index less than 10% (0 plates for the Dharmacon screen, 28 plates (9.5% of all Qiagen plates) for the Qiagen screen). In these plates inhibitory siRNA effects could not be determined without enhanced errors. We assumed that pipetting errors caused such low infection indices. Furthermore, as an siRNA can have an impact on cell viability and/or growth, we defined a cytotoxicity threshold for the screening data: In the Qiagen screen we did not take into account for further analysis wells for which the cell number was less than 75% of the median cell number of the corresponding batch (range between 500 and 1'200 cells / well; see supplementary figure 5.3). Overall 21'415 wells (18.8%) were removed.

As the Dharmacon screen was performed in triplicate, we removed the genes of which mean fold change in the cell number was reduced or enhanced more than 3 times the standard deviation of the fold change of the non-targeting siRNA negative control. The median cell number for non-targeting siRNA controls was 4'260. The calculated cytotoxicity thresholds were 2'199 and 6'328 cells. 1'453 genes (8%) were defined to have a cytotoxic effect after siRNA depletion.

2.1.4.3 Quality Control

After the normalization and correction steps, the quality of the screening data was assessed. A clear distinction between a negative and positive control on infection is an indicator for efficient transfection and good quality. Qualitative plate-well series plots showed a clear difference in most of the plates (see figure 2.4).

Figure 2.5 and supplementary figure 5.4 show example wells of control siRNA, indicating clear effects of positive controls: siRNA against ATP6V1A1 and ATP6V1B2 caused a decrease of infection of 90%; siRNA against DC-SIGN (CD209) reduced infection by 70%; siRNA against N4 caused a decrease of infection of 90%; siRNA against Kif11, PLK1, and AllStarsDeath decreased the cell number by 95%.

To assess quantitatively the quality of the different positive controls within a plate, several statistical procedures are known with advantages and disadvantages (see table 1.4). For our screening data we applied a SSMD metric with threshold criteria for "very strong controls" that is usually used for virus infection siRNA screens (see table 1.4, figure 2.6 & supplementary figure5.5; [146]).

To assess the quality of individual screening plates, we defined a plate threshold criterion. In the Qiagen screen only plates were taken into account for further hit selection process if 75% of the positive controls were classified by the SSMD criteria as good or excellent. This was the case for 285 plates (96%, see supplementary figure 5.5). Since the Dharmacon screen was performed in triplicates, only plates would have been removed when all three replicate plates failed to meet the plate criterion. This was not the case in any instance (see figure 2.6).

Overall, the quality of the screens was good and the number of inferior or poor plates was in the observed range of other screens [144].

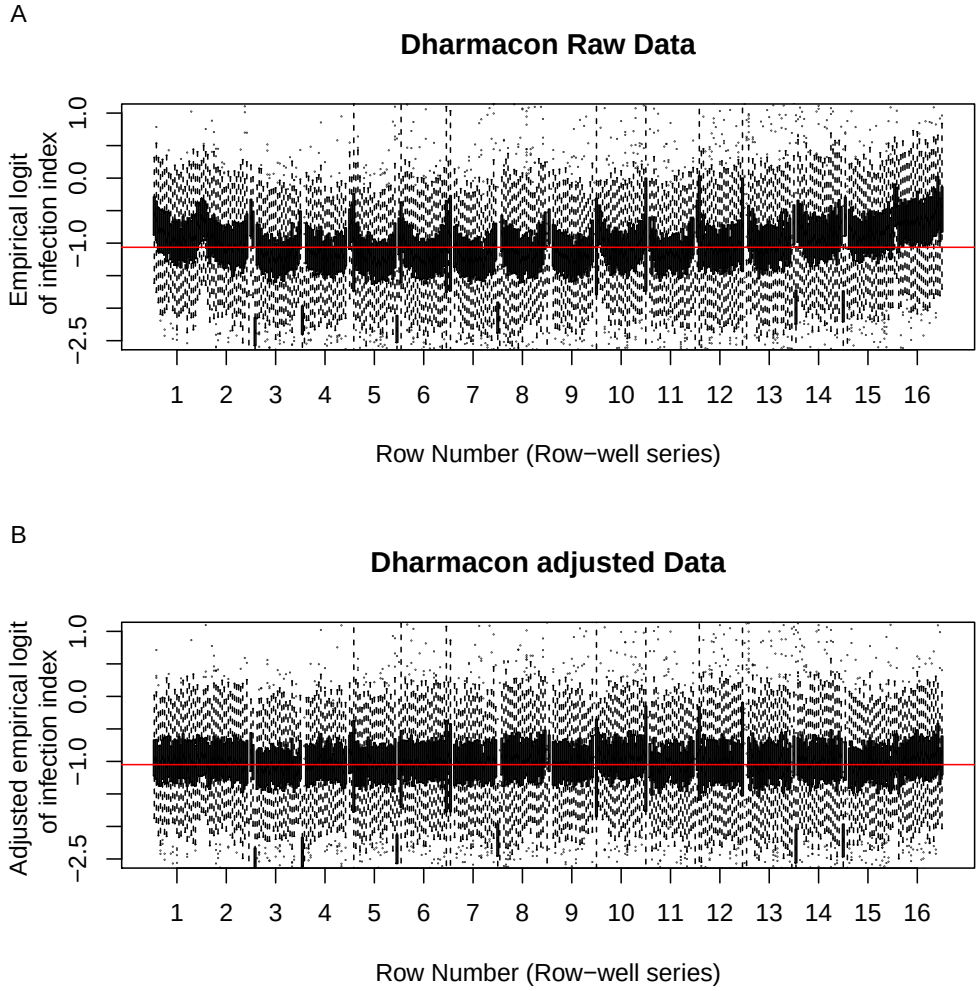

Figure 2.3 Removal of the systematic spatial ("bowl-shaped") effect in the Dharmacon screen. A) Row-well series plot of empirical logit-transformed Dharmacon raw data. The values of the x-axis are the indices of the positions of a well in a row, whereas the labels in the x-axis are the row numbers. The distribution of the well data at the same position is displayed by a box plot. B) As in A but cleaned from the systematic spatial effect using "loess" (locally weighted scatterplot smoothing) method. "Empirical logit of infection index" values 0.5, 0, -0.5, -1, -1.5, and -2 correspond to 62%, 50%, 38%, 27%, 18%, and 12% infection, respectively. Red lines show the corresponding median values of all data to better visualize the infection edge effect.

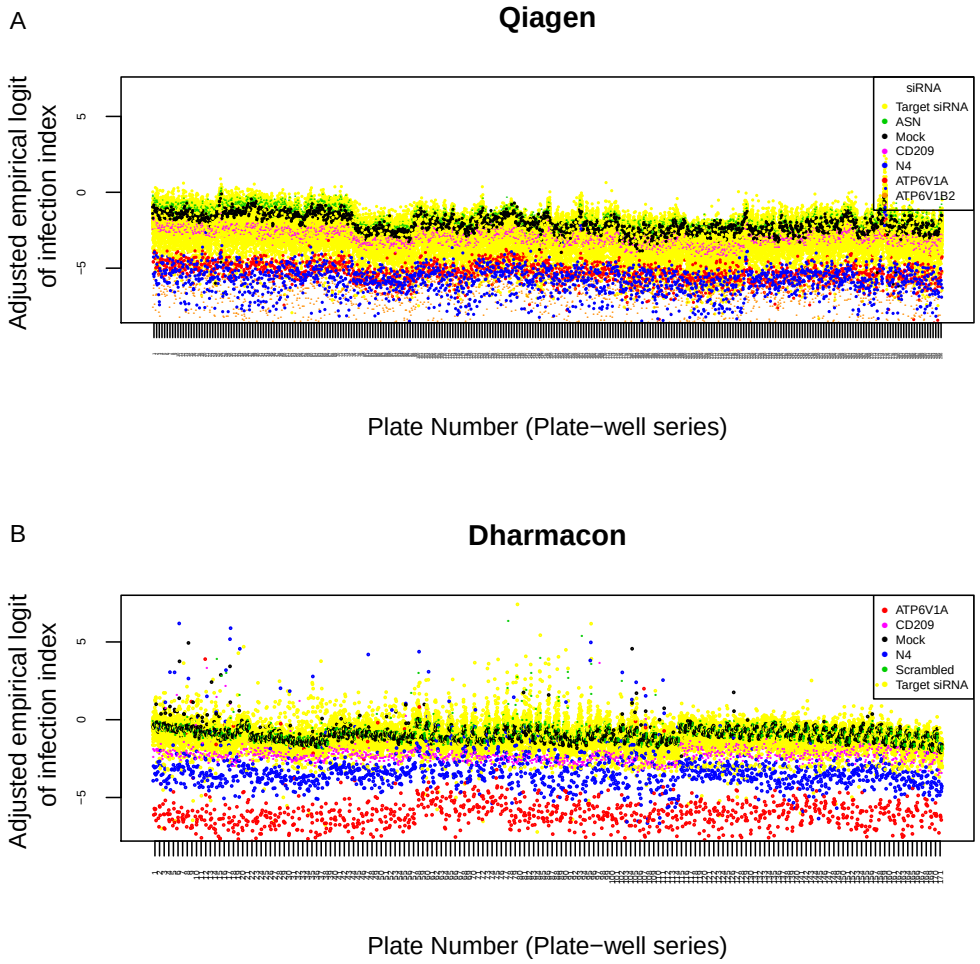

Figure 2.4 Plate-well series plots show efficacy of positive controls. The values of the x-axis is the index of the position of a well in a plate, whereas the labels in the x-axis are the plate numbers. A) Controls of the Qiagen screen. B) Controls of the Dharmacon screen. Negative controls are ASN (AllStarsNegative) and scrambled siRNA and mock wells (no siRNAs). Positive controls are siRNAs against ATP6V1A, ATP6V1B, CD209, and N4 (targeting vacuolar proton pump catalytic subunit A, B, the UUKV receptor DC-SIGN, and the viral nucleoprotein N, respectively). "Empirical logit of infection index values 0.5, 0, -0.5, -1, -1.5, -2 and -5 correspond to 62%, 50%, 38%, 27%,18%, 12%, and 0.7% infection, respectively.

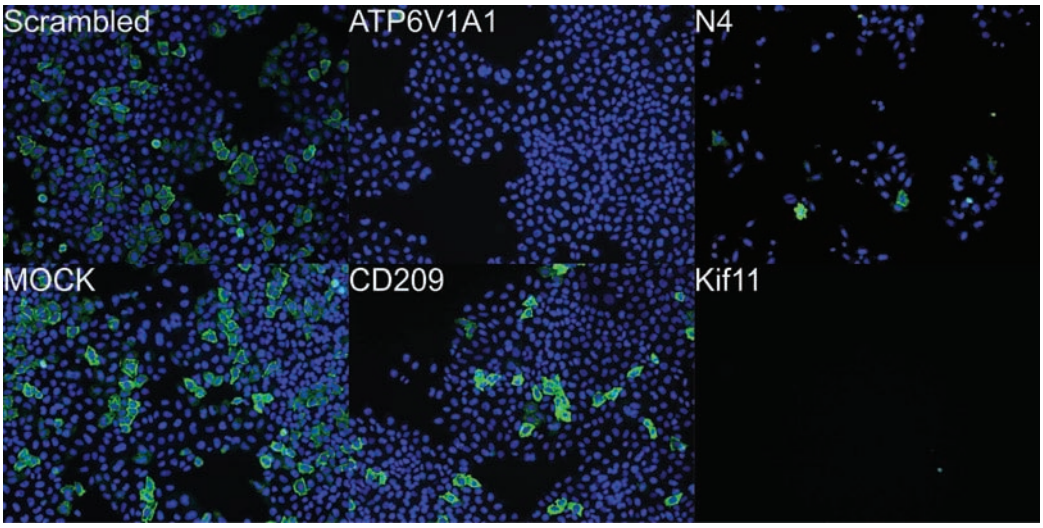

Figure 2.5 Microscopy images of expected Dharmacon control siRNAs effects on UUKV virus infection or cell viability after successful siRNA transfection of cells. The siRNAs against ATP6V1A, DC-SIGN (CD209), and the viral nucleoprotein N (N4) served as positive controls for infection. The siRNA against Kif11 served as positive control for cell death.

2.1.4.4 Up-to-date annotation of Qiagen and Dharmacon siRNA library

As there are still ongoing changes in the nomenclature of the human genome, we performed an up-to-date annotation of the genome-wide libraries. The annotation was performed based on the gene information release from November 2012 by the National Center for Biotechnology Information (NCBI). The up-to-date annotation allows to compare the results revealed by the screens on the same annotation. In addition, Qiagen provides an up-to-date annotation for purchased siRNAs. The annotation revealed that 20% of the siRNAs were designed to target genes, for which an annotation was not longer available. These siRNAs were not taken into account for any further analysis. In addition, 40% of siRNAs were annotated to possess potential off-target effects. Similar findings has been reported by Horn et al. [138].

2.1.5 Hit Selection and Bioinformatic Analysis

2.1.5.1 Preliminary Hit Selection

Plates that passed the quality control were processed to obtain a quantitative scoring that allowed ranking genes according to impact on UUKV infection upon gene depletion. For the Qiagen screen, we applied a statistical method

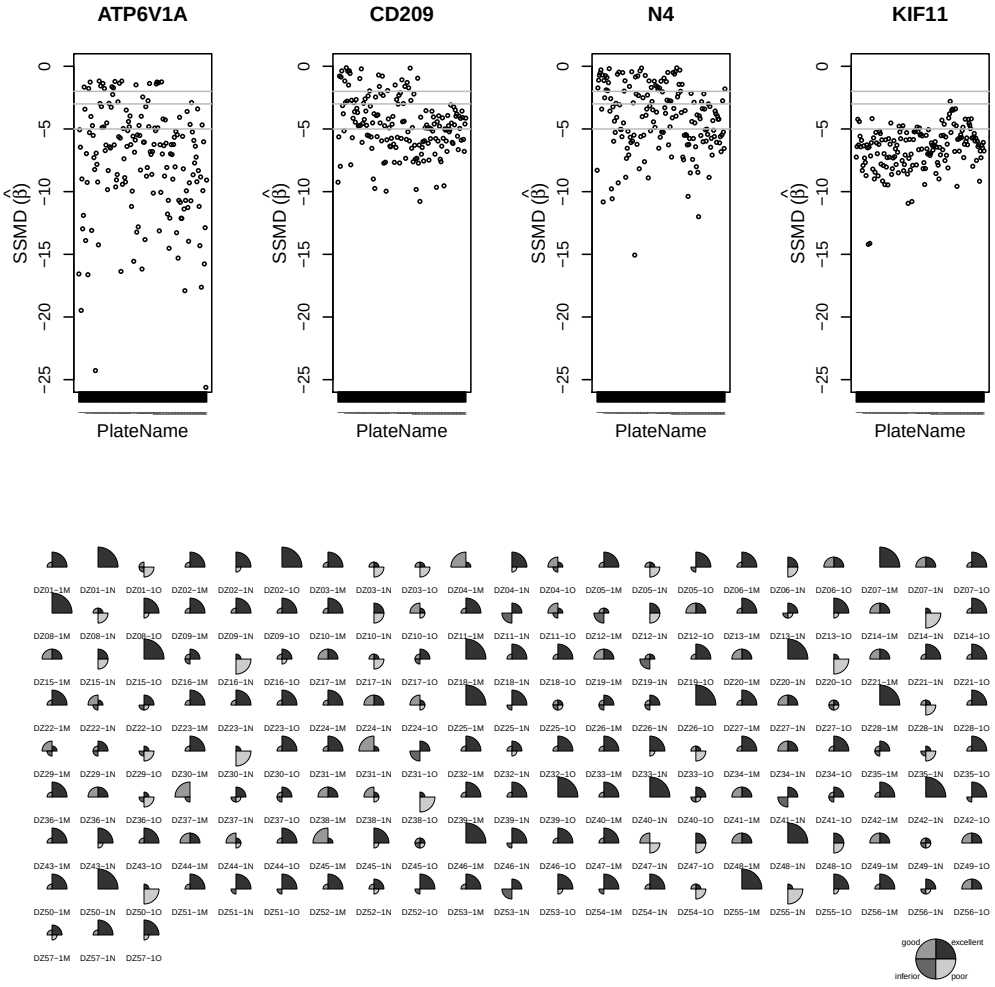

Figure 2.6 Qualtiy assessment of Dharmacon screen A) Quality assessment of within-plate positive siRNA controls based on the strictly standardized means difference (SSMD) cut-off criteria for "very strong controls". Gray lines show $\hat{\beta}$ cutoff values -5, -3, and -2 indicating excellent ($\hat{\beta} \leq$ -5), good (-5 $< \hat{\beta} \leq$ -3), inferior (-3 $< \hat{\beta} \leq$ -2) and poor ($\hat{\beta} >$ -2) quality. B) Star plots indicate single plate quality by summarizing determined SSMD based quality of the four different within-plate positive controls. The letter codes specify single plates. Segmented areas of a star show the amount of positive siRNA controls classified as excellent, good, inferior, or poor.

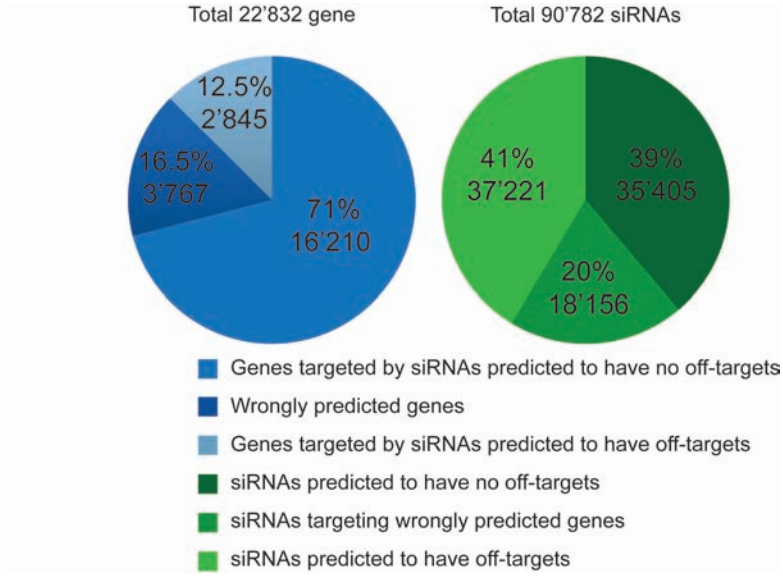

Figure 2.7 Up-to-date-annotation of Qiagen library 2010 The Qiagen library was newly annotated by the vendor 2010. Initially the library contained 22'832 gens and each gene was targeted by 4 different siRNAs. The up-date of the annotation revealed that 39% of all siRNAs may have no off-target and target 71% of all genes. In addition, 41% of all siRNAs are predicted to have off-targets and target 12.5% off all genes. Furthermore, 16.5% off all genes were identified as wrong predicted genes. These genes were targeted by 20% of all siRNAs. Thus these siRNAs have no on-targets anymore. In addition, the changes in the annotation lead to the fact that there were less than 4 siRNAs per gene and 40% of siRNAs may have off-targets.

called "redundant siRNA activity" (RSA). RSA is based on an iterative hypergeometric distribution formula. It examines the rank distribution of all siRNAs targeting the same gene and assigns p-values (see table 1.5) [152]. We ranked the siRNAs according their median absolute deviation (MAD) from the non-targeting controls within a plate. In doing so, we accounted for the plate-to-plate variability. For preliminary hit determination, we applied an arbritary p-value threshold of 0.01 for inhibitor effects and a p-value threshold of 0.001 for enhancer effects. These thresholds led to 461 inhibitor and 60 enhancer hits for the Qiagen screen. The different p-value thresholds were chosen because the siRNA effects on UUKV infection were not normally distributed. Most of the siRNA showed a reduction effect on UUKV infection compared to non-targeting control.

For the Dharmacon screen, we used the SSMD method combined with a fold change approach (see table 1.5) [153]. Since the Dharmacon screen was performed in triplicates, we were able to take into account the inter-replicate variability as an additional quality criterion for each siRNA. SSMD

values could indicate siRNAs to have a strong effect, although the mean fold changes are small - these values might be biologically irrelevant and, hence, result in a false-positive hit. To avoid such errors, we combined the SSMD approach with the fold change method. We used SSMD cutoffs of -3 for inhibitor hits and +2 for enhancers together with corresponding fold change threshold of 0.5 and 1.5. As a result, 256 genes inhibited UUKV infection and were classified as preliminary inhibitor hits, while 38 genes were classified as preliminary enhancers of infection.

Comparing both preliminary hit lists revealed 19 hits that were shared and inhibited UUKV infection (7% of Dharmacon inhibitory hits, 4% of Qiagen inhibitory hits, p-value = 8.815e-05). Furthermore it revealed 2 shared hits that enhanced UUKV infection (5% of Dharmacon enhancer hits, 3% of Qiagen inhibitory hits, p-value = 0.007). Although the number of common hits were significant, the number of common genes was modest. We suggested that this may be due to false-positive hits caused by siRNA off-target effects and false-negative hits caused by poor depletion or toxicity.

2.1.5.2 Off-target Analysis

Transcriptome Correction Identified 30% of Preliminary Hits as False-positives

Many siRNA screens of virus infection published so far have suffered from weak comparability of their hit lists [3, 4]. The discrepancies have mostly been explained with differences in the screening assays, protocols, and hit definition procedures. For example, different cell lines and reverse transfection incubation time has been used. However, since different siRNA libraries were used, siRNA off-targets that enhance false-positive hits might also play an important role.

To minimize false-positive hits, that are based on off-target mRNA silencing, we compared predicted siRNA targets with the transcriptome of HeLa-DC-SIGN cells that we used in the screens. Messenger RNAs (mRNAs) that are not expressed were removed from the preliminary defined hits.

To compare mRNAs of preliminary hits with the transcriptome of HeLa-DC-SIGN cells, we first acquired the total mRNA by a microarray approach using Agilent Humane Gene Expression 8x60k chips (Functional Genomics Center Zurich (fgcz)). Total mRNA was isolated from HeLa-DC-SIGN cells using TRIZOL reagent according to the manufacture's protocol followed by DNAse digestions and two purification steps using Qiagen RNeasy Mini Kit. Integrity, purity and concentration of mRNA was assessed by Nano Drop 1000 Spectrophotometer (Thermo Scientific) and by Agilent 2100 Bioana-

lyzer. Reverse transcription of total mRNA, labeling of cDNA, cDNA and DNA hybridization, scanning, and analysis was performed by the fgcz. Total mRNA of HeLa-DC-SIGN cells was acquired four times independently.

In total, 13'421 transcripts were detected. Both preliminary screening hit lists were then compared with the transcriptome. In the Qiagen screen 178 (32%) of the preliminary inhibitor hits and 21 (35%) of the preliminary enhancer hits were identified as non-expressed genes, hence as false-positives. In the Dharmacon screen 74 (29%) and 11 (30%), respectively. These false-positive hits were eliminated from the preliminary hits. Thus transcriptome corrected hit lists were obtained for Qiagen and Dharmacon screens consisting of 313 inhibitor and 39 enhancer hits and 182 inhibitor and 26 enhancer hits, respectively (see figure 2.8).

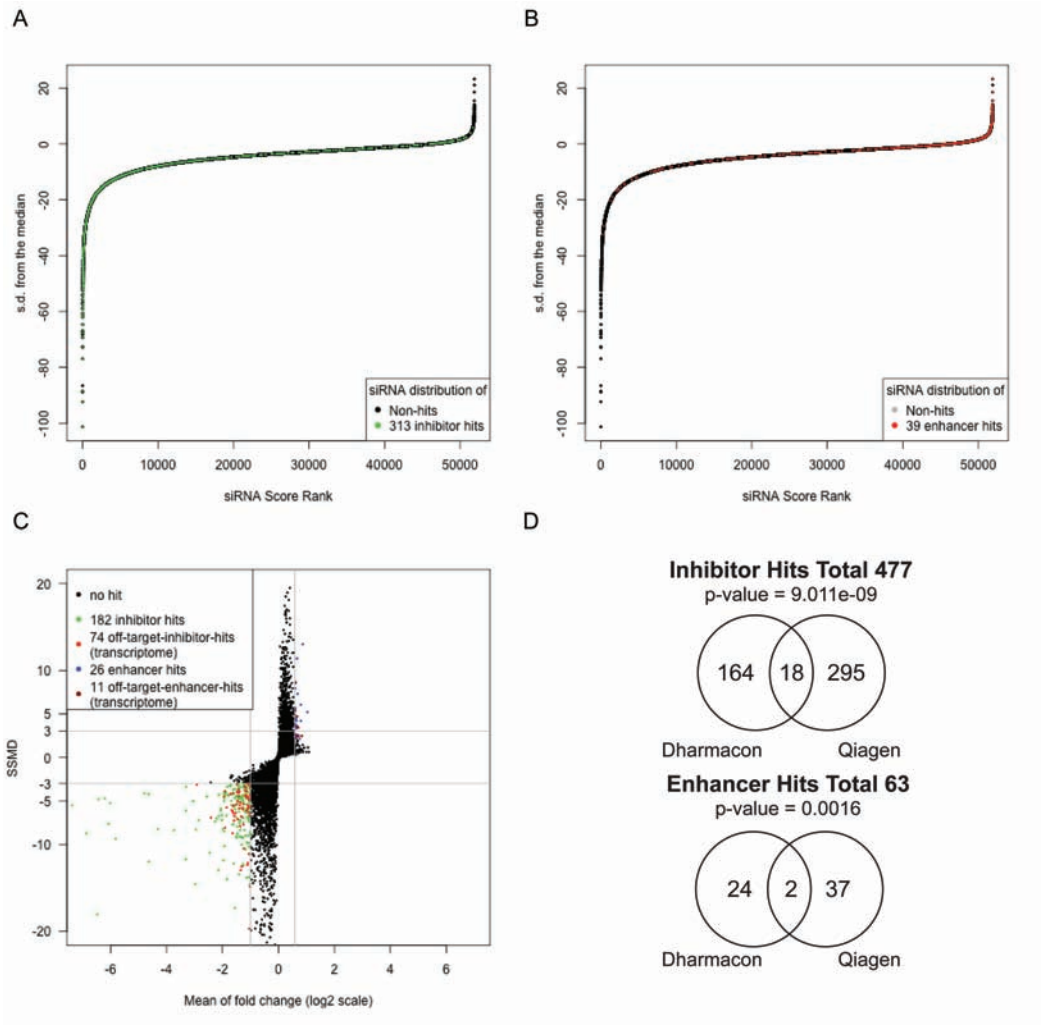

Figure 2.8 Hit selection in Qiagen and Dharmacon screens. A) The distribution of selected Qiagen siRNA inhibitor hits is plotted as a function of standard deviation (s.d.) from the median of the adjusted logit transformed infection indices of the non-targeting siRNA controls. Hits are defined to have a RSA p-values < 0.01. B) Likewise in A but for enhancer hits. Hits are defined to have a RSA p-values < 0.001. C) Dual flash plot for Dharmacon siRNA showing selected hits based on SSMD criteria and fold change. Inhibitor and enhancer hits are defined by SSMD values $<$ -3 and > 2, and a fold change < 0.5 and >1.5, respectively (indicated by the gray horizontal lines). D) Overlaps between Dharmacon and Qiagen inhibitor or enhancer hits. P-values of fisher-exact test are shown.

Off-target Identification by siRNA Seed Region Analysis

It has been shown that siRNAs can interfere with mRNAs in a microRNA like manner (see section 1.4.3.2 and figure 1.4) [135, 136].

To investigate if siRNAs in our screens acted like microRNAs (miRNAs)

and thereby inhibited UUKV infection, we classified all siRNAs of the Qiagen and Dharmacon screens according to their antisense 7 nucleotide (nt) long seed region (nucleotide position 2 to 8 at 5' end). In total, 9'541 different seed classes were observed in the Qiagen screen, 11'890 in the Dharmacon screen (see figure 2.9 and supplementary figure 5.6).

Seeds of seed classes consisting of ≥ 3 different siRNAs were analyzed for their effect on UUKV infection. The analysis was performed using the SSMD method combined with the fold change approach. We found that several seeds inhibited or enhanced the virus infection. In the Qiagen screen 644 seeds showed a "very strong" or "extremely strong" inhibition effect on UUKV infection; one seed showed an "extremely" strong enhancement effect (see figure 2.9). To identify how many of these 644 seeds are present in the "hit siRNAs" (in total 923) targeting the 313 Qiagen inhibitor hits, we compared the 644 seeds with the seeds of the "hit siRNAs". We revealed 181 "hit siRNAs" (20%) to possess such seeds. Of the inhibitor hits, 50% were targeted by at least one siRNA, that may impact UUKV infection either by depletion of its target mRNA and/or by off-target effects via its seed. On average a hit was targeted by three different siRNAs.

In the Dharmacon screen, 2 seeds were identified with a "very strong" inhibitory effect on UUKV infection reducing infection by 50%. Thus, in the Dharmacon screen there were much less seed classes identified to inhibit UUKV infection compared to the Qiagen screen, indicating that off-target effects via the siRNA seed were reduced.

2.1.5.3 Comparison of hit lists and bioinformatic analysis

By comparing transcriptome corrected hit lists of both screens we identified 18 shared inhibitor hits (10% of Dharmacon inhibitor hits, 6% of Qiagen inhibitor hits, p-value = 9.011e-09) and two overlapping enhancer hits (7% of Dharmacon enhancer hits, 5% of Qiagen enhancer hits, p-value = 0.0016, see figure 2.8 and supplementary table 5.1). In contrast, when comparing the non-expressed preliminary hits no overlapping inhibitor hits and one overlapping enhancer hit (p-value = 0.48) was identified (data not shown).

The expressed inhibitor hits from both screens were combined to a final hit list consisting of 477 cellular host factors required for UUKV infection (see figure 2.8). Bioinformatic analysis using the open source softwares Reactome, and STRING revealed 12 functional pathways such as endosomal acidification, that are essential for UUKV infection (see table 2.1 and figure 2.10).

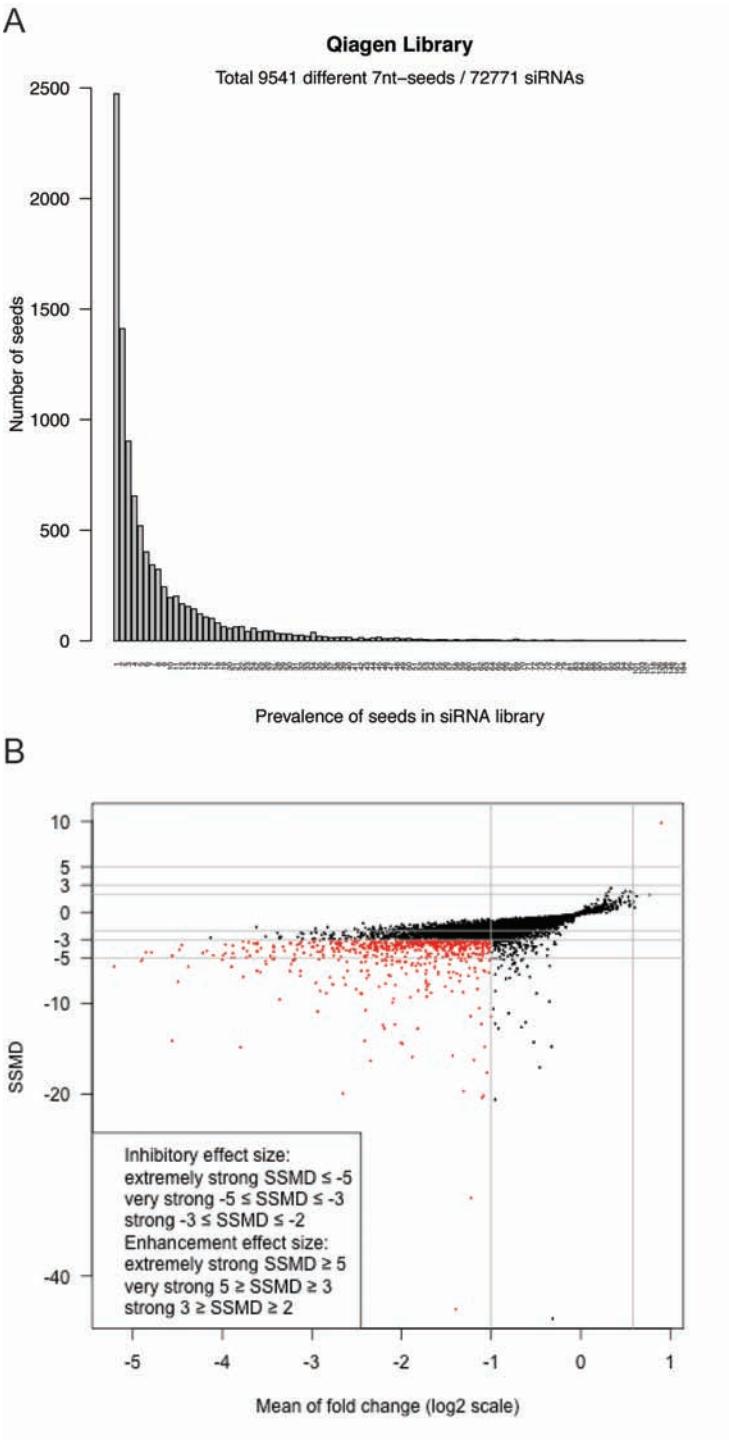

Figure 2.9 Prevalence of 7nt-seeds in Qiagen siRNA library and their effects on UUKV infection. A) 9'541 different 7nt-seeds were identified. 2'473 seeds were present in one siRNA. Remaining seeds were shared by minimal 2 up to maximal 184 siRNAs. B) Effect size on UUKV infection was calculated for all those seeds that were shared by at least 3 different siRNAs (totaly 5658 seeds). To calculate effect size, the SSMD method combined with fold change approach was used. 644 seeds showed a "very strong" or "extremely strong" inhibition effect on UUKV infection with a fold change $\leq$ 0.5 (-1 on log 2 scale). One seed showed an "extremely" strong enhancement effect with a fold change $\geq$ 1.5 (0.58 on log2 scale). Seeds that showed a "very strong" or an "extremely strong" effect are indicated in the figure by red dots.

Table 2.1 Overrepresentation analysis of cellular events for screening hits using Reactome

Name of event	P-value	Total number of hits	Number of D/Q hits	Overlapped hits	Total genes involved in this event	Gene symbol of hits
Endosome acidification	6.07E-17	14	12/10	8	23	ATP6V1H, ATP6V1E1, **ATP6V0D1**, ATP6V0A4, **ATP6V0B**, **ATP6V1D**, ATP6V1C1, ATP6V1F, ATP6V0A1, **ATP6V1B2**, **ATP6V1G1**, **ATP6V0C**, **ATP6V0E1**, **ATP6V1A**
Phagosome maturation (early endosomal stage)	2.10E-14	15	13/10	8	38	ATP6V1H, ATP6V1E1, CYBB, **ATP6V0D1**, ATP6V0A4, **ATP6V0B**, **ATP6V1D**, ATP6V1C1, ATP6V1F, ATP6V0A1, **ATP6V1B2**, **ATP6V1G1**, **ATP6V0C**, **ATP6V0E1**, **ATP6V1A**
Iron uptake and transport	3.33E-14	15	12/11	8	39	ATP6V1H, ATP6V1E1, **ATP6V0D1**, ATP6V0A4, **ATP6V0B**, **ATP6V1D**, ATP6V1C1, FLVCR1, ATP6V1F, ATP6V0A1, **ATP6V1B2**, **ATP6V1G1**, **ATP6V0C**, **ATP6V0E1**, **ATP6V1A**
Latent infection of Homo sapiens with Mycobacterium tuberculosis	2.91E-10	15	13/10	8	68	ATP6V1H, ATP6V1E1, CYBB, **ATP6V0D1**, ATP6V0A4, **ATP6V0B**, **ATP6V1D**, ATP6V1C1, ATP6V1F, ATP6V0A1, **ATP6V1B2**, **ATP6V1G1**, **ATP6V0C**, **ATP6V0E1**, **ATP6V1A**
Signaling by Insulin receptor	2.48E-07	15	13/10	8	109	ATP6V1H, ATP6V1E1, **ATP6V0D1**, ATP6V0A4, **ATP6V0B**, **ATP6V1D**, ATP6V1C1, EIF4E, ATP6V1F, ATP6V0A1, **ATP6V1B2**, **ATP6V1G1**, **ATP6V0C**, **ATP6V0E1**, **ATP6V1A**
Transmembrane transport of small molecules	3.13E-04	25	16/17	8	432	ATP6V1H, ATP6V1E1, RANBP2, SLC22A8, ATP6V1C1, NUP155, ATP2A2, FLVCR1, APOA1, ATP7B, **ATP6V1B2**, **ATP6V1G1**, **ATP6V1A**, **ATP6V0C**, **ATP6V0E1**, SLC6A6, ATP6V0A4, **ATP6V0D1**, **ATP6V0B**, **ATP6V1D**, SLC4A2, PEX19, ATP6V0A1, ATP6V1F, SLC39A7
Unfolded Protein Response	3.85E-04	8	3/6	1	65	ARFGAP1, **ATP6V0D1**, HSPA5, WIPI1, CCL2, ASNS, MBTPS2, ATF6

Continued on next page

Table 2.1 Reactome overrepresentation analysis – Continued from previous page

Name of event	P-value	Total number of hits	Number of D/Q hits	Number of intersected hits	Total genes involved in this event	Gene symbol of hits
Dissociation of ATF6-alpha:BiP Complex	7.61E-04	2	0/2	0	2	HSPA5, ATF6
Cleavage of ATF6-alpha by S2P	7.61E-04	2	0/2	0	2	MBTPS2, ATF6
Activation of Chaperones by ATF6-alpha	1.05E-03	3	0/3	0	8	HSPA5, MBTPS2, ATF6
Metabolism of proteins	1.85E-03	24	11/15	2	461	RPS15A, GPAA1, **RPS25**, PFDN5, SUMF2, EDEM3, EIF2B5, EIF4E, DOLK, EIF3D, TIMM13, TBCA, CHCHD4, EIF3J, EIF2B2, ATP5G1, ATP6AP2, SRP54, **EEF2**, SEC61G, MUC13, PIGT, GRPEL1, PIGQ
Mitochondrial tRNA aminoacylation	2.34E-03	4	1/3	0	21	HARS2, PARS2, QARS, KARS
PERK regulated gene expression	2.92E-03	3	0/3	0	11	ASNS, HSPA5, CCL2
Polo-like kinase mediated events	4.40E-03	2	0/2	0	4	WEE1, PKMYT1
Phosphorylation of MOB1A and B by p-STK3 / p-STK4	4.40E-03	2	1/1	0	4	SAV1, MOB1A
RNA Polymerase I, RNA Polymerase III, and Mitochondrial Transcription	5.51E-03	6	1/5	0	59	POLR3A, GTF3C5, GTF2H4, ERCC2, GTF3C4, KAT2B
tRNA Aminoacylation	5.69E-03	5	1/4	0	42	VARS, HARS2, PARS2, QARS, KARS
Binding of TFIIIC to Type 2 promoter	7.20E-03	2	0/2	0	5	GTF3C5, GTF3C4
Competitive inhibition of translation initiation by ISGylated 4EHP	7.41E-03	3	3/0	0	15	ISG15, EIF4E, EIF4G2
Diabetes pathways	7.56E-03	9	3/6	1	125	ARFGAP1, **ATP6V0D1**, HSPA5, WIPI1, CCL2, ASNS, MBTPS2, EXOC4, ATF6
Translation	8.83E-03	11	2/9	2	151	RPS15A, EIF2B2, **RPS25**, SRP54, **EEF2**, EIF2B5, SEC61G, EIF4E, EIF3D, EIF3J

Abbreviations: D, Dharmacon Screen; Q, Qiagen Screen
Notes: 270 hits were not mapped to Reactome events. Intersected hits are indicated in bold in column "Gene symbol of hits". P-values show un-adjusted probability from hypergeomteric test of seeing given number or more genes in this event by chance.

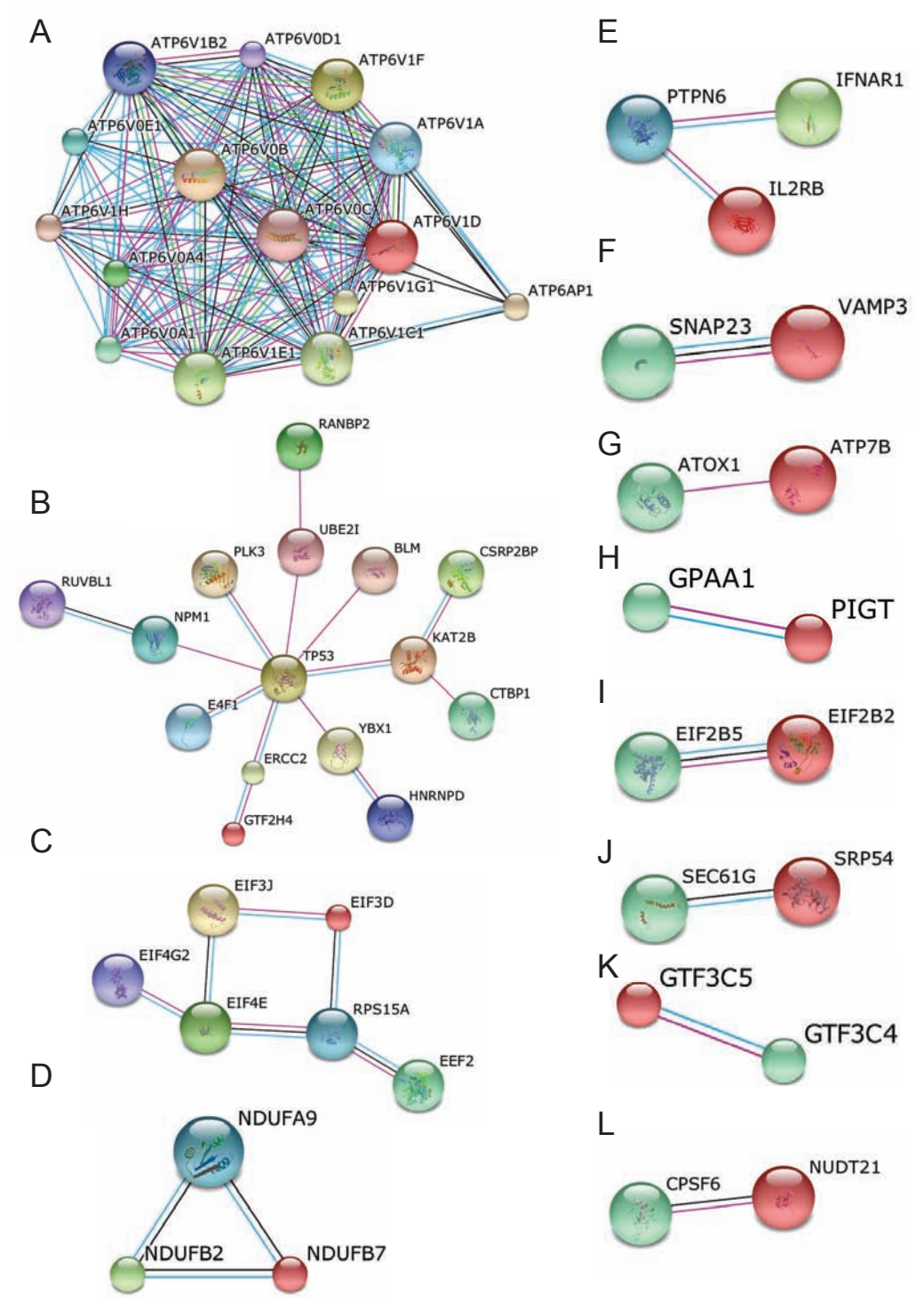

Figure 2.10 Protein-protein interaction analysis using open-source software STRING. STRING analysis revealed 12 protein interaction clusters. A) Endosomal acidification cluster; B) Growth arrest cluster; C) Translation initiation cluster; D) Multisubunit NHAD:ubiquinone oxidoreductase complex1 cluster; E) Interferon - interleukin cluster; F) SNARE cluster; G) Cooper homeostasis cluster; H) Glycosylphosphatidylinositol (GPI)-anchor cluster; I) Translation initiation cluster; J) Protein transport into endoplasmic reticulum (ER) cluster; K) General transcription factor cluster; L) Cleavage and polyadenylation specific factor cluster. Totally 455 proteins of the uploaded 477 hits were recognized by STRING software and revealed 581 protein-protein interactions (settings: highest confidence 0.9; active prediction methods: neighborhood, gene fusion, co-occurrence, co-expression, experiments, database)

2.2 Verification and Characterization of Hits

2.2.1 Verification of Seed-Effects

To verify the observed results, that siRNAs can affect UUKV infection via their 7nt-seed region, we performed UUKV infection experiments in presence of mimic miRNAs (miRs). We selected miRs according to their predicted siRNA seed inhibition effects on UUKV infection. We selected four miRs predicted to have an "extremely strong" inhibition effect (fold changes ranging from 0.05 to 0.09), two miRs for which the seeds showed a "very strong" inhibition effect (fold changes 0.14 and 0.5), five miRs for which the inhibition effect was classified as "strong" (fold changes ranging from 0.2 to 0.55), and three miRs that showed "weak", "very weak", or "extremely weak" inhibition effect (fold changes 0.63, 0.93, 1.1). In addition a miR for which a "very weak" enhancement effect was predicted (fold change 1.3) was selected. MiRs were kindly provided by Prof. Dr. D. Gerlich.

In HeLa-DC-SIGN cells all miRs predicted to have an "extremely strong" or "very strong" effect (miR-124-3p,miR-506-3p,miR-142-3p, miR-1226-5p, miR-921, and miR-518e-5p) inhibited UUKV infection of at least 65% (max. 95%) compared to control siRNA (ASN). The miR-518e-5p did not reduce infection. MiRs for which a "strong" decrease was predicted (miR-1303, miR-885-5p, miR-651, miR-369-3p, and miR513a-3p) inhibited UUKV infection at least 40%, except miR-513a-3p and miR-885-5p which showed a decrease of 30% and 20%. MiRs that were predicted to have a "weak", "very weak", or "extremely weak" inhibition effect (miR-758-3p, miR-20b-5p, and miR-647) did not show any significant decrease. The miR-409-3p predicted to have a weak enhancement effect, did not affect UUKV infection (see figure 2.11).

Taken together, predicted siRNA seed-effects on UUKV infection were accurate and confirmed by infection experiments in cells treated with miRs.

In A549 cells similar inhibition was observed for following miRs: miR-142-3-p, miR-1226, miR-921, and miR-1303 (inhibition range between 50% to 80%; see supplementary figure 5.7) indicating that the observed inhibition effects on UUKV infection in HeLa-DC-SIGN cells was not cell specific and was not linked to DC-SIGN, as A549N did not express DC-SIGN.

To examine if verified miR candidates (miR-1226-5p, miR-124-3p, miR-1303, miR-142-3p, miR-506-3p, and miR-921) inhibited a pre-fusion event, fusion of UUKV or a post-fusion event, endocytosis bypass experiments were performed in HeLa-DC-SIGN cells. UUKV particles bound in the cold to the cell surface were fused with the plasma membrane by treatment with acidic medium for 1 min 30 s. This allowed the virus to release the genome directly into the host cell cytosol, without passing through endocytotic vesicles. If

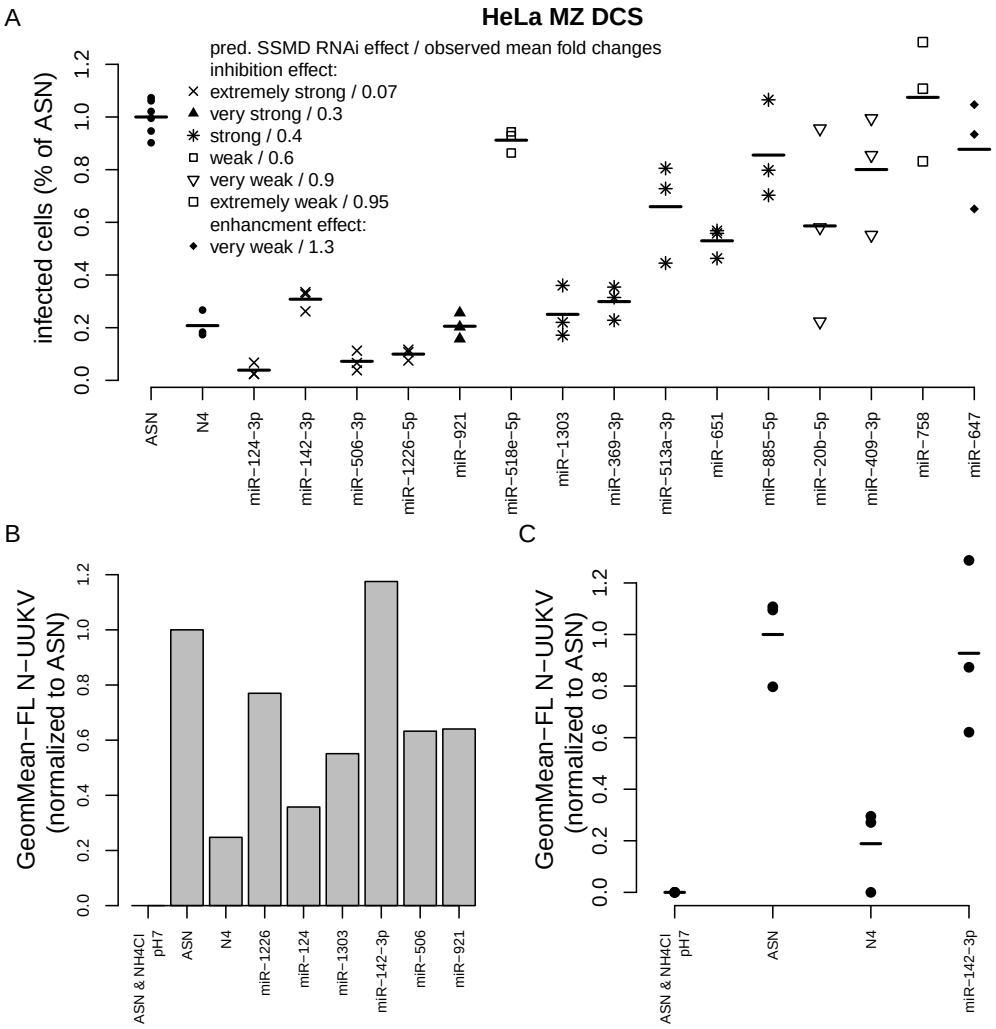

Figure 2.11 Mimic miRNAs (miRs) inhibit UUKV infection at post-fusion or pre-fusion/fusion event. A) We selected miRs according to predicted SSMD seed-effects and their fold change (see figure legend) and investigated their effect on UUKV infection. Cells were treated with miRs, with ASN, or with siRNA N4. Then, cells were infected with UUKV (moi 5), fixed, stained against the virus nucleoprotein N and analyzed using flow cytometry. All miRs predicted to have an "extremely strong" or a "very strong" effect, revealed expected results, except miR-518e-5p that did not affecte UUKV infection. B) Mimic miRNA-142-3p (miR-142-3p) regulates UUKV endocytosis. HeLa-DC-SIGN cells were treated with miRs shown to inhibit UUKV infection, ASN, or N4. Then, UUKV (moi 0.5) was bound to cells on ice in the presence of medium containing NH_4Cl (M-NH_4Cl) for 1 h, washed and exposed to acidic medium (pH 5) or neutral M-NH_4Cl at 37 °C for 1 min 30 s. Then, cells were immediately washed with neutral M-NH_4Cl and further incubated at 37 °C in presence of M-NH_4Cl. For all but inhibiting miR-142-3p, acid bypass did not rescue infection indicating that a post-fusion step is affected. Experiment was performed once. C) Same as for B, except that cells were only transfected with miR-142-3-p, ASN, or N4 and that the experiment was performed in independent triplicate. The inhibitory effect of miR-142-3p was rescued by acid mediated fusion indicating that a pre-fusion event or the fusion step was affected. Thus results confirmed observed results in B. All experiments were performed in HeLa-DC-SIGN cells. ASN serves as negative control siRNA. N4 serves as a positive control siRNA, targeting the nucleoprotein (N) of UUKV. Used concentration for transfection of siRNAs or miRs was 20 nM. Cells were treated with siRNAs or miRs for 72 h before UUKV infection or UUKV binding. Incubation time of UUKV infected cells was 8 h.

infection is blocked at the level of pre-fusion or fusion such an acid-mediated bypass should rescue infection. We identified that the inhibitory effect of miR-142-3p was rescued by acid fusion indicating that a pre-fusion event or the fusion step was affected (see figure 2.11).

Taken together, we found that siRNAs likely acted like miRNAs inhibiting UUKV infection in the screens. All tested miRs inhibited UUKV infection in HeLa-DC-SIGN cells at post-fusion events, except miR-142-3p that inhibited UUKV endocytosis. As miR-142-3p also inhibited UKKV infection in A549N cells that do not express DC-SIGN, we suggest that fusion or a pre-fusion event is affected by the miR-142-3p, but not the endocytotic uptake via DC-SIGN.

2.3 miR-142-3p Regulates UUKV Endocytosis

Critical steps during UUKV infection upstream of fusion comprise cellular receptor expression, virus-receptor binding, internalization, intracellular trafficking, and acidification. To characterize whether one of these early entry steps was miR-142-3p dependent, we measured the level of DC-SIGN surface-expression and performed UUKV binding and internalization experiments in HeLa-DC-SIGN cells treated with miR-142-3p. Neither DC-SIGN surface expression, nor UUKV binding or internalization was affected by miR-142-3p (see 2.12).

To measure how many internalized particles finally fuse with interior vesicle membranes we took advantage of the quenching properties of the lipophilic fluorophore octadecyl rhodamine B chloride (R18) [154].

We labeled UUKV particles with R18 in self-quenching concentrations, and bound them to HeLa-DC-SIGN cells treated with miR-142-3p or ASN at 4 °C. While the virus internalized upon warming, we continuously measured the R18 fluorescence in a spectrofluorometer. The fusion event dilutes R18 into the vesicle membrane, thus lowering its self-quenching effect and causing an increase in fluorescence over time.

Figure 2.12 shows the R18 fluorescence in the presence of miR-142-3p, ASN, as a negative control for not inhibition of fusion, or ASN and ammonium chloride (NH_4Cl), as a positive control for inhibition of fusion. NH_4Cl prevents endosomal acidification. Thus ASN in presence of NH_4Cl serves as a positive control for inhibition of UUKV fusion. The fusion step was strongly reduced over time in miRNA-transfected cells compared to the negative control (70% at 40 min post-internalization).

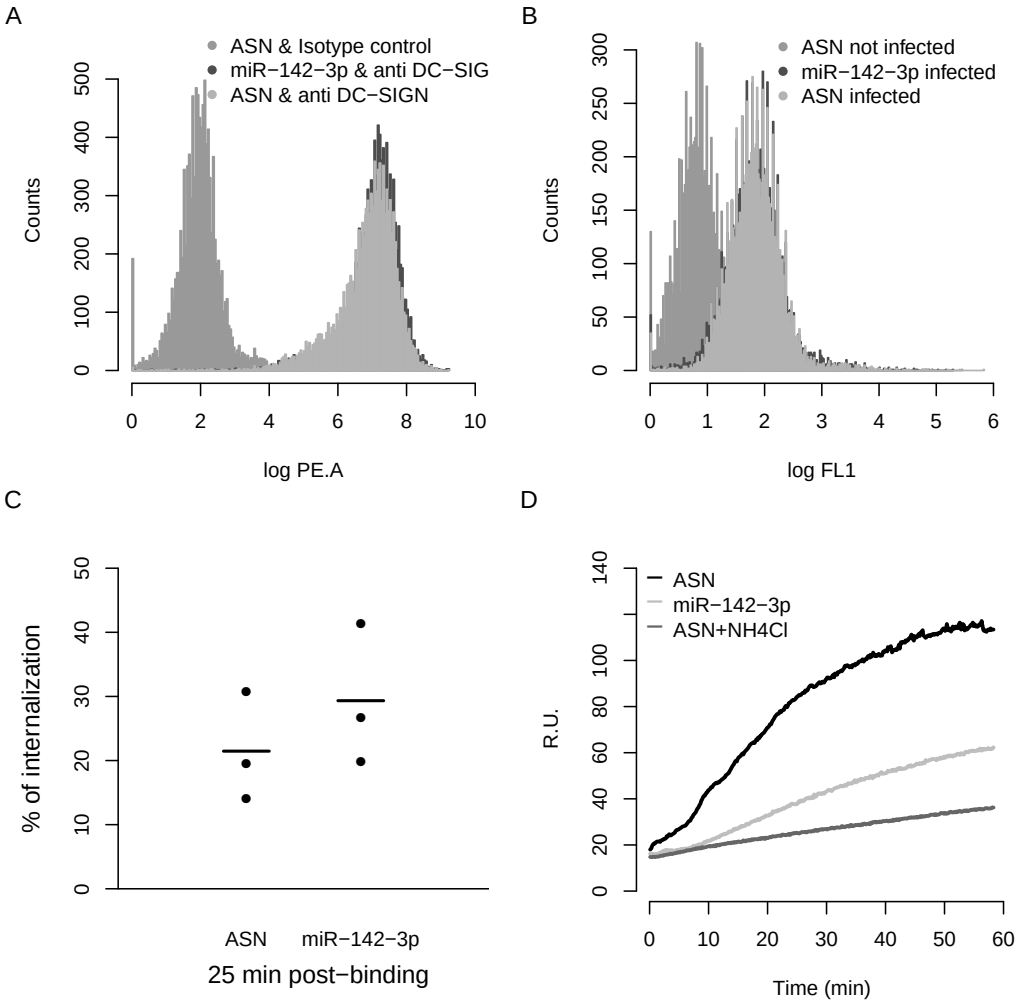

Figure 2.12 miR142-3p affect UUKV fusion or a late-entry step just before fusion. DC-SIGN surface expression (A), binding of UUKV (B), and internalization of UUKV (C) are not affected in cells treated with miRNA142.3p. For DC-SIGN surface expression experiments (exp.), cells were stained against the DC-SIGN with a Phycoerythricin (PE)-conjugated antibody (FAB1621P) on ice for 45 min, washed, fixed and analyzed. The isotype antibody IgG_{2A} was used as control. For binding and internalization exp., UUKV (moi 2), labeled to Alexa Fluor 488 (AF488) dye, was bound to cells on ice for 1 h, washed and either fixed and analyzed (for binding exp.), or shifted to 37 °C for 25 min, fixed and analyzed (for internalization exp.). Analysis of all three experiments were performed using flow cytometry. D) Fusion or pre-fusion of UUKV is inhibited in cells treated with miR142.3p. UUKV-R18 (moi 5) was bound to cells treated with miR-142-3p or ASN on ice for 45 min, washed, and analyzed by recording fusion kinetic using a fluorimeter at 37 °C for 45 min. Cells treated with ASN & NH_4Cl were used as fusion incompetent control. In all experiments HeLa-DC-SIGN cells were reverse transfected with 20 nM of miR-142-3p or negative siRNA control (ASN) for 72 h. The data in A), B), and D) are representatives of three independent exp. Figure C) and D) courtesy by Pierre-Yves Lozach

Together with the acid bypass results, this finding clearly indicated that miR-142-3p impairs fusion or a late-entry step just before fusion.

2.4 miR-142-3p Down-Regulates Screening Hit VAMP3

To investigate the impact of miR-142-3p on gene expression, the expression level of mRNA was monitored in HeLa DC-SIGN cells treated with miR-142-3p. The Agilent microarry approach was used as described before (see 2.1.5.2). We quantified the results using paired t-test and fold change approach. In addition false discovery rate (fdr) method for multiple comparisons correction was applied. Fdr controls the expected proportion of false-positives (see 1.4.3). To select hits, fold change and fdr thresholds of ≤ 0.5 and ≤ 0.01 were used for down-regulated genes and for up-regulated genes ≥ 1.5 and ≤ 0.01, respectively.

We obtained 112 down-regulated and 174 up-regulated genes in the presence of miR-142-3p compared with control (see figure 2.13). When we overlapped these down-regulated hits with the inhibitor hits from Qiagen and Dharmacon screens, VAMP3 (vesicle-associated membrane protein 3) remained. At less stringent conditions, if we overlapped with only one screen, we obtained in addition to VAMP3 also ATP2A2 (ATPase, Ca^{2+} transporting, cardiac muscle, slow twitch 2 [SERCA]) in case of the Dharmacon screen; in case of the Qiagen screen LHX1 (LIM homeobox 1), HSD3B7 (hydroxy-delta-5-steroid dehydrogenase, 3 beta- and steroid delta-isomerase 7), and MTL5 (metallothionein-like 5, testis-specific; see figure 2.13).

Taken together, five genes (VAMP3, SERCA, LHX1, HSD3B7, and MTL5) of the identified genes that were regulated by the miR-142-3p were present in the final hit list of the RNAi screens.

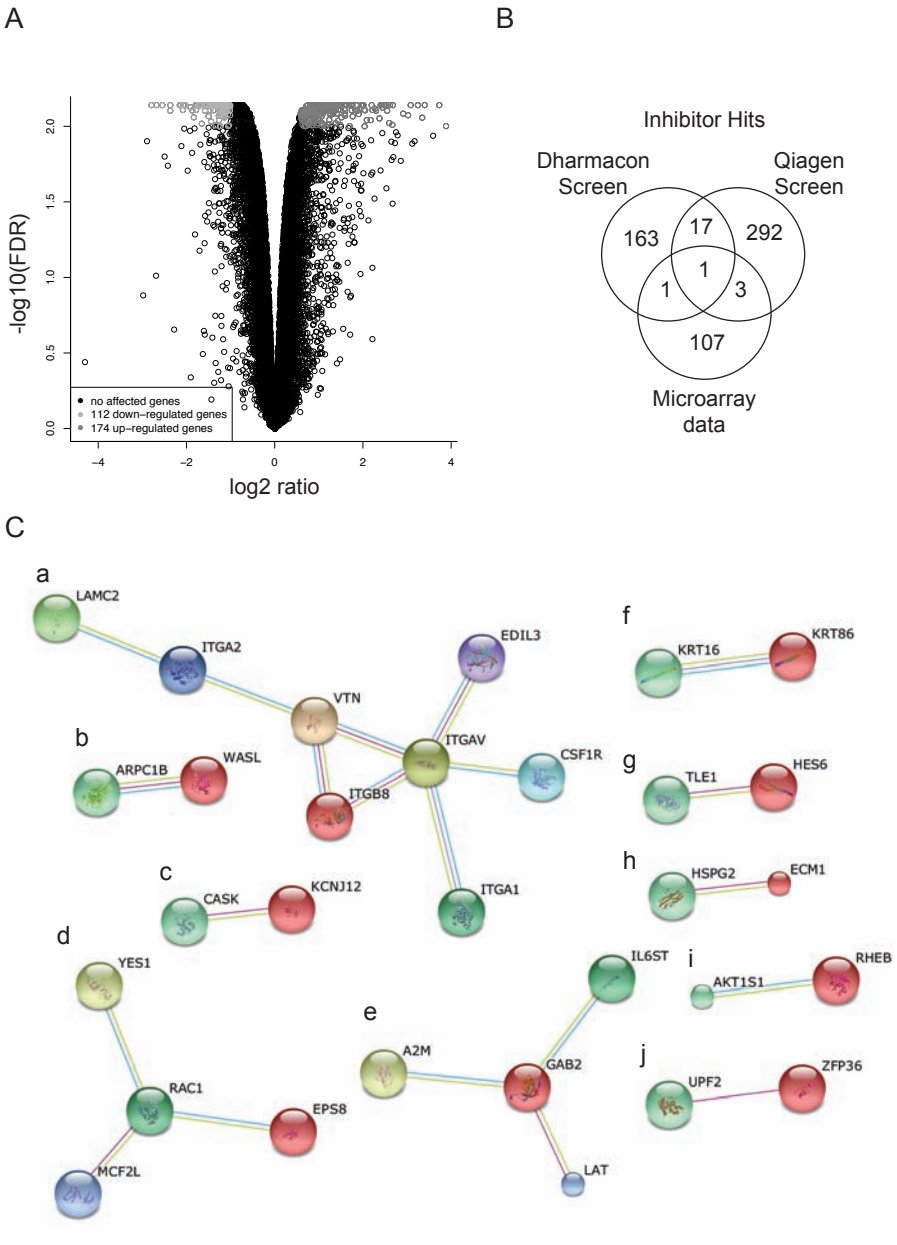

Figure 2.13 Microarray analysis of HeLa-DC-SIGN responses to miRNA142-3p transfection. A) Volcano plot displaying on the x-axis the different gene expression magnitudes in the log2 scale and on y-axis the negative log10 transformed false discovery rate (fdr) values. Gray points indicate top 292 up- and down-regulated genes. B) Overlapping of inhibitory hits from microarray data, Qiagen and Dharmacon genome-wide siRNA screens. The single three-list-overlap is VAMP3. C) Protein-protein interaction analysis using open source software STRING revealed 11 protein-protein interaction clusters: a) Integrin adhesion and signal transduction cluster; b) Actin related cluster; c) Ion channel related cluster; d) Cell growth and cytoskeleone reorganization cluster; e) Regulation of signaling pathways cluster; f) Keratin cluster; g) Transcription cluster; h) Extracellular matrix cluster; i) Cell growth cluster; j) mRNA surveillance cluster (used settings: highest confidence 0.9; active prediction methods: neighborhood, gene fusion, co-occurrence, co-expression, experiments, database, and text mining.)

2.5 VAMP3 Plays a Potential Role in UUKV Infection

VAMP3 was a stringent hit from the screening and microarray data. Its role in UUKV infection was further validated using diverse perturbation approaches. First, we verified that siRNAs against VAMP3 decreased infection under different virus loads. HeLa-DC-SIGN cells were treated with siRNA "VAMP3.1" and challenged with UUKV at moi 2 and moi 5. Flow cytometry analysis showed a decrease in the infection levels of 70% and 50%. In an analogue experiment with siRNA "VAMP3.4" infection was reduced by 85% and 60%, respectively (see figure 2.14).

VAMP3 is a SNARE component involved in vesicle fusion and is, together with VAMP1 and 2, sensitive to the protease activity of tetanus toxin [155]. To investigate if UUKV infection was inhibited in HeLa-DC-SIGN cells transiently expressing the catalytic light chain of tetanus toxin (TeTx), we challenged such cells with UUKV (moi 2). Results showed a significant decrease in UUKV infection of 40% (p-value = 0.013) relative to control (see figure 2.14).

No decrease of infection relative to control was observed in cells transiently expressing a VAMP3 soluble form (VAMP3-sol-eGFP), which is described as a dominant negative construct to endogenous VAMP3 (see figure 2.14, [156]). Also, overexpressing VAMP3-GFP did not affected UUKV infection (see figure 2.14).

To study if incoming UUKV colocalizes with VAMP3, cells were transfected with VAMP3-eGFP 20 h before Texas Red labeled UUKV (UUKV-TR) was bound to cells on ice for 30 min. Cells were then shifted to 37 °C, incubated for different time points (0, 2, 10, 20, an 40 min), fixed and imaged using confocal microscopy. UUKV-TR associated with VAMP3-eGFP containing vesicle and reached a maximum association 20 min after entry. Most of the VAMP3-eGFP containing vesicle, that associated with UUKV-TR after 20 min, were observed in the perinuclear region of the cytoplasm (see figure 2.15).

Taken together, reproducibility of the RNAi effects by flow cytometry, colocalization with UUKV, and sensitivity of the virus for TeTx clearly argue for an essential role of VAMP3 in UUKV infection. Overexpression of dominant negative VAMP3 (VAMP3-sol) may not be potent enough to inhibit endogenous VAMP3.

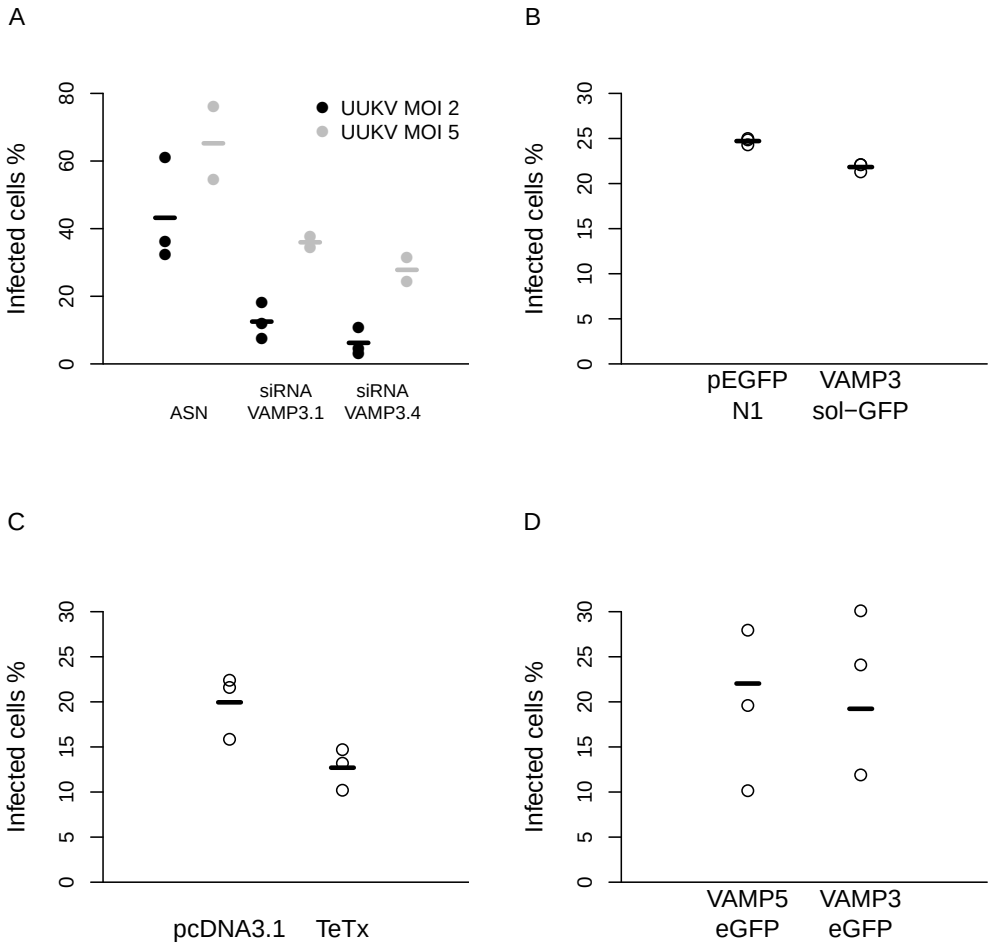

Figure 2.14 VAMP3 plays a potential role in UUKV infection A) Cells treated with 20 nM siRNAs targeting VAMP3 or control siRNA AllStarsNeg (ASN) were infected with UUKV (moi 2 or moi 5). Compared to the control cells, UUKV infection at moi 2 was blocked by 70% (siRNA VAMP3.1) and 85% (siRNA VAMP3.4), while infection at moi 5 was reduced by 45% (siRNA VAMP3.1) and 65% (siRNA VAMP3.4). B) Cells were transfected with empty pEGFP-N1 plasmid (control plasmid) or pEGFP-N1 plasmid expressing VAMP3-soluble-eGFP form (VAMP3-sol-eGFP), and infected with UUKV moi 2. No difference was observed relative to control. C) Cells were transfected with empty plasmid (pcDNA3.1, control) or pcDNA3.1 plasmid expressing the catalytic light chain of the tetanus toxin (TeTx). Compared to control cells, cells expressing TeTx showed a significant decrease in infection of 35% (p-value = 0.013). D) Cells were transfected with VAMP5-eGFP, which served as a negative control, or VAMP3-eGPF containing vector. No difference was observed between control cells and VAMP3-eGFP over-expressing cells. Transfections of plasmids were performed 20 h before infection using transfection reagent lipofectamine 2000 and 1µg of plasmids. To quantitate infection flow cytometry analysis was used in all experiments 8 h post-infection. Data are results of three independent experiments.

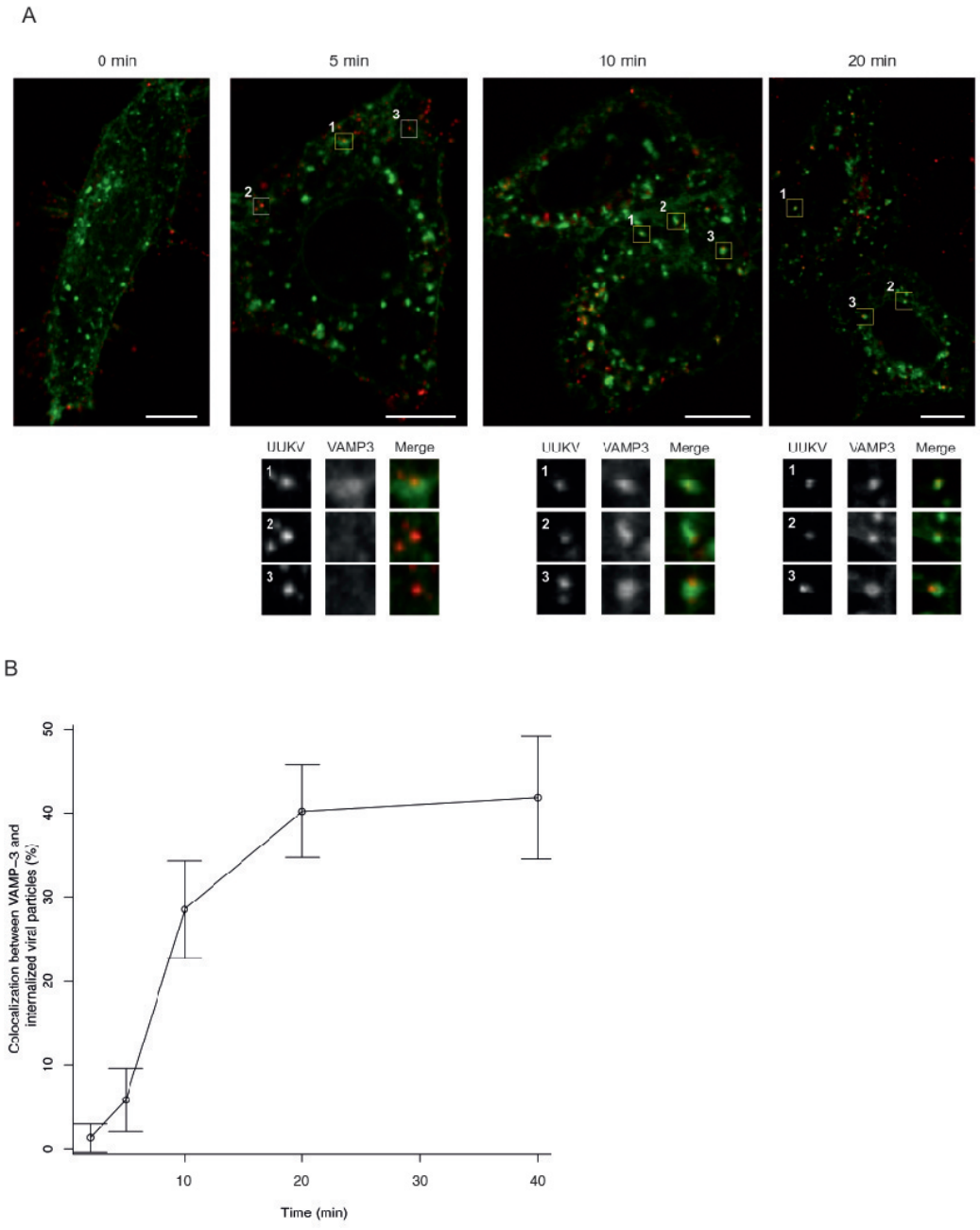

Figure 2.15 UUKV-TR associated with VAMP3-eGFP containing vesicles. A) HeLa-DC-SIGN cells were transfected with VAMP3-eGFP plasmid for 20 h using transfection reagent lipofectamine 2000 and 1µg of plasmids. Thereafter, UUKV-TR (MOI 10) was bound to cells before warming up to 37 °C for 0, 2, 5, 10, 20, and 40 min. Then, cells were fixed and imaged by confocal microscopy. UUKV-TR associated to VAMP3-eGFP containing vesicles. Pictures indicate time points 0, 5, 10, and 20 min. Magnification of association between UUKV-TR and VAMP3-eGFP containing vesicles (yellow squares) or non-colocalizing, internalized particles (white squares) are shown. Scale bars indicate 10 µm. B) Quantification of UUKV-TR association with VAMP3-eGFP containing vesicles. The association was maximal at time point 20 min. The experiment was performed once and for each time point 10 cells were analysed. Error bars represent standard deviation. Figures courtesy by Pierre-Yves Lozach.

Chapter 3

Discussion

The virus family of *Bunyaviridae* comprises many viruses that are important pathogens for humans, livestock and plants. Human infection is associated with high fatality rate. A hantavirus isolated in 2012 from Yosemite National Park in California was associated with a fatality rate of 30%. Another example is the recent identification of the Huaiyangshan virus in China with a fatality rate of 15% [10, 11]. Currently, no treatment or vaccines against bunyaviruses are approved by the Food and Drug Administration (FDA) for human use. Little is known about host proteins that are essential for bunyavirsus entry into host-cells. Identification of cellular factors that are important for bunyavirus infection and understanding of host-pathogen interactions are fundamental for potential drug development.

In this thesis, we performed image-based, genome-wide siRNA screens to identify cellular host factors for Uukuniemi virus (UUKV) infection in HeLa cells stably expressing DC-SIGN. UUKV belongs to the genus of *Phlebovirus* in the *Bunyaviridae* family. The virus has been used for several decades as a model for bunyaviruses and allows work under biosafety level 2 conditions.

Recently, we showed that UUKV and other phleboviruses use DC-SIGN triggered endocytosis to enter immature dendritic cells (DCs) and cells ectopically expressing the lectin [1, 2]. DC-SIGN on the cell surface binds the virus directly via interactions with high-mannose *N*-glycans on the viral glycoproteins. This is followed by clustering of cell surface DC-SIGN receptors and internalization of the virus-DC-SIGN complex into EE. In EE, the virus separates from the DC-SIGN and continues its journey like other late penetrating viruses into the degradative pathway.

DC-SIGN is mainly expressed on the surface of DCs. Due to limited availability and inefficient transfection efficiency of DCs, we used HeLa-DC-SIGN cells as model cells in our screens.

SiRNA screens were performed using libraries from two different vendors,

Dharmacon and Qiagen. The Dharmacon library is a pooled library in which different siRNAs targeting the same genes are applied into the same well of a 384-well plate, the Qiagen library contains four different siRNAs per gene that are pipetted into single wells of different 384-well plates. It had been claimed that pooling of siRNAs targeting the same gene minimizes off-target effects.

The two screens revealed 477 genes that potentially inhibit UUKV infection. These hits represent different cellular machineries such as endosomal acidification, translation initiation and transcription, replication and translation of the viral nucleoprotein N.

3.1 RNAi Screens – Promises and Pitfalls

In the last decade, gene silencing through RNAi has become a tool of choice for genome-scale, high-throughput analysis of gene function in different research fields including signal transduction, cancer progression, and host cell responses to infection. In the field of host cell responses to viral infection alone, numerous studies have been reported [117, 118, 119, 120, 121, 122, 123, 124, 125, 126, 127, 128, 129]. Screens revealed hundreds of new host factors that may affect viral infection and the studies increased the understanding of the complex jigsaw of host-virus interaction. However, many published siRNA screens of virus infection have suffered from weak comparability of their hit lists [3, 4]. In the last year, three siRNA screens were published to identify cellular genes required for HIV infection [117, 122, 129]. The screens showed less than 7% shared hits for any pairwise combination [3, 4]. Similarly, maximal 11% of hits were shared in pairwise comparisons of three genome-wide studies for influenza virus infection [120, 123, 118, 134]. The discrepancies between the hit lists of the performed genome-wide siRNA screens have mostly been explained by differences in the screening assays, protocols, and hit definition procedures such as different cell lines and reverse transfection incubation time [4].

In our case comparing Qiagen and Dharmacon preliminary hits from our screens revealed 19 common inhibitor hits and 2 enhancer hits, respectively. Although this overlap was clearly significant for the inhibitors (p-value 8.815e-05) and significant for enhancers (p-value 0.00713), the number of common hits was modest (for inhibitors 7.4 % for Dharmacon screen, 4% for Qiagen screen, for enhancers 5.4% and 3.3%, respectively). We used the same RNAi liquid handling protocol in both screens, utilized the same virus stock, and used the same cell line. Reverse transfection protocols and incubation times were also the same. Thus different screening protocols and different cell

lines are not sufficient to explain the small number of common hits. Similar observations were made in recent screens by the Swiss InfectX consortium (personal communication) and support the outcome of our screens.

Importantly, our two screens were different in respect to library design and hit selection. Especially the different library designs led to the use of different hit selection procedures. As the Dharmacon library was a pooled library, we were able to do the screen in triplicate. This allowed us to account for the variation within the replicate as an additional quality criterion for each siRNA. The difference in the library design and the different hit selection procedure may contribute to the modest overlap that we observed between screen results from the two screened libraries. Of note, hits are defined in both analysis methods based on arbitrary thresholds influencing the number of shared hits between the screens.

3.1.1 Limitations and Challenges of RNAi Screens

As described in the introduction, RNAi technology has several limitations that can result in false-positive and false-negative hits (see section 1.4.3). By definition, a false-positive hit is an actual non-hit declared as a hit, whereas a false-negative hit is the opposite. The reasons for a false-negative hit are many-fold: insufficient depletion of mRNA levels with the siRNAs used, insufficient degradation of proteins and thus insufficient functional reduction, functional redundancy of depleted genes with other genes, and cytotoxicity due to gene depletion. Several challenges and pitfalls need to be addressed to minimize false-positive and false-negative hits. Amongst them are experimental design (e.g. plate design, number of replicates), normalization procedure, quality control, and hit selection procedure, cell population context effects, off-target effects, and experimental errors during automated liquid handling [3, 4]. In the next subsections we will discuss possibilities for correcting the challenges.

3.1.1.1 Plate Design

Plate design is a fundamental step in HTS experiments. Improper design impairs all subsequent statistical analysis such as normalization, quality control, and hit selection [157]. The optimal plate design would be a fully randomized distribution of control and target siRNAs. This would allow proper normalization and quality control, resulting in less false-positive and false-negative hits. However, many commercial siRNA libraries, including the Qiagen and Dharmacon libraries, are clustered in functional groups and limit the distribution of control siRNAs to the outmost columns in the plates.

3.1.1.2 Normalization

Normalization is the process of identifying and removing systematic errors from the data. Systematic errors are biases in the read-out caused by inhomogenous conditions, e.g. uneven reagent evaporation, temperature differences within plates, liquid handling, and imaging [141].

An easy but very important approach to find biases is to visualize raw data in various ways including different series-plots. This method enabled us to observe a systematic, bowl-shaped edge effect in the infection index that would have drastically influenced subsequent hit determination and needed to be mathematically corrected.

Such spatial plate-effects are well known in HTS experiments. Different methods are suggested to adjust for such positional effects: for linear spatial effects, median polishing methods, robust regression, and linear mixed effect models have been proposed [141, 143, 148]. The bowl-shaped spatial effect in screening data, though, is a non-linear problem and requires a more complex mathematical approach such as diffusion models or locally weighted scatterplot smoothing ("loess") approaches [157, 158]. We chose the "loess" method, since it is an efficient and practicable statistical method, and adjusted to the needs of siRNA screening. Indeed, after applying the "loess" approach, the bow-shaped effect in infection was almost completely eliminated.

With some limitations, normalization of the observed infection edge effect was successful in our case. Negative controls in our screens were located on the first two and last two columns of each plate. Therefore, we could not use the negative controls to adjust for spatial effects, but had to take sample wells. Due to the aforementioned plate design, this approach cannot adjust screening data for systematic errors in an ideal manner and enhances the probability of false-negative hits [157]. Target siRNA were clustered in functional groups and therefore, may affect spatial correction algorithms by their potential pathway-specific impact on infection. This is ruled out when using negative control wells. It emphasizes the importance of the screen design phase which was not under our control in this study.

3.1.1.3 Population Context-Dependent Cell-To-Cell Variability

Besides systematic errors on the plate level, another important source of false-positive or false-negative hits, especially in virus infection screens, is the influence of cell variability on the read-out. Virus infection of cells can be susceptible to cell density [139]. Cell density, in turn, can be influenced by siRNA, when their cellular effects change cell growth or cell viability.

To acccount for this siRNA-mediated change in cell density, the use of so

called "checkerboard" plates is suggested [159]. "Checkerboard" plates are plates in which different amount of cells per well, transfected with a negative control siRNA, are infected. After infection, the fraction of infected cells is calculated for each cell density and a regression function is fitted. This function can be applied to infection indices and the cell number obtained for each well of the screen. Thus infection indices can be normalized to cell density.

We did not perform normalization against cell density of screening data for two main reasons: First, the aforementioned sub-optimal plate design did not allow to normalize "checkerboard" plates to the observed infection edge effect. Regression fitting cannot be performed properly as it can not be differentiated between the effect of the cell density and the edge effect on infection. Correction to such deduced regression function would introduce errors to the data set that may be stronger than without "checkerboard" correction. Secondly, the "checkerboard" approach is based on the assumption that there are no synergistic effects between an siRNA and the virus that influences cell density or cell growth. This is certainly the case for short virus infection time, within no or only low cell growth is expected. However, it is not necessarily true for a long infection incubation time, such as for 20 h used in our screening protocol. In the case of an interaction effect on cell growth, infection indices would be corrected to the wrong cell density and thus enhance the number of false-negative or false-positive hits.

One solution for cell-population effects would be corrections of the cell number obtained from additional screens without virus infection. Thereby, final cell numbers, spatial cell growth effects within a well, cell size etc. may be assigned to the exclusive effect of the siRNA, and further used for normalization e.g. in linear-mixed effect models [148].

3.1.1.4 Quality Control

A clear difference between negative and positive controls is a score for good quality screening data [145]. Many methods have been proposed to measure data quality such as signal-to-background ratio, signal-to-noise ratio, signal window, assay variability ratio, Z-factor, and SSMD [143, 146]. It is important that the quality of the data is assessed after the normalization steps. Otherwise systematic errors may affect the assessment of the quality resulting in wrong conclusions. To assess the quality of our screens after normalization, we used the SSMD method that measures the effect size of the positive siRNA controls. Thereby SSMD accounts for data variability in both controls [145]. We had to remove a total of 39 plates (13%) in the Qiagen screen for further analysis. This is a typical amount of plates in HTS

of such size [157]. For the Dharmacon screen all plates passed our quality criteria.

3.1.2 Preliminary Hit Selection

Once the quality of screening had been assessed and low-quality plates were eliminated, hits were defined. Many statistical analysis methods for this step have been proposed (see table 1.5) [142, 157]. We decided to apply the SSMD method and combined it with the "fold-change" approach for the primary hit selection in the Dharmacon screen. For Qiagen we used the "redundant siRNA activity" (RSA) method. Compared to other methods, like mean ± k x standard deviation (s.d.), median ± k x median deviation (MAD) or multiple t-test, the SSMD method allows to measure the strenght of an siRNA effect and to classify it into different effect classes ranging from "zero", "extremely weak" to "extremely strong". The classification into the different classes is related to the probability, that a value from a certain siRNA is greater / smaller than a value from a negative reference [149].

The RSA method examines the rank distribution of all siRNAs targeting the same gene and assigns them p-values. P-value calculation is based on an iterative hypergeometric distribution function. An advantage of this method is that a hit based on multiple moderately effective siRNAs is considered stronger than a hit based on just one or a few highly effective siRNAs [152]. Using these methods, we revealed preliminary hit lists for Dharmacon and Qiagen screens consisting of 256 inhibitor and 38 enhancer genes affecting UUKV infection and 461 inhibitor and 60 enhancer genes, respectively.

3.1.3 Off-target Analysis

A further important issue to minimize false hits is to filter out off-target effects. Off-target effects may occur when siRNAs act as a microRNAs (miRNAs), and bind to other mRNAs than the predicted, thereby down-regulating often tens to hundreds of genes [135, 136]. Since the length of homology is by far shorter for miRNAs than for siRNAs, the likelihood of binding different mRNAs is accordingly higher. Together with the fact that we used very similar liquid handling protocols for both screens, we hypothesized that miRNA-activity of siRNA may be a major cause of false-positive hits. To filter out off-target effects we applied two different approaches, transcriptome correction and assessment of siRNA seed-effects.

3.1.3.1 Transcriptome correction

SiRNAs that targeted genes not expressed in HeLa-DC-SIGN cells, but inhibited or enhanced UUKV infection were false-positive hits due to off-targets. To address this issue we examined the transcriptome of the HeLa-DC-SIGN cell line used in the screen. The transcriptome of HeLa-DC-SIGN cells was determined by a microarray approach in four independent experiments. In total, 13'421 mRNA transcripts were detected and mapped to their gene ID. Nagarjuna et al. performed proteome and transcriptome analysis in HeLa cells by advanced mass spectrometry and deep transcriptome sequencing and suggested at least 10'000 -12'000 genes to be expressed in HeLa cells [160]. This is comparable to our identified 13'421 expressed genes in HeLa-DC-SIGN cells.

We compared the HeLa-DC-SIGN transcriptome data with the gene hits of the siRNA screens. The comparison revealed genes in our hit lists that are not expressed in HeLa-DC-SIGN cells. Thus, these genes were assumed to be false-positive hits.

The result of comparing the 13'421 expressed genes with the gene hits in our screens confirmed our suspicion. In both screens about 30% of the preliminary hits were false-positive (Qiagen inhibitors 178 and enhancers 21, Dharmacon inhibitors 74 and enhancers 11). Comparing Qiagen and Dharmacon hits after transcriptome correction revealed 18 common inhibitor hits and 2 common enhancer hits. Compared to the frequency of shared preliminary hits, the fraction of shared hits increased for inhibitors from 7.4 % to 9.9% for Dharmacon screen and from 4% to 5.8% for Qiagen screen. For shared enhancer hits the fraction increased from 5.4% to 7.7% in Dharmacon screen and from 3.3% to 5.1 % in Qiagen screen. P-values for overlapping genes was 9'782 times smaller for inhibitor genes and five time smaller for enhancer genes than p-values for overlapping genes of preliminary hits i.e. before transcriptome correction.

These results minimized off-target effects. In general, the transcriptome comparison strategy is an effective method to determine the reliability of screening hits. It should be included in data analysis protocols of RNAi projects. So far, transcriptome correction has not been included in any published screen. In our case, the comparison with the transcriptome clearly showed that a large fraction of the preliminary hits were likely false-positive hits.

3.1.3.2 Assessment of siRNA seed-effects

It is shown that off-targets may occur when siRNAs act like miRNAs. Thus, another strategy to filter off-target siRNAs was based on similar phenotypes observed for homologous siRNAs. Homology amongst siRNAs can be two-fold: seed homology or on-target homology. If a phenotype of a siRNA rather resembles the common phenotype of siRNAs with the same seed region than of the phenotype siRNAs with the same on-target gene, it is likely that this particular siRNA acts as a miRNA.

We classified all siRNAs within our screening libraries according to their 7nt-seed sequences. We identified 9'541 different classes of seeds in the Qiagen library and 11'890 in the Dharmacon library. In both screens, most different classes (75%, Qiagen; 5'657 classes, Dharmacon 7'621 classes) consisted of at least 3 different siRNAs. We assessed the effects of seed classes consisting of at least 3 different siRNAs on UUKV infection. We used the SSMD method combined with the "fold-change" approach. The assessment of the seed-effects revealed for the Qiagen screen 644 seeds with an "extremely strong" or a "very strong" effect that inhibited UUKV infection at least by 50% compared to the negative control. When comparing these 644 seeds with the seeds of the siRNAs targeting the expressed hit genes, we identified that 20% of the siRNAs possessed seeds that can inhibit UUKV infection. These siRNAs most likely acted as miRNAs.

To test this possibility, we chose 6 synthetic miRNAs (miRs) that mimic endogenous miRNAs and share the same seed region with 6 seed classes with inhibitory effect on UUKV infection. We found that all miRs, except for one, reduced UUKV infection by 60 - 90% supporting our hypothesis.

Of the transcriptome corrected hits, 50% were targeted by at least one siRNA that may have acted as a miRNA. On average, hit genes were targeted by 3 different siRNAs. Thus without any further experiments it was not possible to know whether these genes were false-positive hits or real hits.

In the Dharmacon screen, 2 seeds were identified to have a "very strong" inhibitiory effect on UUKV infection. Thus, in the Dharmacon screen there were much less seed classes identified to inhibit UUKV infection. The difference may be due to the different designs of the libraries. The Dharmacon library is a pooled library. It has been claimed that the pooling of the siRNAs reduces false-positives due to the lower single siRNA concentration per well. It seems that the seed off-target effect in the Dharmacon screen was less predominant compared to the Qiagen screen.

Compared to the Qiagen library, the median inhibition effect in the on-target and off-target analysis were in generally weaker in the Dharmacon screen (30% versus 60%). This could indicate that the depletion efficiency

in the Dharmacon screen was less efficient than in the Qiagen screen. An inefficient depletion of genes results in more false-negative hits.

Taken together, the transcriptome correction revealed that approximately 30% of preliminary hits were likely to be false-positive in both screens. In the Qiagen screen, 50% of the hit genes were targeted by at least one siRNA that may act as a miRNA. Since the screening protocols had identical liquid handling, cell line, and virus stock, we concluded that the low overlap between the screening hits was mainly due to off-target effects of siRNAs in the Qiagen screen and mainly due to high number of false-negative hits in the Dharmacon screen. The fraction of common hits after correction increased 1.5 times. However, the fraction of common hits was still modest after transcriptome correction, which may point out that there are further false-positive and false-negative hits.

3.1.4 Final Hit List and Bioinformatic Analysis

After off-target analysis and removal of false-positives, we analyzed both hit lists for common pathway functions involved in UUKV infection using the open source software Reactome. The tool revealed that the lists supplemented each other in most of the functional pathways. Thus we combined hit lists into one list.

The observation that hit lists supplement each other, was found for meta-analysis of published screens for Influenza virus and HIV [3, 4] supporting our strategy to combine the hit lists.

Protein-protein interaction analysis using the open source software STRING reveled 12 clusters such as a VAMP interaction cluster, a growth arrest interaction cluster, and a translation initiation interaction cluster. However, overall the number of observed clusters was modest compared to other published screens.

3.2 Outlook Genome-wide siRNAs Screens

Published and ongoing screens should be checked for their up-to-date annotation of their siRNAs libraries and their hit lists should be adjusted. In general the annotation of the libraries should be regularly up-dated to prevent false hits due do wrong annotation. Although over a long time period, minor changes in hit lists are expected due to up-to-date annotation, regularly up-dating the annotation allows comparison of different screens.

Screens should be corrected against the transcriptome of the cell line used in the screens. In general, transcriptome correction should be included

as standard procedure for any further genome-wide siRNA screen. Transcriptome analysis could be performed using next generation sequencing methods.

To further minimize false hits, MOCK screens should become a standard for siRNA screens to correct against population context cell-to-cell variability.

In addition, so far no siRNA screen was analysed for off-target effects due to the sense strands of siRNAs that are able to regulate gene expression [161] [162]. It would be interesting to develop methods that take this off-target analysis into account.

To perform statistical analysis of siRNA screens on a solid basis, the layout design of the siRNA libraries should be randomized. Vendors should be convinced to take over this responsibility or screeners should do a redesign of the libraries.

More efforts needs to be done to understand in which cases siRNAs act as miRNAs and to assure that siRNAs act accurately. This finding needs to be implemented in the design of new siRNAs. SiRNAs need further be validated against off-targets on mRNA and protein levels using for example next generation sequencing and MASS spectrometry analysis.

Information of single siRNAs concerning their potential to act as miRNAs are lost when pooled siRNA libraries are used. Thus off-target correction due to seed-effects is much more complicated in pooled siRNA screens compared to un-pooled screens. In addition, we assume a high number of false-negative hits in pooled screens, when not all siRNAs in a pool work efficiently. Thus we suggest that future genome-wide siRNA screens should be performed using un-pooled libraries that contain a high number of different siRNAs against the same gene. This would allow to enhance the probability to predict real hits. To determine the minimal number of different siRNAs targeting the same gene that is needed to predicted real hits with high accuracy, mathematical methods need to be developed that consider the probability of siRNAs to act like miRNAs.

3.3 Verification and Characterization of Hits

3.3.1 miR-142-3p and VAMP3

We found that miR-142-3p inhibited UUKV fusion or a pre-fusion event using acid bypass experiments. This finding was confirmed by UUKV fusion experiments in which HeLa-DC-SIGN cells treated with mimic miR-142-3p inhibited fusion of the virus.

Interestingly, miR-142-3p has been reported to be expressed in human dendritic cells (DCs) and T lymphocytes [163]. UUKV is known to infect

human dendritic cells [1]. MiR-142-3p may regulate UUKV infection in a tightly controlled way depending on the expression level of miR-142-3p. Further validation is needed to demonstrate this possibility.

Since miR-142-3p affected UUKV infection, we analyzed gene expression in HeLa-DC-SIGN cells treated with and without miRs. We found 180 up- and 112 down-regulated genes in the presence of miR-142-3p.

Comparison of the miR-142-3p down-regulated genes with inhibitor hits from siRNA screens revealed five shared genes: LIM homeobox1 (LHX1), hydroxy-delta-5-steroid dehydrogenase 3 beta- and steroid delta-isomerase 7 (HSD3B7), metallothionein-like 5, testis-specific (MTL5), ATPase, Ca^{2+} transporting, cardiac muscle, slow twitch 2 (ATP2A2, also known as SERCA), and vesicular associated membrane protein 3 (VAMP3, also known as cellubrevin)

LHX1 is a potential transcription factor. HSD3B7 plays an essential role in the synthesis of bile acids. The function of MTL5 is unknown. ATP2A2 catalyzes the hydrolysis of ATP coupled with the translocation of calcium from the cytosol to the lumen of the sarcoplasmic reticulum. VAMP3 is a v-SNARE (Soluble NSF Attachment Protein Receptor) protein.

VAMP3 was the only gene that decreased UUKV infection in both screens and was also significantly down-regulated by the miR-142-3p. To confirm a role for VAMP3 in UUKV infection, we performed further experiments in HeLa-DC-SIGN cells.

When cells were treated with VAMP3 siRNA, UUKV infection dropped between 45% and 85%, depending on experimental conditions. Further, we used the catalytic light chain of tetanus toxin (TeTx), a protease that cleaves and inactivates VAMP1, VAMP2, and VAMP3. In cells transiently expressing TeTx, UUKV infection was significantly decreased (35%). This led us to conclude that inhibition was due to the VAMP3 inactivation by TeTx. We cannot exclude side effects from inactivation of VAMP1 and/or VAMP2, although they were not hits in the screens.

Colocalization studies revealed that fluorescently labeled UUKV particles were present in VAMP3-GFP-positive, perinuclear vesicles. Maximal colocalization was observed 20 min after UUKV entry. In respect to UUKV infection kinetics, we suggest that VAMP3 may play a role in UUKV infection by interfering with the maturation or function of late endosomes. This is consistent with UUKV being a late penetrating virus [37].

The v-SNARE VAMP3 has been reported to be implicated in recycling of transferrin and integrin receptors [164]. It is suggested that VAMP3-dependent trafficking may include the recycling of a large variety of plasmalemmal proteins [155, 165]. In contrast, VAMP3 knockout mice have no obvious phenotype in constitutive membrane recycling [165].

We observed maximal colocalization between UUKV and VAMP3-GFP-positive, perinuclear vesicles 20 min after UUKV entry. In addition, the DC-SIGN surface expression was not different in HeLa-DC-SIGN cells treated with VAMP3 siRNAs compared to cells treated with non-targeting siRNA control (data not shown). Thus we assume that VAMP-3 does not affect UUKV infection on the level of DC-SIGN recycling.

VAMP3 belongs to the SNARE proteins that mediate membrane fusion in vesicular transport. About 36 different mammalian SNAREs are known. Combinations of the various members create a wide array of SNARE complexes that mediate different transport events. For example, the vesicle-SNARE (v-SNARE) VAMP8 mediates homotypic fusion of EE and LE by interacting with the target-SNARE (t-SNARE) composed of Syn7 (Syntaxin 7), Vti1b (Vesicle transport through interaction with t-SNAREs 1B), and Syn8 (Syntaxin 8) present in the membrane of the target compartment [166]. Alternatively, the same t-SNARE can combine with the v-SNARE VAMP7 for heterotypic fusion between late LE and LYS [167].

Biochemical studies show that VAMP3 binds to plasma membrane t-SNAREs composed of syntaxin1, syntaxin4, SNAP-23, and/or SNAP-25 [168] [169]. It has also been reported the VAMP3 forms ternary complexes with syntaxin1/SNAP-23, syntaxin1/SNAP-25, syntaxin4/SNAP-23 and syntaxin4/SNAP-25 [170, 171, 172]. Fusion capacity of the ternary complexes formed by VAMP3 is shown for syntaxin1/SNAP-25, syntaxin1/SNAP-23, and syntaxin4/SNAP-25, but not for syntaxin4/SNAP-23 [173]. Of note, SNAP23 was present in our final hit list of the screen. Interestingly, it has been suggested that SYN11 and SNAP-23 are present on LE [174]. Whether SNAP-23 and VAMP3 forms the *trans*-SNARE complex that affect UUKV infection needs to be proven. Furthermore the syntaxin protein that is involved in the *trans*-SNARE complex needs to be determined.

VAMP3 has also been shown to be involved in autophagy, a cellular process that degrades obsolete parts of the cell itself. Autophagy starts with the formation of autophagosomes and capturing of cytoplasmic cargo. The autophagosomes fuse with LEs to form amphisomes that in turn fuse with LYS to autolysosomes in which degradation of the cargo occurs. VAMP3 is required for the fusion of late endosomes and autophagosomes to generate amphisomes that allow the maturation of autophagolysosomes [175].

Besides VAMP3, autophagy related 16-like 2 (ATG16L2), BCL2/adenovirus E1B 19kDa interacting protein1 (BNIP1), tumor protein p53 (TP53), RB1-inducible coiled-coil 1 (RB1CC1), WD repeat domain, and phosphoinositide interacting 1 (WIPI1) were inhibitory hits in the screen that may be linked to autophagy.

So far, it is not known if ATG16L2 has a role in autophagy. ATG16L2 is

an isoform of mammalian ATG16L1 that forms the ATG12-5-16L1 complex that is essential for the early maturation steps of mammalian autophagosome [176]. Similar, ATG16L2 forms an ATG12-5-16L2 complex. However, it has been shown that ATG12-5-16L2 did not compensate for the function of ATG16L1 in autophagosome formation [177]. Nevertheless, a genome-wide siRNA screen to discover host factors required for HIV-1 replication in HeLa cells identified several autophagy genes as well as ATG16L2 [117]. Thus, ATG16L2 may be related to autophagy and may play an essential role in infectious diseases.

BNIP1 has been shown to be associated with autophagy receptor p62 [178]. The autophagy receptor p62 promotes clearance of ubiquitinated protein by autophagy [179].

The tumor suppressor protein p53 has been shown to inhibit autophagy by interaction with RB1CC1 [180].

Taken together, we suggest that autophagy may play a role in UUKV entry.

Autophagy has been shown to play essential anti-viral and pro-viral roles [181]. Pro-viral roles have been shown for example for influenza A virus (IAV), DV, and hepatitis C virus that induce autophagy and thus enhance viral replication and yield [182, 183, 184]. Recently, it has been shown that also the bunyavirus SNV induces autophagy in cells that promote virus replication [185].

In addition, autophagy may participate in the viral life cycle at the early entry phase of viral infection. Recent studies show that DV and JEV (japanese encephalitis virus) co-localize with both autophagosome and endosome markers and a potential role for autophagosome - endosome fusion in viral entry/uncoating has been suggested [186, 187, 188].

We previously found that UUKV colocalizes with Rab7a and LAMP-1 positive vacuoles [33]. Considering that VAMP3 is required to generate amphisomes and Rab7a and Lamp-1 localize to both LE and amphisomes, we suggest a working model in which UUKV fusion takes place in amphisomes [189, 190] (see figure 3.1).

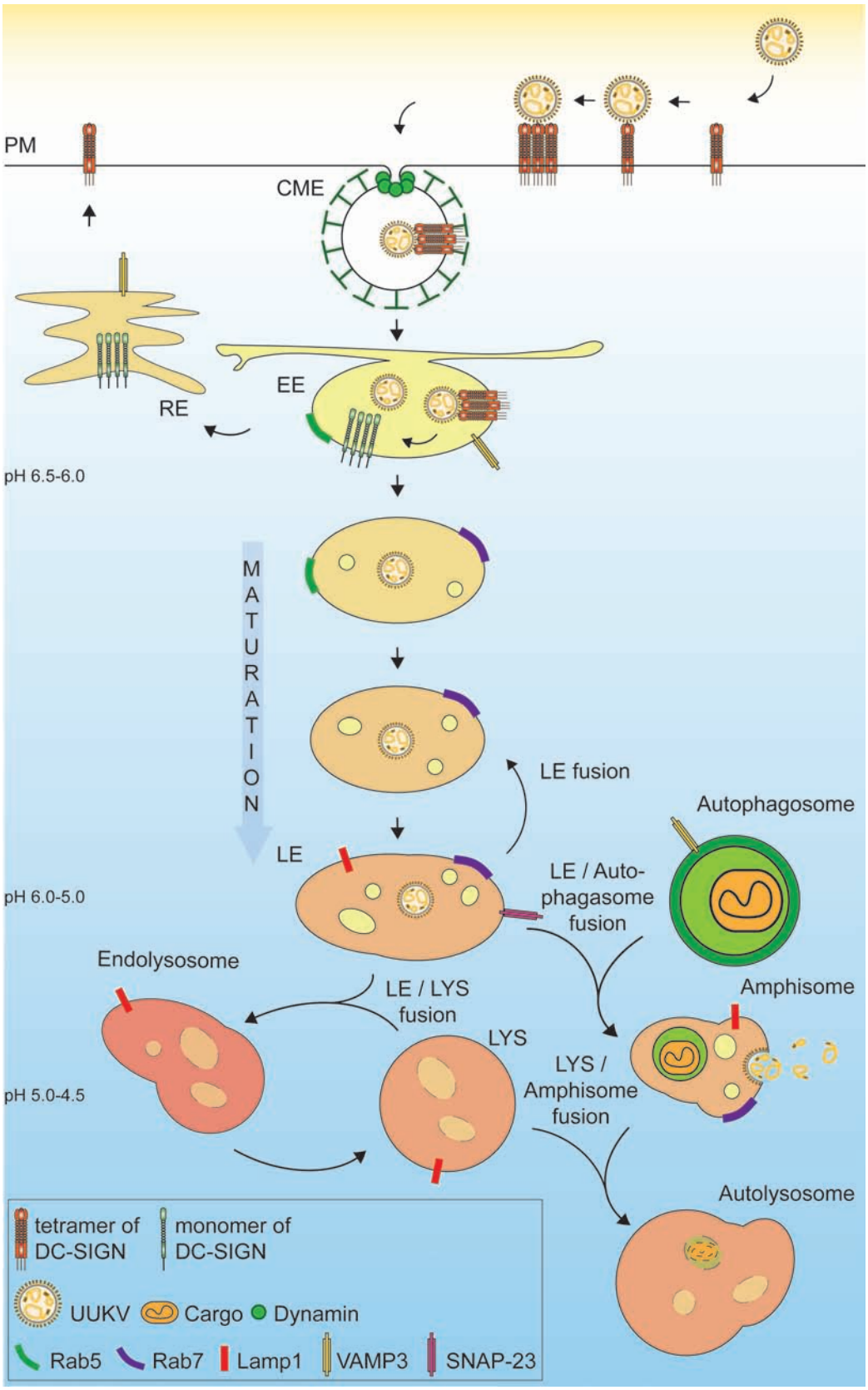

Figure 3.1 UUKV Entry Working Model. UUKV binds to its receptor DC-SIGN followed by receptor clustering and CME. In EE, the virus receptor complex dissociates, triggered by the pH, and DC-SIGN is recycled back to the PM. The UUKV is further processed to LE that fuse with autophagosomes to amphisomes mediated by VAMP3 and SNAP23. In amphisomes, UUKV fuses and penetrates into host cytosol. Abbreviations: CME, clathrin mediated endocytosis; EE, early endosome; LE, late endosome; LYS, Lysosome; PM, plasma membrane; RE, recycling endosome

3.4 Outlook

We showed that miR-142-3p regulated an UUKV pre-fusion or fusion event. In addition we showed that the expression of VAMP3 is regulated by the miR-142-3p using a gene expression microarray approach. To verify that miR-142-3p down regulates VAMP3 expression, Western Blot analysis should be performed. It will also be interesting to study if endogenous miR-142-3p affects UUKV infection. It was proposed that miR-142-3p is expressed in DCs and we showed that UUKV infects DCs. Thus it would be interesting to investigate how anti-microRNAs against the micro-RNA-142-3p affect UUKV infection in DCs.

We showed that VAMP3 depletion and inactivation using siRNAs and TeTx inhibited UUKV infection. To verify that siRNAs against VAMP3 down-regulate cellular VAMP3 levels, Western Blot analysis should be performed using HeLa-DC-SIGN cells.

The role of VAMP3 in UUKV infection needs to be further characterized. Endocytic bypass experiments should be performed to show whether VAMP3 regulates a UUKV pre-fusion or fusion event. If endocytic bypass experiments reveal that pre-fusion or fusion is inhibited, it should be investigated at which endocytic step VAMP3 inhibits UUKV infection. In parallel, infection experiments in cells treated with siRNAs targeting VAMP3 will be performed using late penetrating viruses such as influenza virus and early penetrating viruses such as semliki forest. Performing the infection experiments, the specificity of VAMP3 to inhibit UUKV infection will be investigated.

VAMP3 colocalization experiments in HeLa-DC-SIGN with Rab4, Rab11, Rab5, Rab7 and the microtubule-associated protein1 light chain3 (LC3) will show whether VAMP3 localizes with EEs, LEs, LYS or amphisomes.

To prove our working model, UUKV colocalization experiments with the microtubule-associated protein1 light chain3 (LC3) should be performed to show whether UUKV localizes in amphisomes. Also, it will be interesting to study if UUKV activates autophagy by monitoring autophagy in live cells using dyes that selectively stains autophagic vacuoles.

A general implication of VAMP3 in endocytosis may be investigated by transferrin uptake and recycling and EGF degradation assays.

3.5 Conclusion

We performed two genome-wide siRNAs screens to identify cellular factors that are important in UUKV infection. We identified 477 host genes that may play a role. By performing two strategies – transcriptome correction and effect assessment of homologous seeds shared by different siRNAs on UUKV infection – we aimed at minimizing false-positive hits. Using the transcriptome correction procedure we identified 30% of preliminary hits as false-positive. The seed-effect strategy enabled us to label 25% of the remaining hits as potential false-positives. These results support our approach to minimize off-target effects. The transcriptome comparison strategy is very effective, and should be included in data analysis protocols of RNAi projects. The seed-effect strategy is limited to identify potential false-positive hits in siRNA screens that are performed with only few numbers of different siRNAs that target the same genes. However, this strategy could be very powerful in identifying false-positive hits in infection screens that are performed with several different siRNAs targeting the same gene. It would allow to predict real hits and false-positive hits with much higher probability compared to screens performed with only few siRNAs targeting the same gene.

Our results shows additionally the importance of hit verification by further experimental procedure. We performed verification experiments for a seed hit that is annotated for the endogenous miRNA-142-3p.

We showed that mimic-miRNA-142-3p regulates UUKV endosomal trafficking, prefusion or fusion events. The role of the endogenous miR-142-3p in UUKV infection needs to be proven. Gene expression analysis in cells treated with the miR-142-3p revealed VAMP3 as a potential gene that is regulated by miR-142-3p. VAMP3 was also a hit in both siRNA screens. First validation steps support, that VAMP3 plays a role in UUKV infection. Given that VAMP3 is required for LE and autophagosome fusion to form the amphisomes and considering that UUKV colocalizes with the LE, LYS, and amphisomal markers Rab7a and Lamp-1, we suggest a working model, in which UUKV penetration occurs in amphisomes.

Chapter 4

Material and Methods

4.1 Material

Table 4.1 Chemicals

Chemicals	**Provider**	**Ordering Number**
Acetic acid	VWR International AG; Switzerland	1.00063
Albumin fraction V (bovine serum albumin; BSA)	Sigma; Switzerland	A9418
Ampicillin	Axon Lab AG; Switzerland	A0839
BODIPY TR C_5-Thiosulfate, Sodium Salt	Life technologies^{TM}; Switzerland	T30455
Carboxymethylcellulose sodium low visc.	VWR; Switzerland	276494N
Coomassie Hepes	Sigma Aldrich; Switzerland	S6191
Hoechst 33258 (bis-benzimide)	Life technologies^{TM}; Switzerland	H-3569
Kanamycin	Sigma Aldrich; Switzerland	K1876
LB medium	Prepared in the media kitchen at the Institute of Biochemistry, ETH Zurich; Switzerland	
LB plates, containing different antibiotics	Prepared in the media kitchen at the Institute of Biochemistry, ETH Zurich; Switzerland	
Methanol	Fluka; Switzerland	65543
Saponin	Sigma Aldrich; Switzerland	S4521
Sodium acide (NaN3)	Sigma Aldrich; Switzerland	S2002
Triton X-100	Sigma Aldrich; Switzerland	T8787
TRIzol Reagent	Life technologies^{TM}; Switzerland	15596026

Table 4.2 Material

Material	Provider	Ordering Number
5 mL serological plastic pipettes	Greiner bio-one; Switzerland	606180
10 mL serological plastic pipettes	Greiner bio-one; Switzerland	607160
25 mL serological plastic pipettes	Greiner bio-one; Switzerland	760180
15 mL falcon tubes	Greiner bio-one; Switzerland	188161
50 mL falcon tubes	Greiner bio-one; Switzerland	227280
6-well plates	Greiner bio-one; Switzerland	657160
12-well plates	Greiner bio-one; Switzerland	665180
24-well plates	Greiner bio-one; Switzerland	662160
96-well U-bottom plates	Greiner bio-one; Switzerland	650160
384-well plates	Greiner bio-one; Switzerland	781091
Bovine serum albumine (BSA)	Sigma Life Science; Switzerland	A9576
Cell Strainer, 40 μm Nylon	BD Falcon^{TM}, Europe	352340
Dimethyl sulfoxide (DMSO)	Sigma; Switzerland	D-2650
Dulbecco's Modified Eagle Medium (DMEM)	Gibco, life technologies^{TM}; Switzerland	21063029
EDTA 0.5 M	Gibco, Life technologies^{TM}; Switzerland	AM9260G
Fetal calf serum (FCS)	LabForce; Switzerland	RA111E
Formaldehyde 37%	Sigma Aldrich; Switzerland	47629
Glasgow MEM BHK-21 (GMEM)	Gibco, Life technologies^{TM}; Switzerland	11710035
GlutaMax	Life technologies^{TM}; Switzerland	35050079
Hepes	Gibco, Life technologies^{TM}; Switzerland	15630080
High precision cells made of Quartzs SUPRASIL	Hellma Analytics; Germany	119004FQS
Lipofectamine^{TM} 2000	Life technologies^{TM}; Switzerland	11668-019
Lipofectamine^{TM} RNAiMAX	Life technologies^{TM}; Switzerland	13778150
Non-essential amino acids (NEAA)	Gibco, Life technologies^{TM}; Switzerland	11140050
Penicillin/streptomycin	Life technologies^{TM}; Switzerland	15140163
Phosphate buffered saline 1x (PBS1x)	Prepared in the media kitchen at the Institute of Biochemistry, ETH Zurich; Switzerland	
SW55 Ultra-Celar Centrifuge tubes(25x89 mm)	Beckman; Switzerland	344057
SW28 Ultra-Celar Centrifuge tubes(25x89 mm)	Beckman; Switzerland	344058
T-25 cell culture flasks	Greiner bio-one; Switzerland	690175
T-75 cell culture flasks	Greiner bio-one; Switzerland	658175
T-175 cell culture flasks	BD-Falcon; Switzerland	354780
Trypsin/EDTA 5 M	Gibco, Life technologies^{TM}; Switzerland	15400-054
Tryptose phosphate broth (TPB)	Sigma Aldrich; Switzerland	T8159
10 cm cell culture dishes	Greiner bio-one; Switzerland	664960

Table 4.3 Kits

Kits	Provider	Ordering Number
Calcium Phosphate Transfection Kits/Reagents	Clontech; Switzerland	631312
RNeasy Mini Kit	Qiagen; Switzerland	74104
3,3′-diaminobenzidine (DAB) Substrate Kit for Peroxidase	Vector Laboratories; United Kingdom	SK-4100

Table 4.4 Antibodies

Antibody (Ab)	Raised against	Provider	Source	Dilution
U2	UUKV N-, G_N, and G_C proteins	Produced in house	Rabbit	1:400
8B11A3	UUKV N-protein	Ralf Pettersson; Karolinska Institute; Sweden	Mouse	1:500
FAB1621P	DC-SIGN CRD	R&D Systems; US-MN	Mouse	1:50
IgG2A Phycoerythrin Isotype Control		R&D Systems; US-MN	Mouse	1:50
2^{nd}Ab-AlexaFluor coupled	Various species	Life technologies; Switzerland	Various species	1:1'000

Table 4.5 Buffers

Buffer	Composition
FACS Buffer (FB)	2% FCS, 5 mM EDTA, 0.02% NaN_3 in PBS1x
FACS Perm Buffer (FPB)	2% FCS, 5 mM EDTA, 0.02% NaN_3, 0.1% saponin (w/v) in PBS1x
Fixation buffer	40% MeOH, 10% Acetic Acid, 50% H_2O
Phosphate buffered saline 1x	prepared in the media kitchen at the Institute of Biochemistry, ETH Zurich; Switzerland
Sucrose cushion	30% sucrose in 1x HNE buffer
HNE-buffer 1x	20 mM Hepes, 150 mM NaCl, 2 mM EDTA, pH 7.4

Table 4.6 Plasmids

Name	Insert	Backbone	Resistance	Origin
pVSVG	VSV-G	pcDNA5.1	Amp	[191]
p8.71	HIV Gag and Pol	p8.2	Amp	[191]
pTrip-DC-SIGN	DC-SIGN wt	pTrip	Amp	[192]
p.VAMP-3-eGFP	VAMP3-eGFP	peGFP-N1	Kan	Newly generated
p.VAMP-3-cyto-eGFP	VAMP3-cyto-eGFP	peGFP-N1	Kan	Newly generated
p.VAMP-5-eGFP	VAMP5-eGFP	peGFP-N1	Kan	Newly generated
p.TeTx	catalytic chain of tetanus toxin (TeTx)	pcDNA3.1	Amp	kindly provided by Marc G. Coppolino [156]

Abbreviations: Amp, Ampicillin; Kan, Kanamycin

4.2 Cell Culture

For genome-wide siRNA screens cervix carcinoma cells (HeLa) stably expressing DC-SIGN were used (HeLa-DC-SIGN). Infection-, endocytotic bypass-, binding-, internalization-, and fusion experiments were performed in HeLa-DC-SIGN cells. In addition the endocytotic bypass experiment was performed using the human lung epithelial cell line A549. UUKV was produced in Baby Hamster Kidney (BHK-21) cells. To produce pseudotyped lentivirus particles the epithelial kidney human cell line HEK293T was used.

HeLa, HeLa-DC-SIGN, and Hek293T cells were maintained in Dulbecco's Modified Eagle's Medium (DMEM) supplemented with 10% fetal calf serum (FCS) and 1% GlutaMAX. A549 cells were cultivated in DMEM supplemented with 10% FCS, 1% GlutaMAX, and 1% no essential amino acids (NEAA). BHK-21 cells were grown in Glasgow Medium (GMEM) supplemented with 10% FCS and 10% Tryptose Phosphate Broth (TPB).

4.2.1 Production of HeLa-DC-SIGN Cells

Cell lines stably expressing DC-SIGN were established by transduction of HeLa cells using pseudotyped lentivirus particles followed by fluorescence-activated cell-sorting (see 4.2.1.1, 4.4.0.1, and 4.2.1.2).

4.2.1.1 Transduction of HeLa Cells

75'000 HeLa cells/well of a 12-well plate were seeded and incubated at 37 °C for 24 h. After incubation, cells were washed once with DMEM, the medium was removed and 400 µl/well of transduction solution consisting of 50 µl

(100 μl) virus, 30 μg polybrene, and 350 μl (300 μl) DMEM, was added. After 2 h incubation at 37 °C, 1 ml of culture medium was added, followed by amplification of cells and cell sorting.

4.2.1.2 Fluorescence-activated-Cell-Sorting (FACS)

Cell sorting was conducted at Flow Cytometry Facility of the ETH Zurich. 20e+6 transducted cells were stained against DC-SIGN using FAB1621P or using isotype control IgG2A coupled to phycoerythrin. Antibodies were diluted 1:50 in PBS1x at 4 °C for 45 min. Cells were washed and filtered through a 40 μm BD Falcon Cell Strainer just before cell sorting. Cell sorting was performed by sorting the highest 5% of DC-SIGN expressing cells.

4.3 Transfection of Cells

4.3.1 DNA Transfection

For transient gene expression, 80'000 HeLa-DC-SIGN cells were seeded per well of a 24-well-plate 24 h prior transfection. Per well 2 µl Lipofectamine 2000 were added to 48 µl DMEM and incubated at RT for 5 min. After addition of 50 µl DMEM containing 1 µg of DNA, both solutions were mixed gently by slowly pipetting up and down and incubated at RT for 1 h. The cells were washed once with PBS1x. 100 µl of the Lipofectamine/DNA-mixture were added to the well containing 500 µl culture medium and distributed by moving the plate back and forth. The plates were incubated at 37 °C for 20-22 h.

4.3.2 RNAi Reverse Transfection

All siRNA reverse transfections were performed using a final siRNA concentration of 20 nM. First siRNA, DMEM and RNAiMax mix was prepared (see table 4.7 for volumes and concentrations) and incubated at RT for 1 h. Meanwhile desired cell dilution was prepared (see table 4.7). After the incubation time of the siRNA, DMEM and RNAiMax mix, corresponding volumes of the mix was added per well followed by adding the corresponding volume of diluted cells (see table 4.7). Then, cells were incubated at 37 °C for 72 h before further steps followed according to the need.

Table 4.7 RNAi Reverse Transfection Conditions

Plate format	96 well	24 well	6 well
Cell line	HeLa-DC-SIGN	HeLa-DC-SIGN	HeLa-DC-SIGN
Number of dispensed cells	2'000	40'000	500'000
Total Vol./well (µl)	100	500	2'000
Final siRNA conc./well (nM)	20	20	20
Vol. of diluted cells (µl)	70	400	1'900
Vol. of 10 µM siRNA stock (µl)	0	1	4
Vol. of 133.33 nM siRNA stock (µl)	15	0	0
Vol. DMEM (µl)	14.9	98.5	93
Vol. RNAiMax (µl)	0.1	0.5	3

Abbreviations: Vol., volume; conc., concentration

4.4 Virus Handling

4.4.0.1 UUKV production

UUKV particles were produced using BHK-21 cells. BHK-21 cells that were ∼80% confluent in T175 cell culture flask were splited 1:2 24 h before virus infection. Flasks were put on a flat surface during 10 min before incubation at 37 °C. 24 h after seeding, cells were ∼70% to ∼80% confluent and were washed once with GMEM containing FCS, 10%TPB, 1% Glu. Virus dilution (moi ∼0.1; ∼3.00e+6 ffu) was prepared using 15 ml of GMEM, 10%TPB, 1% Glu/T175 cell culture flask. Cell medium was removed and 15 ml/flask of diluted virus was added to cells, except for one flask that served as control to monitor virus production. Cells were incubated at 37 °C for 1 h. Then medium was removed and 35 ml/flask of GMEM containing 10%TPB, 1% Glu was added. Cells were incubated for 40 h at 37 °C. and regularly monitored. Supernatant was collected when the cells showed a clear cytotoxic effect compared to the control BHK-21 cells i.e. when they started to float in the medium. Supernatant was centrifuged at 2'000 g, at 4 °C, for 20 min, collected in 50 ml tubes, and Hepes was added (10 mM final concentration (conc.)). Depending on requirement supernatant was concentrated and purified or the supernatant was frozen.

4.4.0.2 Production of VSV Pseudotyped Lentivirus Particles

VSV pseudotyped lentivirus particles were produced by cotransfection of HEK293T cells with the p8.71 plasmid, encoding the gag and pol proteins of the human immunodeficiency virus (HIV), the pVSVG plasmid, encoding for

the glycoprotein of vesicular stomatitis virus (VSV-G), and the vector pTrip encoding for DC-SIGN (pTrip-DC-SIGN).

2x10e+06 HEK293T cells were seeded per Petri Dish (100x20 mm) and incubated for ∼16 h (cells should be 50%-80% confluent for transfection step). 3 h before transfection using the CalPhos^{TM} mammalian transfection kit, cells were washed once with culture medium. 500 μl of transfection mix was prepared containing 250 mM $CaCl_2$ and 6 μg of plasmids. Plasmids, p8.71, pTrip-DC-SIGN, pVSVG, were used in a proportion of 1.5:1.5:1. After vortexing gently, the mix was incubated at RT for 20 min. 2.5 ml 2x HBS buffer were added in a 50 ml falcon tube and the transfection mix was added slowly while vortexing carefully. Transfection solution was incubated at RT for 20 min. Then 1 ml of the transfection solution was added dropwise to each dish, dishes were moved gently back and forth to distribute transfection solution evenly, and cells were incubated at 37 °C for 16 h. After incubation time cells were washed once with culture medium and further incubated in culture medium containing 20% Hepes for 30 h to 50 h, depending on the shape of the cells. Finally, supernatant was harvest, centrifuged at 2'000 g, at 4 °C, for 20 min, and virus was concentrated (see subsection 4.4.0.3).

4.4.0.3 Virus Concentration

33.5 ml of supernatant was added to a SW28 Beckmann plastic tube. 2.5 ml/ SW28 tube of 20% sucrose diluted in HNE buffer was added on the bottom of the tube (a volume of 3 ml of 20% sucrose was imbibed during pipetting). Tubes were centrifuged at 96'000 g, at 8 °C for 2 h. Thereafter, supernatant was disposed and additional droplets were dried with a tissue by not touching the pellet. Then, 300 μl of HNE buffer was added, the tube was covered by Parafilm and incubated on ice for at least 1 h. The pellet was resuspended by pipetting several times up and down, the virus was collected in a 2 ml tube and centrifuged at 3'000 g at 4 °C for 15 min. Then, the virus was aliquoted and stored at −80 °C.

4.4.0.4 Virus Labeling

Virus was labeled with BodipyTR by directly adding the dye at 5-fold molar excess over viral glycoproteins to the purified virus, which was followed by mixing shortly and incubating for 2 h at 4 °C.

4.4.0.5 Virus Purification

Labeled viruses were purified over a linear sucrose gradient (20% to 40% w/v in HNE buffer) by centrifugation at 100'000 g, at 4 °C for 2 h. Sucrose gradi-

ent was prepared in SW55 Beckmann plastic tube using Gradient Master^{TM} apparatus with the following settings: time 1 min 20 s, tilt angle 85 °, and speed of rotation 20 rpm.

4.4.0.6 Virus Quantification

To determine virus concentration of produced viruses a focus-forming unit assay was performed. 200'000 BHK-21 cells per well of a 24-well plate were seeded and incubated at 37 °C for 16 h. Tenfold serial dilutions of virus were prepared in MEM medium containing 5% TPB, 2% Hepes. Cells were washed and 200 μl/well of MEM medium containing 5% TPB, 2% Hepes was added. Then 200 μl/well of diluted viruses were added and cells were incubated at 37 °C for 1 h. Meanwhile, CMC/MEM 10% FCS, 10%TPB, and 2% Hepes (1:2) mix was prepared and incubated at RT on a roller till incubation time of cells was over. After the incubation of the cells 400 μl/well of CMC/MEM mix was added and the cells incubated at 37 °C for 48 h. Then, cells were washed once with 1 ml/well of MEM medium and 300 μl of FA 4% was added for 20 min. Cells were washed once with 1 ml of FPB. 200 μl/well of the U2 antibody (1:1000, diluted in FBP) was added and cells were incubated at RT for 1 h. Thereafter, cells were washed once with FPB, 200 μl/well of the secondary antibody α rabbit HRP (1/400, diluted in FPB) was added, and cells were incubated at RT for 45 min. Then cells were washed once with 1 ml/well FPB, FPB was removed, and 200 μl/well of DAB solution was added for 2 min to 10 min. Cells were washed with 1 ml of PBS1x, PBS1x was removed and cells were air dried. Finally, foci were counted and foci forming units (ffu)/ml was calculated.

The amount of the viral glycoproteins was estimated by running different volumes of viruses (2 μl, 5 μl, and 12 μl) in presence of LDS sample buffer under non-reducing conditions in a 4%-12% gradient gel. In parallel, different amounts of BSA (0.125 μg, 0.25 μg, 0.5 μg, and 1 μg) were loaded as calibration standard to allow semi-quantification of glycoproteins. Gels were fixed for 1 h using fixation buffer followed by staining with Coomassie blue solution over night. Semi-quantification was done by colorimetric analysis using open source software ImageJ.

4.5 Infection Assay

Infection of cells treated with siRNA or miRNA was performed 72 h after reverse transfection. Cells were washed and detached using PBS1x, EDTA 0.5 nM. Subsequently cells were counted and 300'00 cells diluted in infection

medium were challenged with UUKV moi 0.5 to moi 5 (titer determined on BHK-21 cells) at 37 °C for 1 h. Thereafter, virus inoculum was replaced by culture medium and cells were further incubated for 8 h. Then, cells were washed using PBS1x, detached by Trypsin/EDTA 0.5 mM, and transferred into 96 well plates. Then cells were fixed with 4% Formaldehyde (FA) at RT for 20 min followed by two washing steps with FPB. Washing steps were performed by pelleting and resuspending cells in FPB. Afterwards, cells were either permeabilized with 100 μl FPB at RT for 20 min followed by incubating cells with 100 μl of primary antibody 8B11A3 (mouse α N, 1:500, diluted in FPB) at RT for 1.5 h or cells were directly incubated with 100 μl of primary antibody 8B11A3 (1:500, diluted in FPB) at 4 °C over night. After incubation with the first antibody two washing steps were performed and cells were incubated with 100 μl of secondary antibody goat α mouse Alexa Fluor 647 at RT for 45 min. Finally, cells were washed once with FPB and once with PBS1x followed by flow cytometry analysis.

4.6 Endocytosis Bypass Assay

400'000 cells were reverse transfected with miRs, ASN and N4 in 24-well plates for 72 h (see 4.3.2). Then, cells were washed with pre-chilled binding buffer (BB) and incubated for 10 min on ice followed by pre binding of UUKV (moi 0.5) to cells for 1.5 h in pre-chilled BB by gently rocking. Thereafter, cells were washed twice with BB on ice, BB was removed and the plate was transferred to RT. 1 ml/well of pre-warmed pH buffer was added by starting from higher pH and cells were incubated in water bath at 37 °C for 1.5 min. Cells were immediately transferred back on ice and washed three times with 1 ml of post-infection medium (PIM) by pelleting and resuspending cells using centrifugation (1'200 g, 4 °C for 3 min). The supernatant was removed and 1 ml/well of pre-warmed culture medium containing 30 mM Hepes, 1x NEAA, and 50 mM NH_4Cl pH 7.4 was added. Then cells were incubated at 37 °C for 8 h and detached using Trypsin/EDTA 0.5 mM. Detached cells were transferred to 96-well plate and fixed using 4% FA at RT for 20 min. Then cells were stained for flow cytometry analysis as described under 4.5.

4.7 DC-SIGN Surface Expression Assay

Cells were reverse transfected with miR-142-3p and ASN in 6-well plates. 72 h post-transfection, cells were washed and detached using PBS1x, containing 0.5 mM EDTA for 10 min. Subsequently, PBS1x was added to dilute

PBS1x/EDTA solution and detached cells were transferred to a 15 ml falcon tube. After centrifugation at 1'300 g at 4 °C for 3 min, cells were resuspended in 5 ml pre-chilled PBS1x. 300'000 cells were transferred into a well of a 96-well plate and washed once by pelleting and resuspending cells in PBS1x. All steps were performed on ice. Staining of DC-SIGN was performed with 100 μl/well FAB1621P or with isotype control (IgG2A coupled to phycoerythrin) for 45 min. All antibodies were diluted 1:50 in pre-chilled PBS1x containing 0.2% BSA. After staining, flow cytometry of the cells resuspended in 400 μl PBS1x were immediately performed using FACS Calibur. The PE signal was acquired in the FL-2 channel.

4.8 Binding Assay

Cells were reverse transfected with miR-142-3p and ASN in 6-well plates. 72 h post-transfection, cells were washed and detached using PBS1x, containing 0.5 mM EDTA for 10 min. Subsequently, PBS1x was added to dilute PBS1x/EDTA solution and detached cells were transferred to a 15 ml falcon tube. Cells were washed by pelleting and resuspending cells in BB. Then, 300'000 cells were added to a well of a 96-well plate and incubated on ice for 10 min. Afterwards cells were centrifuged, the supernatant was removed and 100 μl/well of UUKV coupled to Alexa Fluor 488 (UUKV-AF488, moi 2, diluted in BB) was added on ice for 1 h. After incubation, cells were washed using 200 μl/well of cold FB buffer and cells were fixed using 4% FA at RT for 20 min. Finally, cells were washed using PBS1x and flow cytometry analysis was performed.

4.9 Internalization Assay

Cells were reverse transfected with miR-142-3p and ASN in 6-well plates. 72 h post-transfection, cells were washed and detached using PBS1x, containing 0.5 mM EDTA for 10 min. Subsequently, PBS1x was added to dilute PBS1x/EDTA solution and detached cells were transferred to a 15 ml falcon tube. Cells were washed by pelleting and resuspending cells in BB. Then, 300'000 cells were added to a well of a 96-well plate and incubated on ice for 10 min. Afterwards cells were centrifuged, the supernatant was removed and 100 μl/well of UUKV coupled to Alexa Fluor 488 (UUKV-AF488, moi 5, diluted in BB) was added on ice for 45 min. Then cells were washed, supernatant was removed, and pre-warmed infection medium was added and cells were incubated at 37 °C in the waterbath for 10 min. After cells were

washed with PBS1x on ice and fixed using 4% FA for 20 min. Then cell were washed once and flow cytometry of the cells resuspended in 400 μl PBS1x were performed using FACS Calibur.

4.10 Fusion Assay

Cells were reverse transfected with miR-142-3-p and ASN in 6-well plates. 72 h post-transfection, cells were washed three times using 1 ml of PBS1x, detached using PBS1x, 0.5 mM EDTA and transferred to 15 ml falcon tube. Then cells were washed by pelleting and resuspending cells in culture medium, counted and diluted in culture medium to a conc. of 500'000 cells/1 ml. 1 ml of cells were added to a 1.5 ml Eppendorf tube for each condition. Then cells were exposed to R18-labelled UUKV (UUKV-R18, moi 5, diluted in BB) on ice, in the dark for 1 h. After incubation time, cells were washed using DMEM containing 0.2% BSA and 20 mM Hepes. The medium was replaced by medium with or without NH_4Cl (50 mM) and cells were transferred to "high-precision cells" (Hellma Analytics). Finally, fusion kinetics was monitored at 37 °C over a time range from 0 min to 1 h using a Varian Cary Eclipse Fluorescence Spectrophotometer (Agilent Technologies). For normalization steps, cells were lysed using Triton-X-100 at the end of the monitoring time.

4.11 Co-localization Assay

5'000 cells per well of a 8-well chamber were dispensed in culture medium and incubated at 37 °C over night. Then, cells were washed using BB and transfected with 100 ng of VAMP-3-GFP plasmid using Lipofectamine 2'000 according to manufacture protocol. After 20 h incubation at 37 °C, cells were washed and UUKV-R18 (moi 5) was bound to cells on ice for 45 min. Then, cells were washed using PBS1x and fixed by FA 4% for 20 min. Afterwards, cells were washed, PBS1x was added to each well and cells were analyzed using confocal fluorescence Zeiss 510M microscope. 63x 1.4 NA Plan-Apochromat immersion oil objective was used. Light excitation was done with an Argon laser (488) at 2.4 mW intensity and a HeNe laser at 1 mW intensity.

4.12 Microarray Gene Expression Analysis

Microarray experiments were performed by the Functional Genomics Center Zurich using Agilent Humane Gene Expression 8x60k chips. Total mRNA was isolated from HeLa-DC-SIGN cells using TRIZOL reagent according to manufacture protocol followed by DNase digestions and two purification steps using Qiagen RNeasy Mini Kit. Integrity, purity and concentration of mRNA was assessed by Nano Drop 1000 Spectrophotometer (Thermo Scientific) and by Agilent 2100 Bioanalyzer. Only, when total mRNA showed A260/A280 purity ≥ 2 and no degradation products, samples were further processed.

Microarray data were normalized using quantile normalization method. Hit selection based on two group analysis combined with fold change calculation using limma package written for open source software R (www.bioconductor.org/packages/release/bioc/html/limma.html)

.

4.13 Protocols for RNAi screening

4.13.1 siRNA Libraries

Screens were performed with genome-wide siRNA libraries from two different vendors, Qiagen (Leiden, Germany) and Dharmacon (Thermo Fisher Scientific, Waltham, Massachusetts, US). The Qiagen library consisted of 296 384-well plates and originally 4 different siRNA per gene. SiRNAs that targeted the same gene were located in different plates at the same well position. The Dharmacon library comprised 57 384-well plates, and each well contained a pool of four different siRNAs targeting the same gene

4.13.2 Liquid Handling

All liquid handling steps during the screening procedures were performed using "EL406 Microplate Washer & Dispenser" and "BioStack Microplate Stacker" from BioTek.

4.13.2.1 Reverse Transfection

Reverse transfection was performed by adding 25 μl/well of DMEM-Lipofectamine RNAiMAX mix to pre-dispensed siRNAs followed by an incubation at RT for 1 h to form lipid-siRNA complexes. DMEM-Lipofectamine RNAiMAX mix consisted of 24.9 μl of DMEM and 0.1 μl RNAiMax. After

the incubation time, 400 HeLa-DC-SIGN cells diluted in 50 μ culture medium was added per well. The cells were incubated at 37 °C for 72 h.

4.13.3 UUKV Infection

Cells were washed with DMEM and challenged with UUKV (15'000 ffu, approximately moi 5, titer determined on BHK-21 cells) diluted in infection medium. Then cells were incubated at 37 °C for 1 h. Thereafter, virus inoculum was replaced by culture medium and cells were further incubated for 19 h followed by the staining phase.

4.13.4 Staining Procedures

Cells were washed twice with PBS1x followed by incubation with 50 μl/well of the primary antibody 8B11A3 (mouse αN, 1:500 diluted in Triton-X-100 0.1%, 0.2% BSA) at RT for 1.5 h. Afterwards, cells were washed twice with PBS1x and incubated with 50 μl/well of a mix containing Hoechst 33258 (final conc. 1 μg/ml) and the secondary antibody goat α mouse Alexa Fluor 488 at RT for 45 min (1:1'000, diluted in PBS1x, 0.2% BSA). Finally, cells were washed twice with PBS1x, 0.04% NaN_3, plates were sealed and pictures were acquired by microscopy.

4.13.5 Fluorescence Microscopy

Stained screening plates were imaged using automated inverted epifluorescent microscopes (MD ImageXpress, Molecular Devices, Wals-Siezenheim, Austria). 9 pictures per well for each channel (cellular DNA / Hoechst 33258 and UUKV N / Alexa Fluor 488) were acquired using 10x 0.3 NA Plan Fluor objective. MD was equipped with the photometric CoolSNAP HQ CCD (charge-coupled device) camera, with a 14-bit digitizer (10 MHz and 20 MHz) to produce monochrome images at a resolution of 1392 x 1040 pixel size of 6.45 μm x 6.45 μm.

4.13.6 Imaging

4.13.6.1 Segmentation

Segmentation was performed to identify cells in the digital images received from the microscopy of stained screening plates using adapted MATLAB open-source software CellProfiler [150].

4.13.6.2 Classifcation

To classify identified cells in the segmentation phase into infected and non-infected cells open-source software Advanced Cell Classifier was used. Classification was performed using Vote-Weka method [151].

4.13.7 Up-to-date Annotation of siRNA Libraries

The up-to-data annotation was performed based on the gene information release from November 2012 by the National Center for Biotechnology Information (NCBI).

4.13.8 Statistics

For statistical analysis we used the open source software environment R (http://cran.r-project.org/). Data received from flow cytometry were evaluated using the software FlowJo. Experiments were performed in three independent replicates except the Qiagen screen and the bypass experiment, which were performed once.

4.13.8.1 Normalization

To normalize systematic "bowl-shaped" infection edge effect that we observed in the screening data we used local polynomial regression fitting "loess" implemented in the open source software R. Robust settings (family = "symmetric") were chosen and surface fitting was computed exactly (control = loess.control [surface = "direct"]). Plates of the Qiagen screen were normalized using MAD with the adjusting factor 1.4826 for asymptotically normal consistency.

4.13.8.2 Quality Control

Quality assessment of controls was performed using SSMD method (see table 1.4). Stars plots were used to summarize the overall quality of screening plates. For the Qiagen screen, only plates for which at least three controls were classified as good or excellent by the SSMD method were taken into account for further analysis. For the Dharmacon screen, plates were skipped when in two plates of the three replicates ≥ 2 controls were classified by the SSMD method as inferior or poor.

4.13.8.3 Hit Definition

For the Qiagen screen genes that showed a p-value $\leq$0.01 or $\leq$0.001 were defined as preliminary inhibitor or enhancer hits. In the Dharmacon screen the SSMD method combined with fold change approach was uses to define hits. To define a gene as a preliminary inhibitor hit, a fold change threshold of ≤ 0.5 and a SSMD value $\leq$ -3 were chosen. To define a gene as a preliminary enhancer hit, a fold change threshold of 1.5 and a SSMD value ≥ 2 were chosen.

4.13.9 Bioinformatics Tools

For classification of the screening hits and the down- or upregulated genes by miR-142-3p into known or predicted protein interactions or functional pathways we used the open-source tools STRING 9.0 (http://string-db.org) and REACTOME (http://www.reactome.org).

Chapter 5

Supplementary Data

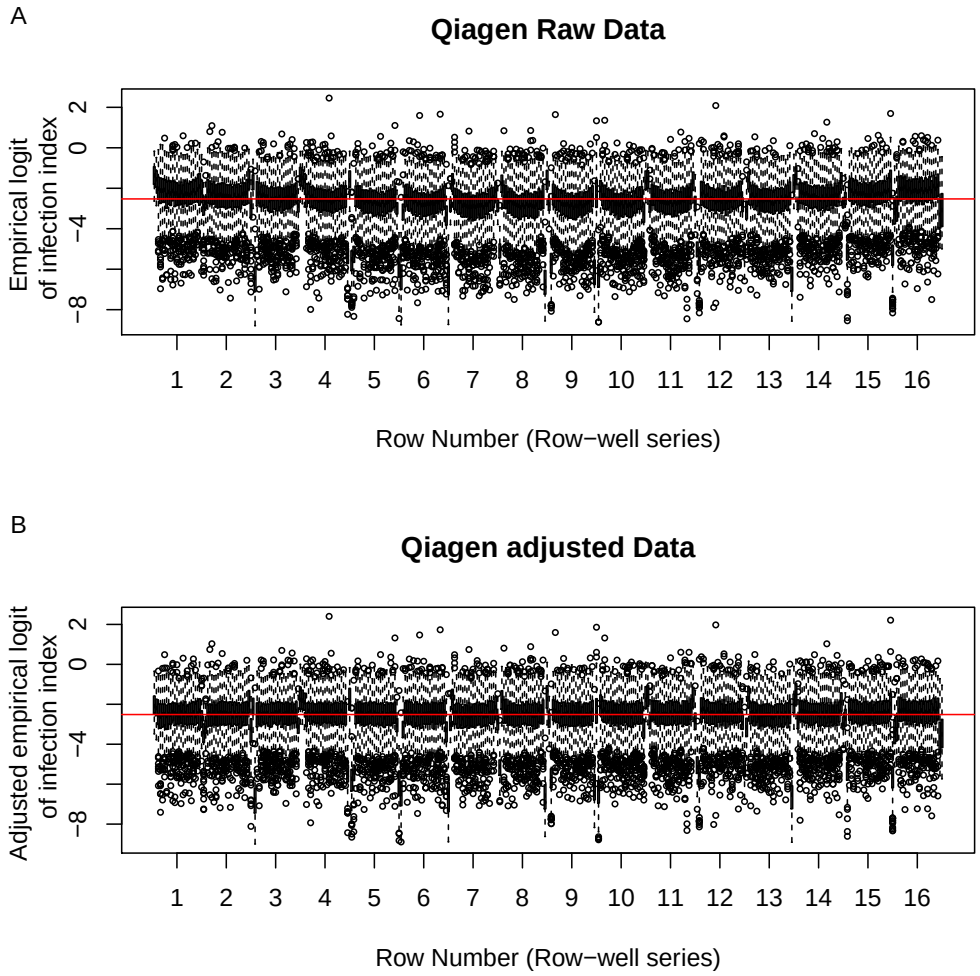

Supplementary figure 5.1 Adjustment of systematic spatial effect in Qiagen screen. A) Row-well series plot of empirical logit transformed Qiagen raw data. The values of the x-axis are the indices of the positions of a well in a row, whereas the labels in the x-axis are the row numbers. The distribution of the well data at the same position is displayed by a box plot. B) Row-well series plot of empirical logit transformed Qiagen data adjusted to systematic spatial effect using loess (locally weighted scatterplot smoothing) method. Empirical logit values 0, -0.5, -1, -2, -4, and -6 of infection index correspond to infection index of 50%, 38%, 27%,12%, 2%, and 0.2%, respectively. Red lines show median empirical logit of infection index over all data to better visualize the infection edge effect.

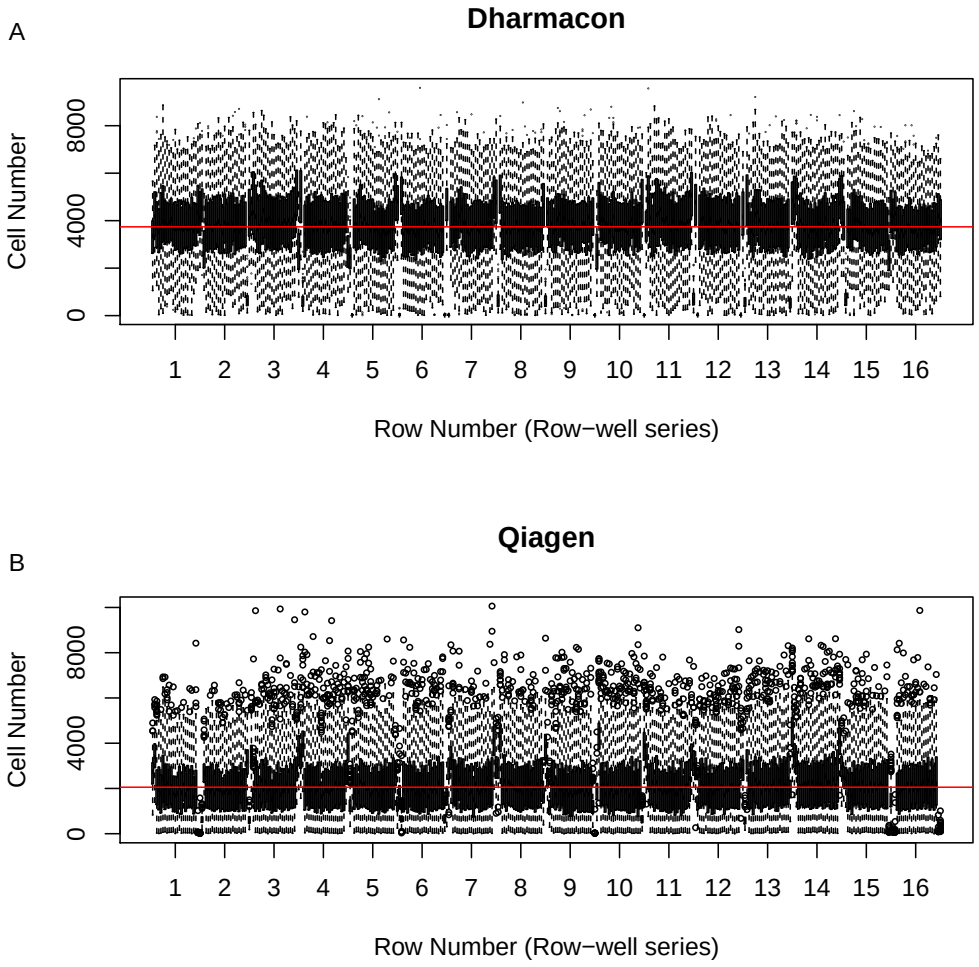

Supplementary figure 5.2 Row series plot for cell number of Dharmacon (A) and Qiagen (B) screen. The values of the x-axis are the indices of the positions of a well in a row, whereas the labels in the x-axis are the row numbers. The distribution of the well data at the same position is displayed by a box plot.

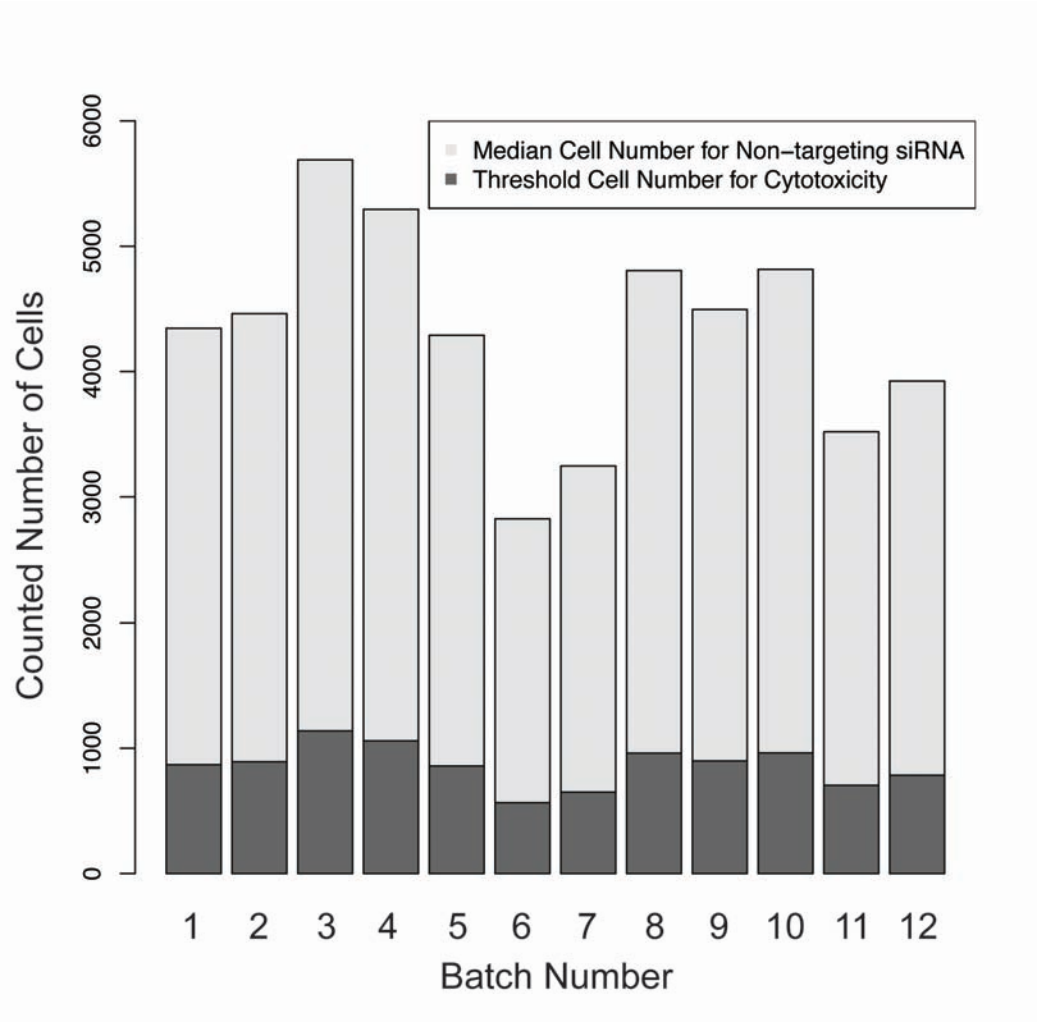

Supplementary figure 5.3 Cell number thresholds that defines cytotoxicity for each batch in the Qiagen screen. Batch thresholds were defined as 25% of the median cell number calculated from all the non-targeting controls within a batch.

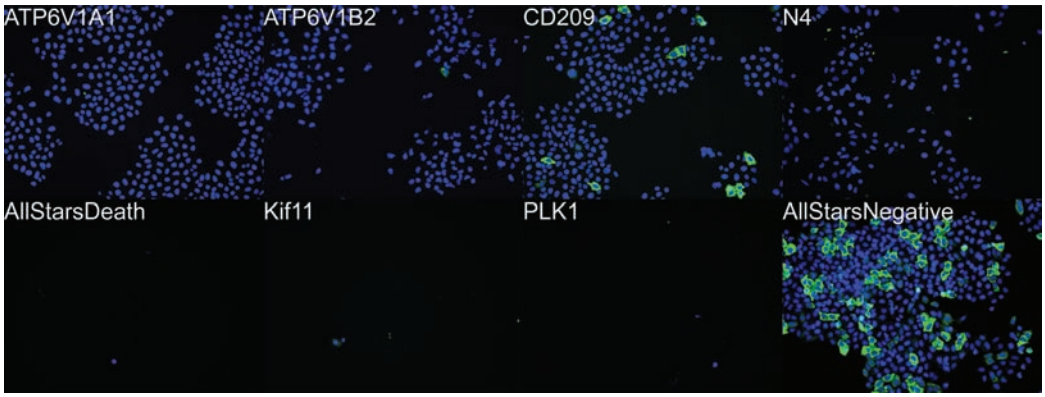

Supplementary figure 5.4 Microscopy pictures of expected Qiagen control siRNAs effects on UUKV virus infection or cell viability after successful siRNA transfection of cells. The siRNAs ATP6V1A1, ATP6V1B2, CD209, N4, Kif11, and PLK1 targeting vacuolar proton pump catalytic subunit A, the UUKV receptor DC-SIGN, the viral nucleoprotein N, kinesin family member 11, and polo-like kinase1 serve as positive controls for infection or cell death. AllStarsDeath is a company design positive control siRNA for cell viability.

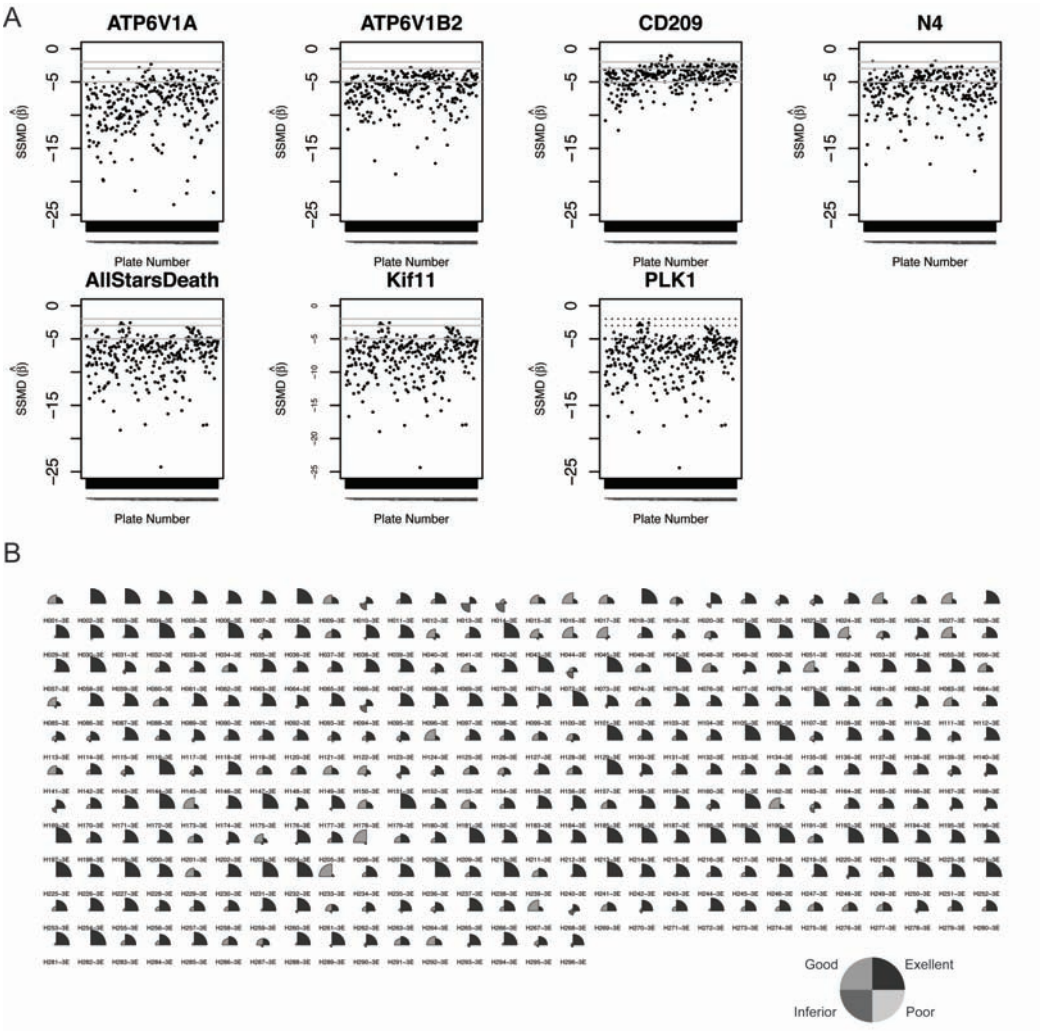

Supplementary figure 5.5 Qualtiy assessment of Qiagen screen A) Assessment of quality for single within-plate positive siRNA controls based on strictly standardized means difference (SSMD) cutoff criteria for very strong controls. Gray lines show $\hat{\beta}$ cutoff values -5, -3, and -2 indicating excellent ($\hat{\beta} \leq$ -5), good (-5 $< \hat{\beta} \leq$ -3), inferior (-3 $< \hat{\beta} \leq$ -2) and poor ($\hat{\beta} >$ -2) quality. B) Star plots indicates single plate quality by summarizing determined SSMD based quality of the seven single within-plate positive controls. The letter codes specify single plates. Segments area of a stars show the amount of positive siRNA controls classified as excellent, good, inferior, or poor.

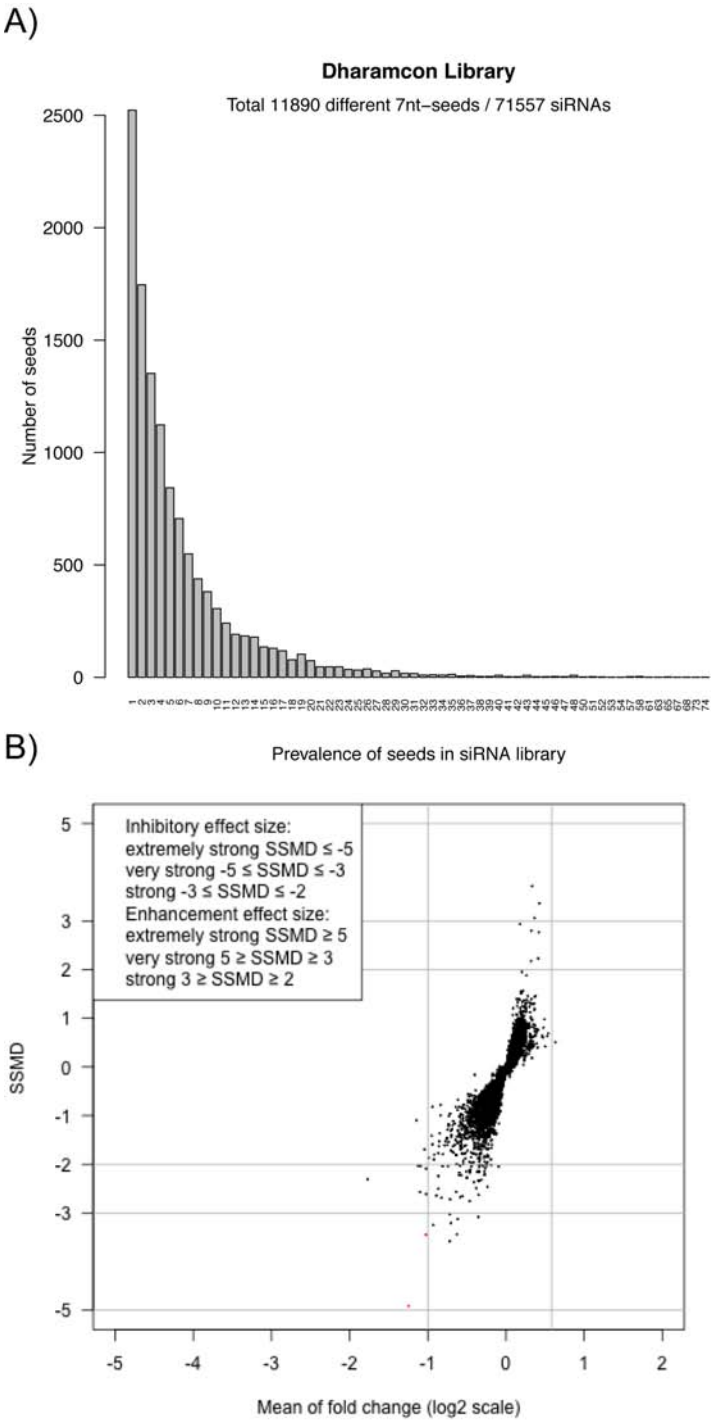

Supplementary figure 5.6 Prevalence of 7nt-seeds in Dharmacon library and their effects on UUKV infection A) 11890 different 7nt-seeds were identified. 2523 seeds were present in one siRNA. Remaining seeds were shared by minimal 2 up to maximal 74 siRNAs. B) Effect size on UUKV infection was calculated for all those seeds that were shared by at least 3 different siRNAs (totally 7622 seeds). To calculate effect size, the SSMD method combined with fold-change approach was used. 2 seeds showed a "very" strong inhibition effect on UUKV infection with a fold-change ≤ 0.5 (-1 on log2 scale) and are indicated in the figure by red dots.

Supplementary table 5.1 Intersect Qiagen and Dharmacon Hits

Intersect Hits (Gene Symbol)	Description
ALDH18A1	aldehyde dehydrogenase 18 family, member A1
ATP6V0B	ATPase, H+ transporting, lysosomal 21kDa, V0 subunit b; Proton-conducting pore forming subunit of the membrane integral V0 complex of vacuolar ATPase. V-ATPase is responsible for acidifying a variety of intracellular compartments in eukaryotic cells
ATP6V0C	ATPase, H+ transporting, lysosomal 16kDa, V0 subunit c; Proton-conducting pore forming subunit of the membrane integral V0 complex of vacuolar ATPase. V-ATPase is responsible for acidifying a variety of intracellular compartments in eukaryotic cells
ATP6V0D1	ATPase, H+ transporting, lysosomal 38kDa, V0 subunit d1; Subunit of the integral membrane V0 complex of vacuolar ATPase. Vacuolar ATPase is responsible for acidifying a variety of intracellular compartments in eukaryotic cells, thus providing most of the energy required for transport processes in the vacuolar system. May play a role in coupling of proton transport and ATP hydrolysis
ATP6V0E1	ATPase, H+ transporting, lysosomal 9kDa, V0 subunit e1; Vacuolar ATPase is responsible for acidifying a variety of intracellular compartments in eukaryotic cells
ATP6V1A	ATPase, H+ transporting, lysosomal 70kDa, V1 subunit A; Catalytic subunit of the peripheral V1 complex of vacuolar ATPase. V-ATPase vacuolar ATPase is responsible for acidifying a variety of intracellular compartments in eukaryotic cells
ATP6V1B2	ATPase, H+ transporting, lysosomal 56/58kDa, V1 subunit B2; Non-catalytic subunit of the peripheral V1 complex of vacuolar ATPase. V-ATPase is responsible for acidifying a variety of intracellular compartments in eukaryotic cells
ATP6V1D	ATPase, H+ transporting, lysosomal 34kDa, V1 subunit D; Subunit of the peripheral V1 complex of vacuolar ATPase. Vacuolar ATPase is responsible for acidifying a variety of intracellular compartments in eukaryotic cells, thus providing most of the energy required for transport processes in the vacuolar system
ATP6V1G1	ATPase, H+ transporting, lysosomal 13kDa, V1 subunit G1; Catalytic subunit of the peripheral V1 complex of vacuolar ATPase (V-ATPase). V-ATPase is responsible for acidifying a variety of intracellular compartments in eukaryotic cells
DNAJC17	DnaJ (Hsp40) homolog, subfamily C, member 17
EEF2	eukaryotic translation elongation factor 2; This protein promotes the GTP-dependent translocation of the nascent protein chain from the A-site to the P-site of the ribosome

Continued on next page

Supplementary table 5.1 Intersect Qiagen and Dharmacon Hits – Continued from previous page

Intersect Hits (Gene Symbol)	Description
HUWE1	HECT, UBA and WWE domain containing 1; E3 ubiquitin-protein ligase which mediates ubiquitination and subsequent proteasomal degradation of target proteins. Regulates apoptosis by catalyzing the polyubiquitination and degradation of MCL1. Also ubiquitinates the p53 tumor suppressor and core histones including H1, H2A, H2B, H3 and H4. Binds to an upstream initiator-like sequence in the preprodynorphin gene. Regulates neural differentiation and proliferation by catalyzing the polyubiquitination and degradation of MYCN. May regulate abundance of CDC6 after DNA damage by polyubiquitinating
LY6E	lymphocyte antigen 6 complex, locus E
RHBDL1	rhomboid, veinlet-like 1 (Drosophila); May be involved in regulated intramembrane proteolysis and the subsequent release of functional polypeptides from their membrane anchors
RNASEK	ribonuclease, RNase K; Endoribonuclease which preferentially cleaves ApU and ApG phosphodiester bonds. Hydrolyzes UpU bonds at a lower rate
RPS25	ribosomal protein S25
VAMP3	vesicle-associated membrane protein 3 (cellubrevin); Trafficking protein from a constitutively recycling pathway
WDR7	WD repeat domain 7

Protein description adapted from STRING 9.0 (string-db-org)

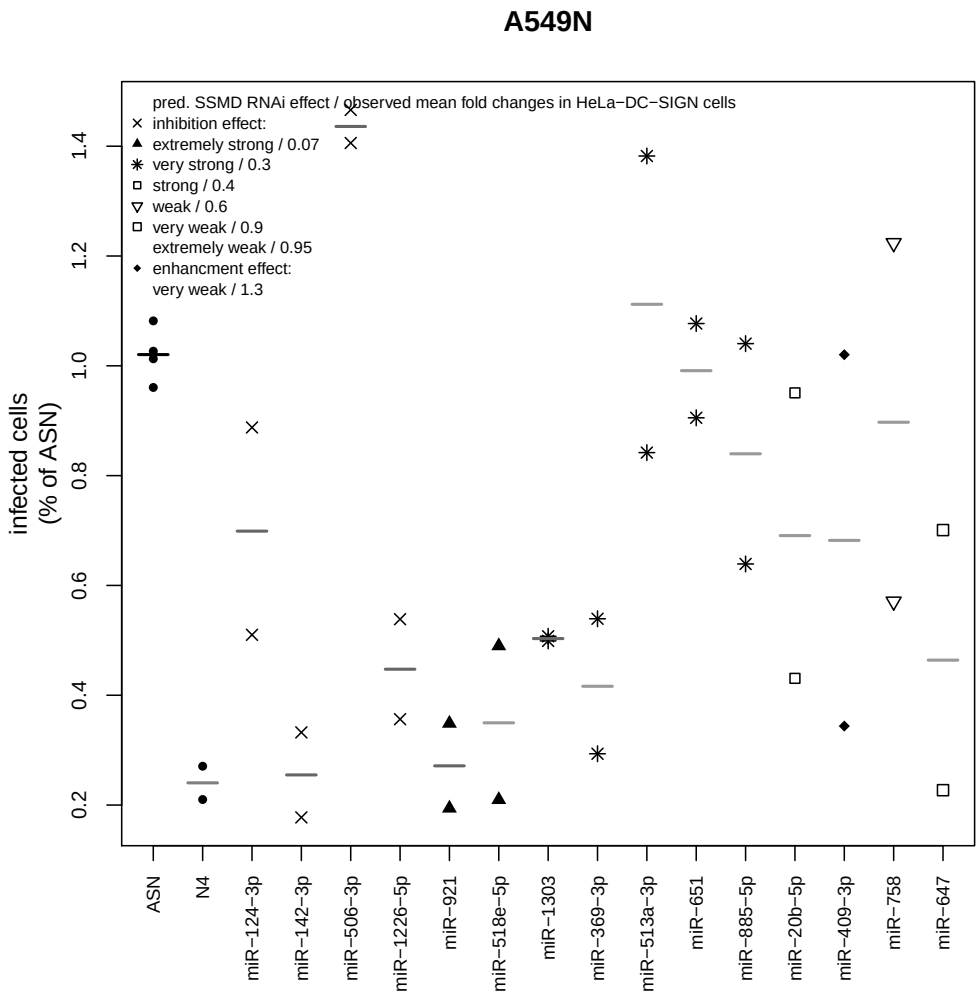

Supplementary figure 5.7 Predicted inhibitor miRNA blocks UUKV infection in A549 cells

Bibliography

[1] P.-Y. Lozach, A. Kühbacher, R. Meier, R. Mancini, D. Bitto, M. Bouloy, and A. Helenius, "DC-SIGN as a Receptor for Phleboviruses," *Cell Host and Microbe*, vol. 10, pp. 75–88, July 2011.

[2] R. Meier, A. Helenius, and P.-Y. Lozach, "DC-SIGN, un récepteur des phlébovirus," *médecine/sciences*, vol. 28, pp. 16–18, Jan. 2012.

[3] F. D. Bushman, N. Malani, J. Fernandes, I. D'Orso, G. Cagney, T. L. Diamond, H. Zhou, D. J. Hazuda, A. S. Espeseth, R. König, S. Bandyopadhyay, T. Ideker, S. P. Goff, N. J. Krogan, A. D. Frankel, J. A. T. Young, and S. K. Chanda, "Host Cell Factors in HIV Replication: Meta-Analysis of Genome-Wide Studies," *PLoS Pathogens*, vol. 5, p. e1000437, May 2009.

[4] S. Cherry, "What have RNAi screens taught us about viral–host interactions?," *Current Opinion in Microbiology*, vol. 12, pp. 446–452, Aug. 2009.

[5] A. Fire, S. Xu, M. K. Montgomery, S. A. Kostas, S. E. Driver, and C. C. Mello, "Potent and specific genetic interference by double-stranded RNA in Caenorhabditis elegans," *Nature*, vol. 391, no. 6669, pp. 806–811, 1998.

[6] J. C. Venter, M. D. Adams, E. W. Myers, P. W. Li, R. J. Mural, G. G. Sutton, H. O. Smith, M. Yandell, C. A. Evans, R. A. Holt, J. D. Gocayne, P. Amanatides, R. M. Ballew, D. H. Huson, J. R. Wortman, Q. Zhang, C. D. Kodira, X. H. Zheng, L. Chen, M. Skupski, G. Subramanian, P. D. Thomas, J. Zhang, G. L. G. Miklos, C. Nelson, S. Broder, A. G. Clark, J. Nadeau, V. A. McKusick, N. Zinder, A. J. Levine, R. J. Roberts, M. Simon, C. Slayman, M. Hunkapiller, R. Bolanos, A. Delcher, I. Dew, D. Fasulo, M. Flanigan, L. Florea, A. Halpern, S. Hannenhalli, S. Kravitz, S. Levy, C. Mobarry, K. Reinert, K. Remington, J. Abu-Threideh, E. Beasley, K. Biddick, V. Bonazzi, R. Brandon, M. Cargill, I. Chandramouliswaran, R. Charlab, K. Chaturvedi, Z. Deng, V. Di Francesco, P. Dunn, K. Eilbeck, C. Evangelista, A. E. Gabrielian, W. Gan, W. Ge, F. Gong, Z. Gu, P. Guan, T. J. Heiman, M. E. Higgins, R. R. Ji, Z. Ke, K. A. Ketchum, Z. Lai, Y. Lei, Z. Li, J. Li, Y. Liang, X. Lin, F. Lu, G. V. Merkulov, N. Milshina, H. M. Moore, A. K. Naik, V. A. Narayan, B. Neelam, D. Nusskern, D. B. Rusch, S. Salzberg, W. Shao, B. Shue, J. Sun, Z. Wang, A. Wang, X. Wang, J. Wang, M. Wei, R. Wides, C. Xiao, C. Yan, A. Yao, J. Ye, M. Zhan, W. Zhang, H. Zhang, Q. Zhao, L. Zheng, F. Zhong, W. Zhong, S. Zhu, S. Zhao, D. Gilbert, S. Baumhueter, G. Spier, C. Carter, A. Cravchik, T. Woodage, F. Ali, H. An, A. Awe, D. Baldwin, H. Baden, M. Barnstead, I. Barrow, K. Beeson, D. Busam, A. Carver, A Center, M. L. Cheng, L. Curry, S. Danaher, L. Davenport, R. Desilets, S. Dietz, K. Dodson, L. Doup, S. Ferriera, N. Garg, A. Gluecksmann,

B. Hart, J. Haynes, C. Haynes, C. Heiner, S. Hladun, D. Hostin, J. Houck, T. Howland, C. Ibegwam, J. Johnson, F. Kalush, L. Kline, S. Koduru, A. Love, F. Mann, D. May, S. McCawley, T. McIntosh, I. McMullen, M. Moy, L. Moy, B. Murphy, K. Nelson, C. Pfannkoch, E. Pratts, V. Puri, H. Qureshi, M. Reardon, R. Rodriguez, Y. H. Rogers, D. Romblad, B. Ruhfel, R. Scott, C. Sitter, M. Smallwood, E. Stewart, R. Strong, E. Suh, R. Thomas, N. N. Tint, S. Tse, C. Vech, G. Wang, J. Wetter, S. Williams, M. Williams, S. Windsor, E. Winn-Deen, K. Wolfe, J. Zaveri, K. Zaveri, J. F. Abril, R. Guigó, M. J. Campbell, K. V. Sjolander, B. Karlak, A. Kejariwal, H. Mi, B. Lazareva, T. Hatton, A. Narechania, K. Diemer, A. Muruganujan, N. Guo, S. Sato, V. Bafna, S. Istrail, R. Lippert, R. Schwartz, B. Walenz, S. Yooseph, D. Allen, A. Basu, J. Baxendale, L. Blick, M. Caminha, J. Carnes-Stine, P. Caulk, Y. H. Chiang, M. Coyne, C. Dahlke, A. Mays, M. Dombroski, M. Donnelly, D. Ely, S. Esparham, C. Fosler, H. Gire, S. Glanowski, K. Glasser, A. Glodek, M. Gorokhov, K. Graham, B. Gropman, M. Harris, J. Heil, S. Henderson, J. Hoover, D. Jennings, C. Jordan, J. Jordan, J. Kasha, L. Kagan, C. Kraft, A. Levitsky, M. Lewis, X. Liu, J. Lopez, D. Ma, W. Majoros, J. McDaniel, S. Murphy, M. Newman, T. Nguyen, N. Nguyen, M. Nodell, S. Pan, J. Peck, M. Peterson, W. Rowe, R. Sanders, J. Scott, M. Simpson, T. Smith, A. Sprague, T. Stockwell, R. Turner, E. Venter, M. Wang, M. Wen, D. Wu, M. Wu, A. Xia, A. Zandieh, and X. Zhu, "The sequence of the human genome.," *Science*, vol. 291, pp. 1304–1351, Feb. 2001.

[7] X. P. Chen, M. L. Cong, M. H. Li, Y. J. Kang, Y. M. Feng, A. Plyusnin, J. Xu, and Y. Z. Zhang, "Infection and pathogenesis of Huaiyangshan virus (a novel tick-borne bunyavirus) in laboratory rodents," *Journal of General Virology*, vol. 93, pp. 1288–1293, May 2012.

[8] L. K. McMullan, S. M. Folk, A. J. Kelly, A. MacNeil, C. S. Goldsmith, M. G. Metcalfe, B. C. Batten, C. G. Albariño, S. R. Zaki, P. E. Rollin, W. L. Nicholson, and S. T. Nichol, "A New Phlebovirus Associated with Severe Febrile Illness in Missouri," *New England Journal of Medicine*, vol. 367, pp. 834–841, Aug. 2012.

[9] B. Xu, L. Liu, X. Huang, H. Ma, Y. Zhang, Y. Du, P. Wang, X. Tang, H. Wang, K. Kang, S. Zhang, G. Zhao, W. Wu, Y. Yang, H. Chen, F. Mu, and W. Chen, "Metagenomic Analysis of Fever, Thrombocytopenia and Leukopenia Syndrome (FTLS) in Henan Province, China: Discovery of a New Bunyavirus," *PLoS Pathogens*, vol. 7, p. e1002369, Nov. 2011.

[10] X.-J. Yu, M.-F. Liang, S.-Y. Zhang, Y. Liu, J.-D. Li, Y.-L. Sun, L. Zhang, Q.-F. Zhang, V. L. Popov, C. Li, J. Qu, Q. Li, Y.-P. Zhang, R. Hai, W. Wu, Q. Wang, F.-X. Zhan, X.-J. Wang, B. Kan, S.-W. Wang, K.-L. Wan, H.-Q. Jing, J.-X. Lu, W.-W. Yin, H. Zhou, X.-H. Guan, J.-F. Liu, Z.-Q. Bi, G.-H. Liu, J. Ren, H. Wang, Z. Zhao, J.-D. Song, J.-R. He, T. Wan, J.-S. Zhang, X.-P. Fu, L.-N. Sun, X.-P. Dong, Z.-J. Feng, W.-Z. Yang, T. Hong, Y. Zhang, D. H. Walker, Y. Wang, and D.-X. Li, "Fever with Thrombocytopenia Associated with a Novel Bunyavirus in China," *New England Journal of Medicine*, vol. 364, pp. 1523–1532, Apr. 2011.

[11] Y. Z. Zhang, Y. W. He, Y. A. Dai, Y. Xiong, H. Zheng, D. J. Zhou, J. Li, Q. Sun, X. L. Luo, Y. L. Cheng, X. C. Qin, J. H. Tian, X. P. Chen, B. Yu, D. Jin, W. P. Guo, W. Li, W. Wang, J. S. Peng, G. B. Zhang, S. Zhang, X. M. Chen, Y. Wang, M. H. Li, Z. Li, S. Lu, C. Ye, M. D. de Jong, and J. Xu, "Hemorrhagic Fever Caused by a Novel Bunyavirus in China: Pathogenesis and Correlates of Fatal Outcome," *Clinical Infectious Diseases*, vol. 54, pp. 527–533, Jan. 2012.

[12] M. Pepin, M. Bouloy, B. H. Bird, A. Kemp, and J. Paweska, "Rift Valley fever virus (Bunyaviridae: Phlebovirus): an update on pathogenesis, molecular epidemiology, vectors, diagnostics and prevention," *Veterinary Research*, vol. 41, p. 61, May 2010.

[13] S. S. Soldan and F. González-Scarano, "Emerging infectious diseases: The Bunyaviridae," *Journal of Neurovirology*, vol. 11, pp. 412–423, Jan. 2005.

[14] C. H. C. von Bonsdorff and R. R. Pettersson, "Surface structure of Uukuniemi virus.," *Journal of Virology*, vol. 16, pp. 1296–1307, Oct. 1975.

[15] H. Rönkä, P. Hildén, C. H. Von Bonsdorff, and E. Kuismanen, "Homodimeric association of the spike glycoproteins G1 and G2 of Uukuniemi virus.," *Virology*, vol. 211, pp. 241–250, May 1995.

[16] R. F. R. Pettersson, M. J. M. Hewlett, D. D. Baltimore, and J. M. J. Coffin, "The genome of Uukuniemi virus consists of three unique RNA segments.," *Cell*, vol. 11, pp. 51–63, Apr. 1977.

[17] C. T. Walter and J. N. Barr, "Recent advances in the molecular and cellular biology of bunyaviruses," *Journal of General Virology*, vol. 92, pp. 2467–2484, Oct. 2011.

[18] J. Fontana, N. López-Montero, R. M. Elliott, J. J. Fernández, and C. Risco, "The unique architecture of Bunyamwera virus factories around the Golgi complex," *Cellular Microbiology*, vol. 10, pp. 2012–2028, Oct. 2008.

[19] X. Shi, A. Kohl, V. H. J. Leonard, P. Li, A. McLees, and R. M. Elliott, "Requirement of the N-Terminal Region of Orthobunyavirus Nonstructural Protein NSm for Virus Assembly and Morphogenesis," *Journal of Virology*, vol. 80, pp. 8089–8099, July 2006.

[20] R. R. Kormelink, M. M. Storms, J. J. Van Lent, D. D. Peters, and R. R. Goldbach, "Expression and subcellular location of the NSM protein of tomato spotted wilt virus (TSWV), a putative viral movement protein.," *Virology*, vol. 200, pp. 56–65, Mar. 1994.

[21] S. R. Gerrard, B. H. Bird, C. G. Albariño, and S. T. Nichol, "Synthesis, proteolytic processing and complex formation of N-terminally nested precursor proteins of the Rift Valley fever virus glycoproteins," *Virology*, vol. 359, pp. 124–133, Mar. 2007.

[22] A. Kohl, "Complementarity, sequence and structural elements within the 3' and 5' non-coding regions of the Bunyamwera orthobunyavirus S segment determine promoter strength," *Journal of General Virology*, vol. 85, pp. 3269–3278, Nov. 2004.

[23] M. A. MIR and A. T. Panganiban, "Trimeric Hantavirus Nucleocapsid Protein Binds Specifically to the Viral RNA Panhandle," *Journal of Virology*, vol. 78, pp. 8281–8288, July 2004.

[24] M. A. MIR, "The bunyavirus nucleocapsid protein is an RNA chaperone: Possible roles in viral RNA panhandle formation and genome replication," *RNA*, vol. 12, pp. 272–282, Feb. 2006.

[25] M. Bouloy and C. Hannoun, "Studies on lumbo virus replication. I. RNA-dependent RNA polymerase associated with virions.," *Audio and Electroacoustics Newsletter, IEEE*, vol. 69, pp. 258–264, Jan. 1976.

[26] A. T. Panganiban, "Bunyavirus N: elF4F surrogate and cap-guardian," *Cell Cycle*, vol. 8, pp. 1332–1337, Feb. 2009.

[27] J. N. Barr, "Bunyavirus mRNA synthesis is coupled to translation to prevent premature transcription termination," *RNA*, vol. 13, pp. 731–736, May 2007.

[28] A. M. Andersson, L. Melin, A. Bean, and R. F. Pettersson, "A retention signal necessary and sufficient for Golgi localization maps to the cytoplasmic tail of a Bunyaviridae (Uukuniemi virus) membrane glycoprotein.," *Journal of Virology*, vol. 71, pp. 4717–4727, May 1997.

[29] A. M. A. Andersson and R. F. R. Pettersson, "Targeting of a short peptide derived from the cytoplasmic tail of the G1 membrane glycoprotein of Uukuniemi virus (Bunyaviridae) to the Golgi complex.," *Journal of Virology*, vol. 72, pp. 9585–9596, Nov. 1998.

[30] E. Kuismanen, J. Saraste, and R. F. Pettersson, "Effect of monensin on the assembly of Uukuniemi virus in the Golgi complex.," *Journal of Virology*, vol. 55, pp. 813–822, Aug. 1985.

[31] A. K. Overby, V. L. Popov, R. F. Pettersson, and E. P. A. Neve, "The Cytoplasmic Tails of Uukuniemi Virus (Bunyaviridae) GN and GC Glycoproteins Are Important for Intracellular Targeting and the Budding of Virus-Like Particles," *Journal of Virology*, vol. 81, pp. 11381–11391, Sept. 2007.

[32] N. Oker-Blom, A. Salminen, M. Brummer-Korvenkontio, L. Kaeaeriaeinen, and P. Weckstroem, "Isolation of some viruses other than typical tick-borne encephalitis viruses from Ixodes Ricinus ticks in Finlad.," *Ann Med Exp Biol Fenn*, vol. 42, pp. 109–112, Jan. 1964.

[33] P.-Y. Lozach, R. Mancini, D. Bitto, R. Meier, L. Oestereich, A. K. Överby, R. F. Pettersson, and A. Helenius, "Entry of Bunyaviruses into Mammalian Cells," *Cell Host and Microbe*, vol. 7, pp. 488–499, June 2010.

[34] A. K. Overby, R. F. Pettersson, K. Grünewald, and J. T. Huiskonen, "Insights into bunyavirus architecture from electron cryotomography of Uukuniemi virus.," *Audio, Transactions of the IRE Professional Group on*, vol. 105, pp. 2375–2379, Feb. 2008.

[35] R. F. Pettersson and C. H. Von Bonsdorff, "Ribonucleoproteins of Uukuniemi virus are circular.," *Journal of Virology*, vol. 15, pp. 386–392, Feb. 1975.

[36] B. Geiger, J. P. Spatz, and A. D. Bershadsky, "Environmental sensing through focal adhesions," *Nature Publishing Group*, vol. 10, pp. 21–33, Jan. 2009.

[37] P.-Y. Lozach, J. Huotari, and A. Helenius, "Late-penetrating viruses," *Current Opinion in Virology*, vol. 1, pp. 35–43, July 2011.

[38] M. Marsh and A. Helenius, "Virus Entry: Open Sesame," *Cell*, vol. 124, pp. 729–740, Feb. 2006.

[39] A. E. Smith, "How Viruses Enter Animal Cells," *Science*, vol. 304, pp. 237–242, Apr. 2004.

[40] I. N. I. Gavrilovskaya, M. M. Shepley, R. R. Shaw, M. H. M. Ginsberg, and E. R. E. Mackow, "Beta3 Integrins mediate the cellular entry of hantaviruses that cause respiratory failure.," *PNAS*, vol. 95, pp. 7074–7079, May 1998.

[41] C. M. Filone, S. L. Hanna, M. C. Caino, S. Bambina, R. W. Doms, and S. Cherry, "Rift Valley Fever Virus Infection of Human Cells and Insect Hosts Is Promoted by Protein Kinase C Epsilon," *PLoS ONE*, vol. 5, p. e15483, Nov. 2010.

[42] M. Simon, C. Johansson, Å. Lundkvist, and A. Mirazimi, "Microtubule-dependent and microtubule-independent steps in Crimean-Congo hemorrhagic fever virus replication cycle," *Virology*, vol. 385, pp. 313–322, Mar. 2009.

[43] B. S. Hollidge, N. B. Nedelsky, M. V. Salzano, J. W. Fraser, F. Gonzalez-Scarano, and S. S. Soldan, "Orthobunyavirus Entry into Neurons and Other Mammalian Cells Occurs via Clathrin-Mediated Endocytosis and Requires Trafficking into Early Endosomes," *Journal of Virology*, vol. 86, pp. 7988–8001, July 2012.

[44] M. Jin, J. Park, S. Lee, B. Park, J. Shin, K.-J. Song, T.-I. Ahn, S.-Y. Hwang, B.-Y. Ahn, and K. Ahn, "Hantaan Virus Enters Cells by Clathrin-Dependent Receptor-Mediated Endocytosis," *Virology*, vol. 294, pp. 60–69, Mar. 2002.

[45] R. I. M. Santos, A. H. Rodrigues, M. L. Silva, R. A. Mortara, M. A. Rossi, M. C. l. Jamur, C. Oliver, and E. Arruda, "Oropouche virus entry into HeLa cells involves clathrin and requires endosomal acidification," *Virus Research*, pp. 1–5, Oct. 2008.

[46] M. Simon, C. Johansson, and A. Mirazimi, "Crimean-Congo hemorrhagic fever virus entry and replication is clathrin-, pH- and cholesterol-dependent," *Journal of General Virology*, vol. 90, pp. 210–215, Jan. 2009.

[47] G. J. Doherty and H. T. McMahon, "Mechanisms of Endocytosis," *Annual Review of Biochemistry*, vol. 78, pp. 857–902, June 2009.

[48] J. Mercer, M. Schelhaas, and A. Helenius, "Virus Entry by Endocytosis," *Annual Review of Biochemistry*, vol. 79, pp. 803–833, June 2010.

[49] B. M. B. Collins, A. J. A. McCoy, H. M. H. Kent, P. R. P. Evans, and D. J. D. Owen, "Molecular Architecture and Functional Model of the Endocytic AP2 Complex," *Cell*, vol. 109, pp. 13–13, May 2002.

[50] I. Gaidarov and J. H. Keen, "Phosphoinositide-AP-2 interactions required for targeting to plasma membrane clathrin-coated pits.," *Journal of Cell Biology*, vol. 146, pp. 755–764, Aug. 1999.

[51] G. Rohde, "A phosphatidylinositol (4,5)-bisphosphate binding site within micro2-adaptin regulates clathrin-mediated endocytosis," *The Journal of Cell Biology*, vol. 158, pp. 209–214, July 2002.

[52] S. Ahle and E. Ungewickell, "Auxilin, a newly identified clathrin-associated protein in coated vesicles from bovine brain.," *Journal of Cell Biology*, vol. 111, pp. 19–29, June 1990.

[53] B. B. Doray, I. I. Lee, J. J. Knisely, G. G. Bu, and S. S. Kornfeld, "The gamma/sigma1 and alpha/sigma2 hemicomplexes of clathrin adaptors AP-1 and AP-2 harbor the dileucine recognition site.," *Molecular Biology of the Cell*, vol. 18, pp. 1887–1896, Apr. 2007.

[54] A. Fotin, Y. Cheng, N. Grigorieff, T. Walz, S. C. Harrison, and T. Kirchhausen, "Structure of an auxilin-bound clathrin coat and its implications for the mechanism of uncoating.," *Nature*, vol. 432, pp. 649–653, Dec. 2004.

[55] Y. Kanaoka, S. H. Kimura, I. Okazaki, M. Ikeda, and H. Nojima, "GAK: a cyclin G associated kinase contains a tensin/auxilin-like domain 1The accession number of GAK in the DDBJ/EMBL/GenBank is D38560.1," *FEBS Letters*, vol. 402, pp. 73–80, Feb. 1997.

[56] B. T. Kelly, A. J. McCoy, K. Späte, S. E. Miller, P. R. Evans, S. Höning, and D. J. Owen, "A structural explanation for the binding of endocytic dileucine motifs by the AP2 complex," *Nature*, vol. 456, pp. 976–979, Oct. 2008.

[57] U. Scheele, C. Kalthoff, and E. Ungewickell, "Multiple interactions of auxilin 1 with clathrin and the AP-2 adaptor complex.," *Journal of Biological Chemistry*, vol. 276, pp. 36131–36138, Sept. 2001.

[58] D. M. Schlossman, S. L. Schmid, W. A. Braell, and J. E. Rothman, "An enzyme that removes clathrin coats: purification of an uncoating ATPase.," *Journal of Cell Biology*, vol. 99, pp. 723–733, July 1984.

[59] S. M. Sweitzer and J. E. Hinshaw, "Dynamin Undergoes a GTP-Dependent Conformational Change Causing Vesiculation," *Cell*, vol. 93, pp. 9–9, June 1998.

[60] E. Ungewickell, H. Ungewickell, S. E. Holstein, R. Lindner, K. Prasad, W. Barouch, B. Martin, L. E. Greene, and E. Eisenberg, "Role of auxilin in uncoating clathrin-coated vesicles.," *Nature*, vol. 378, pp. 632–635, Dec. 1995.

[61] R. G. Anderson, "The caveolae membrane system.," *Annual Review of Biochemistry*, vol. 67, pp. 199–225, 1998.

[62] B. Moren, C. Shah, M. T. Howes, N. L. Schieber, H. T. McMahon, R. G. Parton, O. Daumke, and R. Lundmark, "EHD2 regulates caveolar dynamics via ATP-driven targeting and oligomerization," *Molecular Biology of the Cell*, vol. 23, pp. 1316–1329, Mar. 2012.

[63] K. G. Rothberg, J. E. Heuser, W. C. Donzell, Y. S. Ying, J. R. Glenney, and R. G. Anderson, "Caveolin, a protein component of caveolae membrane coats.," *Cell*, vol. 68, pp. 673–682, Feb. 1992.

[64] M. Stoeber, I. K. Stoeck, C. H. a. nni, C. K. E. Bleck, G. Balistreri, and A. Helenius, "Oligomers of the ATPase EHD2 confine caveolae to the plasma membrane through association with actin," *The EMBO Journal*, pp. 1–15, Apr. 2012.

[65] S. Kumari and S. Mayor, "ARF1 is directly involved in dynamin-independent endocytosis," *Nature Cell Biology*, vol. 10, pp. 30–41, Dec. 2007.

[66] R. Lundmark, G. J. Doherty, M. T. Howes, K. Cortese, Y. Vallis, R. G. Parton, and H. T. McMahon, "The GTPase-Activating Protein GRAF1 Regulates the CLIC/GEEC Endocytic Pathway," *Current Biology*, vol. 18, pp. 1802–1808, Nov. 2008.

[67] S. Sabharanjak, P. Sharma, R. G. Parton, and S. Mayor, "GPI-anchored proteins are delivered to recycling endosomes via a distinct cdc42-regulated, clathrin-independent pinocytic pathway.," *Developmental Cell*, vol. 2, pp. 411–423, Apr. 2002.

[68] O. O. Glebov, N. A. Bright, and B. J. Nichols, "Flotillin-1 defines a clathrin-independent endocytic pathway in mammalian cells," *Nature Cell Biology*, vol. 8, pp. 46–54, Dec. 2005.

[69] J. Mercer and A. Helenius, "Gulping rather than sipping: macropinocytosis as a way of virus entry," *Current Opinion in Microbiology*, vol. 15, pp. 490–499, Aug. 2012.

[70] F. I. Schmidt, C. K. E. Bleck, A. Helenius, and J. Mercer, "Vaccinia extracellular virions enter cells by macropinocytosis and acid-activated membrane rupture," *The EMBO Journal*, vol. 30, pp. 3647–3661, July 2011.

[71] I. Gaidarov, Q. Chen, J. R. Falck, K. K. Reddy, and J. H. Keen, "A functional phosphatidylinositol 3,4,5-trisphosphate/phosphoinositide binding domain in the clathrin adaptor AP-2 alpha subunit. Implications for the endocytic pathway.," *Journal of Biological Chemistry*, vol. 271, pp. 20922–20929, Aug. 1996.

[72] S. Honing, D. Ricotta, M. Krauss, K. Spate, B. Spolaore, A. Motley, C. Robinson, V. Haucke, and D. Owen, "Phosphatidylinositol-(4,5)-Bisphosphate Regulates Sorting Signal Recognition by the Clathrin-Associated Adaptor Complex AP2," *Molecular Cell*, vol. 18, pp. 519–531, May 2005.

[73] M. S. Robinson and J. S. Bonifacino, "Adaptor-related proteins.," *Current Opinion in Cell Biology*, vol. 13, pp. 444–453, Aug. 2001.

[74] L. P. Jackson, B. T. Kelly, A. J. McCoy, T. Gaffry, L. C. James, B. M. Collins, S. Höning, P. R. Evans, and D. J. Owen, "A Large-Scale Conformational Change Couples Membrane Recruitment to Cargo Binding in the AP2 Clathrin Adaptor Complex," *Cell*, vol. 141, pp. 1220–1229, June 2010.

[75] D. Ricotta, "Phosphorylation of the AP2 micro subunit by AAK1 mediates high affinity binding to membrane protein sorting signals," *The Journal of Cell Biology*, vol. 156, pp. 791–795, Mar. 2002.

[76] D. J. Owen, Y. Vallis, M. E. Noble, J. B. Hunter, T. R. Dafforn, P. R. Evans, and H. T. McMahon, "A structural explanation for the binding of multiple ligands by the α-adaptin appendage domain," *Cell*, vol. 97, no. 6, pp. 805–815, 1999.

[77] A. Sorkin, "Cargo recognition during clathrin-mediated endocytosis: a team effort," *Current Opinion in Cell Biology*, vol. 16, pp. 392–399, Aug. 2004.

[78] S. Ferguson, A. Raimondi, S. Paradise, H. Shen, K. Mesaki, A. Ferguson, O. Destaing, G. Ko, J. Takasaki, O. Cremona, E. O. Toole, and P. D. Camilli, "Coordinated Actions of Actin and BAR Proteins Upstream of Dynamin at Endocytic Clathrin-Coated Pits," *Developmental Cell*, vol. 17, pp. 811–822, Dec. 2009.

[79] P. P. Wigge, K. K. Köhler, Y. Y. Vallis, C. A. C. Doyle, D. D. Owen, S. P. S. Hunt, and H. T. H. McMahon, "Amphiphysin heterodimers: potential role in clathrin-mediated endocytosis.," *Molecular Biology of the Cell*, vol. 8, pp. 2003–2015, Sept. 1997.

[80] S. M. Ferguson and P. D. Camilli, "Dynamin, a membrane-remodelling GTPase," *Nature Publishing Group*, vol. 13, pp. 75–88, Jan. 2012.

[81] S. L. Newmyer, A. Christensen, and S. Sever, "Auxilin-dynamin interactions link the uncoating ATPase chaperone machinery with vesicle formation.," *Developmental Cell*, vol. 4, pp. 929–940, May 2003.

[82] E. Eisenberg and L. E. Greene, "Multiple Roles of Auxilin and Hsc70 in Clathrin-Mediated Endocytosis," *Traffic*, vol. 8, pp. 640–646, May 2007.

[83] R. G. Parton, B. Joggerst, and K. Simons, "Regulated internalization of caveolae.," *Journal of Cell Biology*, vol. 127, pp. 1199–1215, Dec. 1994.

[84] M. Kalia, S. Kumari, R. Chadda, M. M. Hill, R. G. Parton, and S. Mayor, "Arf6-independent GPI-anchored protein-enriched early endosomal compartments fuse with sorting endosomes via a Rab5/phosphatidylinositol-3'-kinase-dependent machinery.," *Molecular Biology of the Cell*, vol. 17, pp. 3689–3704, July 2006.

[85] J. Mercer and A. Helenius, "Vaccinia Virus Uses Macropinocytosis and Apoptotic Mimicry to Enter Host Cells," *Science*, vol. 320, pp. 531–535, Apr. 2008.

[86] J. Huotari and A. Helenius, "Endosome maturation," *The EMBO Journal*, vol. 30, pp. 3481–3500, Aug. 2011.

[87] C. Raiborg and H. Stenmark, "The ESCRT machinery in endosomal sorting of ubiquitylated membrane proteins," *Nature*, vol. 458, pp. 445–452, Mar. 2009.

[88] V. Haucke, "Phosphoinositide regulation of clathrin-mediated endocytosis.," *Biochemical Society Transactions*, vol. 33, pp. 1285–1289, Nov. 2005.

[89] H. Stenmark, "Rab GTPases as coordinators of vesicle traffic," *Nature Publishing Group*, vol. 10, pp. 513–525, July 2009.

[90] P. Del Conte-Zerial, L. Brusch, J. C. Rink, C. Collinet, Y. Kalaidzidis, M. Zerial, and A. Deutsch, "Membrane identity and GTPase cascades regulated by toggle and cut-out switches," *Molecular Systems Biology*, vol. 4, July 2008.

[91] A. Vonderheit and A. Helenius, "Rab7 Associates with Early Endosomes to Mediate Sorting and Transport of Semliki Forest Virus to Late Endosomes," *PLoS Biology*, vol. 3, no. 7, p. e233, 2005.

[92] R. Mattera and J. S. Bonifacino, "Ubiquitin binding and conjugation regulate the recruitment of Rabex-5 to early endosomes," *The EMBO Journal*, vol. 27, pp. 2484–2494, Sept. 2008.

[93] B. L. B. Grosshans, D. D. Ortiz, and P. P. Novick, "Rabs and their effectors: achieving specificity in membrane traffic.," *PNAS*, vol. 103, pp. 11821–11827, July 2006.

[94] Poteryaev, Datta, Ackema, Zerial, and Spang, "Identification of the Switch in Early-to-Late Endosome Transition," *Cell*, vol. 141, pp. 12–12, Apr. 2010.

[95] J. M. Kinchen and K. S. Ravichandran, "Identification of two evolutionarily conserved genes regulating processing of engulfed apoptotic cells," *Nature*, vol. 464, pp. 778–782, Jan. 2010.

[96] M. A. Lemmon, "Membrane recognition by phospholipid-binding domains," *Nature Publishing Group*, vol. 9, pp. 99–111, Feb. 2008.

[97] M. Vicinanza, G. D'Angelo, A. Di Campli, and M. A. De Matteis, "Function and dysfunction of the PI system in membrane trafficking," *The EMBO Journal*, vol. 27, pp. 2457–2470, Sept. 2008.

[98] O. C. Ikonomov, "Mammalian Cell Morphology and Endocytic Membrane Homeostasis Require Enzymatically Active Phosphoinositide 5-Kinase PIKfyve," *Journal of Biological Chemistry*, vol. 276, pp. 26141–26147, Apr. 2001.

[99] I. Roxrud, H. Stenmark, and L. Malerød, "ESCRT & Co," *Biology of the Cell*, vol. 102, pp. 293–318, Jan. 2012.

[100] T. Wang, Z. Ming, W. Xiaochun, and W. Hong, "Rab7: Role of its protein interaction cascades in endo-lysosomal traffic," *Cellular Signalling*, vol. 23, pp. 516–521, Mar. 2011.

[101] M. Zhang, L. Chen, S. Wang, and T. Wang, "Rab7: roles in membrane trafficking and disease," *Bioscience Reports*, vol. 29, p. 193, June 2009.

[102] M. A. De Matteis and A. Godi, "PI-loting membrane traffic.," *Nature Cell Biology*, vol. 6, pp. 487–492, June 2004.

[103] V. Marshansky and M. Futai, "The V-type H+-ATPase in vesicular trafficking: targeting, regulation and function," *Current Opinion in Cell Biology*, vol. 20, pp. 415–426, Aug. 2008.

[104] C. C. Scott and J. Gruenberg, "Ion flux and the function of endosomes and lysosomes: pH is just the start," *BioEssays*, vol. 33, pp. 103–110, Dec. 2010.

[105] F. Gu, F. Aniento, R. G. Parton, and J. Gruenberg, "Functional dissection of COP-I subunits in the biogenesis of multivesicular endosomes.," *Journal of Cell Biology*, vol. 139, pp. 1183–1195, Nov. 1997.

[106] F. Gu and J. Gruenberg, "Biogenesis of transport intermediates in the endocytic pathway.," *FEBS Letters*, vol. 452, pp. 61–66, June 1999.

[107] P. Saftig and J. Klumperman, "Lysosome biogenesis and lysosomal membrane proteins: trafficking meets function," *Nautre Reviews Molecular Cell Biology*, vol. 10, pp. 1–13, Aug. 2009.

[108] A. Gennerich and R. D. Vale, "Walking the walk: how kinesin and dynein coordinate their steps," *Current Opinion in Cell Biology*, vol. 21, pp. 59–67, Feb. 2009.

[109] M. Ghildiyal and P. D. Zamore, "Small silencing RNAs: an expanding universe," *Nature Reviews Genetics*, vol. 10, pp. 94–108, Feb. 2009.

[110] M. Jinek and J. A. Doudna, "A three-dimensional view of the molecular machinery of RNA interference," *Nature*, vol. 457, pp. 405–412, Jan. 2009.

[111] R. F. Ketting, "The Many Faces of RNAi," *Developmental Cell*, vol. 20, pp. 148–161, Feb. 2011.

[112] R. W. Carthew and E. J. Sontheimer, "Origins and Mechanisms of miRNAs and siRNAs," *Cell*, vol. 136, pp. 642–655, Feb. 2009.

[113] C. Ender and G. Meister, "Argonaute proteins at a glance," *Journal of Cell Science*, vol. 123, pp. 1819–1823, May 2010.

[114] A. A. Khvorova, A. A. Reynolds, and S. D. S. Jayasena, "Functional siRNAs and miRNAs Exhibit Strand Bias," *Cell*, vol. 115, pp. 8–8, Oct. 2003.

[115] D. S. Schwarz, G. Hutvágner, T. Du, Z. Xu, N. Aronin, and P. D. Zamore, "Asymmetry in the assembly of the RNAi enzyme complex.," *Cell*, vol. 115, pp. 199–208, Oct. 2003.

[116] S. M. Elbashir, J. Harborth, W. Lendeckel, A. Yalcin, K. Weber, and T. Tuschl, "Duplexes of 21-nucleotide RNAs mediate RNA interference in cultured mammalian cells.," *Nature*, vol. 411, pp. 494–498, May 2001.

[117] A. L. Brass, D. M. Dykxhoorn, Y. Benita, N. Yan, A. Engelman, R. J. Xavier, J. Lieberman, and S. J. Elledge, "Identification of Host Proteins Required for HIV Infection Through a Functional Genomic Screen," *Science*, vol. 319, pp. 921–926, Feb. 2008.

[118] A. L. Brass, I.-C. Huang, Y. Benita, S. P. John, M. N. Krishnan, E. M. Feeley, B. J. Ryan, J. L. Weyer, L. van der Weyden, E. Fikrig, D. J. Adams, R. J. Xavier, M. Farzan, and S. J. Elledge, "The IFITM Proteins Mediate Cellular Resistance to Influenza A H1N1 Virus, West Nile Virus, and Dengue Virus," *Cell*, vol. 139, pp. 1243–1254, Nov. 2009.

[119] L. Hao, A. Sakurai, T. Watanabe, E. Sorensen, C. A. Nidom, M. A. Newton, P. Ahlquist, and Y. Kawaoka, "Drosophila RNAi screen identifies host genes important for influenza virus replication," *Nature*, vol. 454, pp. 890–893, July 2008.

[120] A. Karlas, N. Machuy, Y. Shin, K.-P. Pleissner, A. Artarini, D. Heuer, D. Becker, H. Khalil, L. A. Ogilvie, S. Hess, A. P. Mäurer, E. Müller, T. Wolff, T. Rudel, and T. F. Meyer, "Genome-wide RNAi screen identifies human host factors crucial for influenza virus replication," *Nature*, vol. 463, pp. 818–822, Nov. 2010.

[121] M. N. Krishnan, A. Ng, B. Sukumaran, F. D. Gilfoy, P. D. Uchil, H. Sultana, A. L. Brass, R. Adametz, M. Tsui, F. Qian, R. R. Montgomery, S. Lev, P. W. Mason, R. A. Koski, S. J. Elledge, R. J. Xavier, H. Agaisse, and E. Fikrig, "RNA interference screen for human genes associated with West Nile virus infection," *Nature*, vol. 455, pp. 242–245, Aug. 2008.

[122] R. König, Y. Zhou, D. Elleder, T. L. Diamond, G. M. C. Bonamy, J. T. Irelan, C.-y. Chiang, B. P. Tu, P. D. De Jesus, C. E. Lilley, S. Seidel, A. M. Opaluch, J. S. Caldwell, M. D. Weitzman, K. L. Kuhen, S. Bandyopadhyay, T. Ideker, A. P. Orth, L. J. Miraglia, F. D. Bushman, J. A. Young, and S. K. Chanda, "Global Analysis of Host-Pathogen Interactions that Regulate Early-Stage HIV-1 Replication," *Cell*, vol. 135, pp. 49–60, Oct. 2008.

[123] R. König, S. Stertz, Y. Zhou, A. Inoue, H. H. Hoffmann, S. Bhattacharyya, J. G. Alamares, D. M. Tscherne, M. B. Ortigoza, Y. Liang, Q. Gao, S. E. Andrews, S. Bandyopadhyay, P. De Jesus, B. P. Tu, L. Pache, C. Shih, A. Orth, G. Bonamy, L. Miraglia, T. Ideker, A. GarcIa-Sastre, J. A. T. Young, P. Palese, M. L. Shaw, and S. K. Chanda, "Human host factors required for influenza virus replication," *Nature*, vol. 463, pp. 813–817, Dec. 2009.

[124] Q. Li, A. L. Brass, A. Ng, Z. Hu, R. J. Xavier, T. J. Liang, and S. J. Elledge, "A genome-wide genetic screen for host factors required for hepatitis C virus propagation," *Proceedings of the National Academy of Sciences*, vol. 106, pp. 16410–16415, Sept. 2009.

[125] J. Mercer, B. Snijder, R. Sacher, C. Burkard, C. K. E. Bleck, H. Stahlberg, L. Pelkmans, and A. Helenius, "RNAi Screening Reveals Proteasome- and Cullin3-Dependent Stages in Vaccinia Virus Infection," *CellReports*, vol. 2, pp. 1036–1047, Oct. 2012.

[126] D. Panda, A. Das, P. X. Dinh, S. S. Subramaniam, D. Nayak, N. J. Barrows, J. L. Pearson, J. Thompson, D. L. D. Kelly, I. I. Ladunga, and A. K. A. Pattnaik, "RNAi screening reveals requirement for host cell secretory pathway in infection by diverse families of negative-strand RNA viruses.," *PNAS*, vol. 108, pp. 19036–19041, Nov. 2011.

[127] J. A. Smith, E. A. White, M. E. Sowa, M. L. C. Powell, M. Ottinger, J. W. Harper, and P. M. Howley, "Genome-wide siRNA screen identifies SMCX, EP400, and Brd4 as E2-dependent regulators of human papillomavirus oncogene expression," *Proceedings of the National Academy of Sciences*, vol. 107, pp. 3752–3757, Feb. 2010.

[128] A. W. Tai, Y. Benita, L. F. Peng, S.-S. Kim, N. Sakamoto, R. J. Xavier, and R. T. Chung, "A Functional Genomic Screen Identifies Cellular Cofactors of Hepatitis C Virus Replication," *Cell Host and Microbe*, vol. 5, pp. 298–307, Mar. 2009.

[129] H. Zhou, M. Xu, Q. Huang, A. T. Gates, X. D. Zhang, J. C. Castle, E. Stec, M. Ferrer, B. Strulovici, D. J. Hazuda, and A. S. Espeseth, "Genome-Scale RNAi Screen for Host Factors Required for HIV Replication," *Cell Host and Microbe*, vol. 4, pp. 495–504, Nov. 2008.

[130] U. Krueger, T. Bergauer, B. Kaufmann, I. Wolter, S. Pilk, M. Heider-Fabian, S. Kirch, C. Artz-Oppitz, M. Isselhorst, and J. Konrad, "Insights into Effective RNAi Gained from Large-Scale siRNA Validation Screening," *Oligonucleotides*, vol. 17, pp. 237–250, June 2007.

[131] B. D. Parsons, A. Schindler, D. H. Evans, and E. Foley, "A Direct Phenotypic Comparison of siRNA Pools and Multiple Individual Duplexes in a Functional Assay," *PLoS ONE*, vol. 4, p. e8471, Dec. 2009.

[132] R. Kittler, V. Surendranath, A.-K. Heninger, M. Slabicki, M. Theis, G. Putz, K. Franke, A. Caldarelli, H. Grabner, K. Kozak, J. Wagner, E. Rees, B. Korn, C. Frenzel, C. Sachse, B. Sönnichsen, J. Guo, J. Schelter, J. Burchard, P. S. Linsley, A. L. Jackson, B. Habermann, and F. Buchholz, "Genome-wide resources of endoribonuclease-prepared short interfering RNAs for specific loss-of-function studies," *Nature Methods*, Mar. 2007.

[133] J. Moffat, D. A. Grueneberg, X. Yang, S. Y. Kim, A. M. Kloepfer, G. Hinkle, B. Piqani, T. M. Eisenhaure, B. Luo, J. K. Grenier, A. E. Carpenter, S. Y. Foo, S. A. Stewart, B. R. Stockwell, N. Hacohen, W. C. Hahn, E. S. Lander, D. M. Sabatini, and D. E. Root, "A Lentiviral RNAi Library for Human and Mouse Genes Applied to an Arrayed Viral High-Content Screen," *Cell*, vol. 124, pp. 1283–1298, Mar. 2006.

[134] L. Houzet and K. T. Jeang, "Genome-wide screening using RNA interference to study host factors in viral replication and pathogenesis," *Experimental Biology and Medicine*, vol. 236, pp. 962–967, Aug. 2011.

[135] A. Birmingham, E. M. Anderson, A. Reynolds, D. Ilsley-Tyree, D. Leake, Y. Fedorov, S. Baskerville, E. Maksimova, K. Robinson, J. Karpilow, W. S. Marshall, and A. Khvorova, "3' UTR seed matches, but not overall identity, are associated with RNAi off-targets," *Nature Methods*, vol. 3, pp. 199–204, Mar. 2006.

[136] X. Lin, "siRNA-mediated off-target gene silencing triggered by a 7 nt complementation," *Nucleic Acids Research*, vol. 33, pp. 4527–4535, Aug. 2005.

[137] A. L. A. Jackson, S. R. S. Bartz, J. J. Schelter, S. V. S. Kobayashi, J. J. Burchard, M. M. Mao, B. B. Li, G. G. Cavet, and P. S. P. Linsley, "Expression profiling reveals off-target gene regulation by RNAi.," *Nature Biotechnology*, vol. 21, pp. 635–637, May 2003.

[138] T. Horn, T. Sandmann, and M. Boutros, "Design and evaluation of genome-wide libraries for RNA interference screens," *Genome Biology*, vol. 11, no. 6, p. R61, 2010.

[139] B. Snijder, R. Sacher, P. Rämö, E.-M. Damm, P. Liberali, and L. Pelkmans, "Population context determines cell-to-cell variability in endocytosis and virus infection," *Nature*, vol. 461, pp. 520–523, Sept. 2009.

[140] S. Engel, T. Heger, R. Mancini, F. Herzog, J. Kartenbeck, A. Hayer, and A. Helenius, "Role of Endosomes in Simian Virus 40 Entry and Infection," *Journal of Virology*, vol. 85, pp. 4198–4211, Apr. 2011.

[141] V. Makarenkov, P. Zentilli, D. Kevorkov, A. Gagarin, N. Malo, and R. Nadon, "An efficient method for the detection and elimination of systematic error in high-throughput screening," *Bioinformatics*, vol. 23, pp. 1648–1657, July 2007.

[142] A. Birmingham, L. M. Selfors, T. Forster, D. Wrobel, C. J. Kennedy, E. Shanks, J. Santoyo-Lopez, D. J. Dunican, A. Long, D. Kelleher, Q. Smith, R. L. Beijersbergen, P. Ghazal, and C. E. Shamu, "Statistical methods for analysis of high-throughput RNA interference screens," *Nature Publishing Group*, vol. 6, pp. 569–575, Aug. 2009.

[143] N. Malo, J. A. Hanley, S. Cerquozzi, J. Pelletier, and R. Nadon, "Statistical practice in high-throughput screening data analysis," *Nature Biotechnology*, vol. 24, pp. 167–175, Feb. 2006.

[144] X. D. Zhang, *Optimal high-throughput screening*. Cambridge University Press, Feb. 2011.

[145] X. D. Zhang, "Novel Analytic Criteria and Effective Plate Designs for Quality Control in Genome-Scale RNAi Screens," *Journal of Biomolecular Screening*, vol. 13, pp. 363–377, June 2008.

[146] X. D. Zhang, "A pair of new statistical parameters for quality control in RNA interference high-throughput screening assays," *Genomics*, vol. 89, pp. 552–561, Apr. 2007.

[147] B. Luo, H. W. Cheung, A. Subramanian, T. Sharifnia, M. Okamoto, X. Yang, G. Hinkle, J. S. Boehm, R. Beroukhim, B. A. Weir, C. Mermel, D. A. Barbie, T. Awad, X. Zhou, T. Nguyen, B. Piqani, C. Li, T. R. Golub, M. Meyerson, N. Hacohen, W. C. Hahn, E. S. Lander, D. M. Sabatini, and D. E. Root, "Highly parallel identification of essential genes in cancer cells.," *Proceedings of the National Academy of Sciences*, vol. 105, pp. 20380–20385, Dec. 2008.

[148] D. Yu, J. Danku, I. Baxter, S. Kim, O. K. Vatamaniuk, D. E. Salt, and O. Vitek, "Noise reduction in genome-wide perturbation screens using linear mixed-effect models," *Bioinformatics*, vol. 27, pp. 2173–2180, Aug. 2011.

[149] X. D. Zhang, P. F. Kuan, M. Ferrer, X. Shu, Y. C. Liu, A. T. Gates, P. Kunapuli, E. M. Stec, M. Xu, S. D. Marine, D. J. Holder, B. Strulovici, J. F. Heyse, and A. S. Espeseth, "Hit selection with false discovery rate control in genome-scale RNAi screens," *Nucleic Acids Research*, vol. 36, pp. 4667–4679, June 2008.

[150] A. E. Carpenter, T. R. Jones, M. R. Lamprecht, C. Clarke, I. Kang, O. Friman, D. A. Guertin, J. Chang, R. A. Lindquist, J. Moffat, P. Golland, and D. M. Sabatini, "CellProfiler: image analysis software for identifying and quantifying cell phenotypes," *Genome Biology*, vol. 7, no. 10, p. R100, 2006.

[151] P. Horvath, T. Wild, U. Kutay, and G. Csucs, "Machine Learning Improves the Precision and Robustness of High-Content Screens: Using Nonlinear Multiparametric Methods to Analyze Screening Results," *Journal of Biomolecular Screening*, vol. 16, pp. 1059–1067, Oct. 2011.

[152] R. König, C.-y. Chiang, B. P. Tu, S. F. Yan, P. D. DeJesus, A. Romero, T. Bergauer, A. Orth, U. Krueger, Y. Zhou, and S. K. Chanda, "A probability-based approach for the analysis of large-scale RNAi screens," *Nature Methods*, vol. 4, pp. 847–849, Sept. 2007.

[153] X. D. Zhang, "A New Method with Flexible and Balanced Control of False Negatives and False Positives for Hit Selection in RNA Interference High-Throughput Screening Assays," *Journal of Biomolecular Screening*, vol. 12, pp. 645–655, Aug. 2007.

[154] T. Sakai, M. Ohuchi, M. Imai, T. Mizuno, K. Kawasaki, K. Kuroda, and S. Yamashina, "Dual Wavelength Imaging Allows Analysis of Membrane Fusion of Influenza Virus inside Cells," *Journal of Virology*, vol. 80, pp. 2013–2018, Jan. 2006.

[155] T. Galli, T. Chilcote, O. Mundigl, T. Binz, H. Niemann, and P. De Camilli, "Tetanus Toxin-mediated Cleavage of Cellubrevin Impairs Exocytosis of Transferrin Receptor-Containing Vesicles in CHO Cells," *The Journal of Cell Biology*, vol. 125, pp. 1015–1024, June 1994.

[156] M. J. Kean, K. C. Williams, M. Skalski, D. Myers, A. Burtnik, D. Foster, and M. G. Coppolino, "VAMP3, syntaxin-13 and SNAP23 are involved in secretion of matrix metalloproteinases, degradation of the extracellular matrix and cell invasion," *Journal of Cell Science*, vol. 122, pp. 4089–4098, Nov. 2009.

[157] Zhang, *Optimal High-Throughput Screening*. Cambridge University Press, Feb. 2011.

[158] J. P. Carralot, A. Ogier, A. Boese, A. Genovesio, P. Brodin, P. Sommer, and T. Dorval, "A novel specific edge effect correction method for RNA interference screenings," *Bioinformatics*, vol. 28, pp. 261–268, Jan. 2012.

[159] J. W. Engels, "Gene silencing by chemically modified siRNAs," *New BIOTECHNOLOGY*, pp. 1–6, Aug. 2012.

[160] N. Nagaraj, J. R. Wisniewski, T. Geiger, J. Cox, M. Kircher, J. Kelso, S. P. a. a. bo, and M. Mann, "Deep proteome and transcriptome mapping of a human cancer cell line," *Molecular Systems Biology*, vol. 7, pp. 1–8, Nov. 2011.

[161] P. R. Clark, J. S. Pober, and M. S. Kluger, "Knockdown of TNFR1 by the sense strand of an ICAM-1 siRNA: dissection of an off-target effect," *Nucleic Acids Research*, vol. 36, pp. 1081–1097, Dec. 2007.

[162] J.-X. Wei, J. Yang, J.-F. Sun, L.-T. Jia, Y. Zhang, H.-Z. Zhang, X. Li, Y.-L. Meng, L.-B. Yao, and A.-G. Yang, "Both strands of siRNA have potential to guide posttranscriptional gene silencing in mammalian cells.," *PLoS ONE*, vol. 4, no. 4, p. e5382, 2009.

[163] Y. Sun, S. Varambally, C. A. Maher, Q. Cao, P. Chockley, T. Toubai, C. Malter, E. Nieves, I. Tawara, Y. Wang, P. A. Ward, A. Chinnaiyan, and P. Reddy, "Targeting of microRNA-142-3p in dendritic cells regulates endotoxin-induced mortality," *Blood*, vol. 117, pp. 6172–6183, June 2011.

[164] K. A. Riggs, N. Hasan, D. Humphrey, C. Raleigh, C. Nevitt, D. Corbin, and C. Hu, "Regulation of integrin endocytic recycling and chemotactic cell migration by syntaxin 6 and VAMP3 interaction," *Journal of Cell Science*, vol. 125, pp. 3827–3839, Oct. 2012.

[165] V. Proux-Gillardeaux, R. Rudge, and T. Galli, "The Tetanus Neurotoxin-Sensitive and Insensitive Routes to and from the Plasma Membrane: Fast and Slow Pathways?," *Traffic*, vol. 6, pp. 366–373, Mar. 2005.

[166] W. Antonin, C. Holroyd, R. Tikkanen, S. Honing, and R. Jahn, "The R-SNARE endobrevin/VAMP-8 mediates homotypic fusion of early endosomes and late endosomes.," *Molecular Biology of the Cell*, vol. 11, pp. 3289–3298, Sept. 2000.

[167] P. R. Pryor, B. M. Mullock, N. A. Bright, M. R. Lindsay, S. R. Gray, S. C. W. Richardson, A. Stewart, D. E. James, R. C. Piper, and J. P. Luzio, "Combinatorial SNARE complexes with VAMP7 or VAMP8 define different late endocytic fusion events," *EMBO Reports*, vol. 5, pp. 590–595, May 2004.

[168] T. Chilcote, T. Galli, O. Mundigl, L. Edelmann, P. S. McPberson, K. Takei, and P. De Camilli, "Cellubrevin and Synaptobrevins: Similar Subcellular Localization and Biochemical Properties in PC12 Ceils," *The Journal of Cell Biology*, vol. 129, no. 1, pp. 219–231, 1995.

[169] R. Z. Murray, "A Role for the Phagosome in Cytokine Secretion," *Science*, vol. 310, pp. 1492–1495, Dec. 2005.

[170] R. Flaumenhaft, K. Croce, E. Chen, B. Furie, and B. C. Furie, "Proteins of the exocytotic core complex mediate platelet alpha-granule secretion. Roles of vesicle-associated membrane protein, SNAP-23, and syntaxin 4.," *Journal of Biological Chemistry*, vol. 274, pp. 2492–2501, Jan. 1999.

[171] J. Polgar, "Vesicle-associated membrane protein 3 (VAMP-3) and VAMP-8 are present in human platelets and are required for granule secretion," *Blood*, vol. 100, pp. 1081–1083, July 2002.

[172] V. Ravichandran, A. Chawla, and P. A. Roche, "Identification of a novel syntaxin- and synaptobrevin/VAMP-binding protein, SNAP-23, expressed in non-neuronal tissues.," *Journal of Biological Chemistry*, vol. 271, pp. 13300–13303, June 1996.

[173] C. Hu, D. Hardee, and F. Minnear, "Membrane fusion by VAMP3 and plasma membrane t-SNAREs," *Experimental Cell Research*, vol. 313, pp. 3198–3209, Sept. 2007.

[174] A. C. A. Valdez, J. P. J. Cabaniols, M. J. M. Brown, and P. A. P. Roche, "Syntaxin 11 is associated with SNAP-23 on late endosomes and the trans-Golgi network.," *Journal of Cell Science*, vol. 112 (Pt 6), pp. 845–854, Feb. 1999.

[175] C. M. Fader, D. G. Sánchez, M. B. Mestre, and M. I. Colombo, "TI-VAMP/VAMP7 and VAMP3/cellubrevin: two v-SNARE proteins involved in specific steps of the autophagy/multivesicular body pathways," *BBA - Molecular Cell Research*, vol. 1793, pp. 1901–1916, Dec. 2009.

[176] T. Saitoh, N. Fujita, M. H. Jang, S. Uematsu, B.-G. Yang, T. Satoh, H. Omori, T. Noda, N. Yamamoto, M. Komatsu, K. Tanaka, T. Kawai, T. Tsujimura, O. Takeuchi, T. Yoshimori, and S. Akira, "Loss of the autophagy protein Atg16L1

enhances endotoxin-induced IL-1β production," *Nature*, vol. 456, pp. 264–268, Oct. 2008.

[177] K. Ishibashi, N. Fujita, E. Kanno, H. Omori, T. Yoshimori, T. Itoh, and M. Fukuda, "Atg16L2, a novel isoform of mammalian Atg16L that is not essential for canonical autophagy despite forming an Atg12-5-16L2 complex," *Autophagy*, vol. 7, pp. 1500–1513, Dec. 2011.

[178] F. Tang, B. Wang, N. Li, Y. Wu, J. Jia, T. Suo, Q. Chen, Y.-J. Liu, and J. Tang, "RNF185, a Novel Mitochondrial Ubiquitin E3 Ligase, Regulates Autophagy through Interaction with BNIP1," *PLoS ONE*, vol. 6, p. e24367, Sept. 2011.

[179] T. Lamark, V. Kirkin, I. Dikic, and T. Johansen, "NBR1 and p62 as cargo receptors for selective autophagy of ubiquitinated targets.," *Cell Cycle*, vol. 8, pp. 1986–1990, July 2009.

[180] E. Morselli, S. Shen, C. Ruckenstuhl, M. A. Bauer, G. Mariño, L. Galluzzi, A. Criollo, M. Michaud, M. C. Maiuri, T. Chano, F. Madeo, and G. Kroemer, "p53 inhibits autophagy by interacting with the human ortholog of yeast Atg17, RB1CC1/FIP200," *Cell Cycle*, vol. 10, pp. 2763–2769, Aug. 2011.

[181] S. B. Kudchodkar and B. Levine, "Viruses and autophagy," *Reviews in Medical Virology*, vol. 19, pp. 359–378, Nov. 2009.

[182] M. Ait-Goughoulte, T. Kanda, K. Meyer, J. S. Ryerse, R. B. Ray, and R. Ray, "Hepatitis C Virus Genotype 1a Growth and Induction of Autophagy," *Journal of Virology*, vol. 82, pp. 2241–2249, Feb. 2008.

[183] Y.-R. Lee, H.-Y. Lei, M.-T. Liu, J.-R. Wang, S.-H. Chen, Y.-F. Jiang-Shieh, Y.-S. Lin, T.-M. Yeh, C.-C. Liu, and H.-S. Liu, "Autophagic machinery activated by dengue virus enhances virus replication," *Virology*, vol. 374, pp. 240–248, May 2008.

[184] Z. Zhou, X. Jiang, D. Liu, Z. Fan, X. Hu, J. Yan, M. Wang, and G. F. Gao, "Autophagy is involved in influenza A virus replication.," *Autophagy*, vol. 5, pp. 321–328, Apr. 2009.

[185] I. T. M. Hussein, E. Cheng, S. S. Ganaie, M. J. Werle, S. Sheema, A. Haque, and M. A. MIR, "Autophagic Clearance of Sin Nombre Hantavirus Glycoprotein Gn Promotes Virus Replication in Cells," *Journal of Virology*, vol. 86, pp. 7520–7529, June 2012.

[186] J.-K. Li, J.-J. Liang, C.-L. Liao, and Y.-L. Lin, "Autophagy is involved in the early step of Japanese encephalitis virus infection," *Microbes and Infection*, vol. 14, pp. 159–168, Feb. 2012.

[187] M. Panyasrivanit, A. Khakpoor, N. Wikan, and D. R. Smith, "Co-localization of constituents of the dengue virus translation and replication machinery with amphisomes," *Journal of General Virology*, vol. 90, pp. 448–456, Feb. 2009.

[188] J. Shi and H. Luo, "Interplay between the cellular autophagy machinery and positive-stranded RNA viruses," *Acta Biochimica et Biophysica Sinica*, vol. 44, pp. 375–384, Apr. 2012.

[189] M. G. Gutierrez, "Rab7 is required for the normal progression of the autophagic pathway in mammalian cells," *Journal of Cell Science*, vol. 117, pp. 2687–2697, June 2004.

[190] S. Jager, "Role for Rab7 in maturation of late autophagic vacuoles," *Journal of Cell Science*, vol. 117, pp. 4837–4848, Oct. 2004.

[191] V. Zennou, C. Petit, D. Guetard, U. Nerhbass, L. Montagnier, and P. Charneau, "HIV-1 genome nuclear import is mediated by a central DNA flap," *Cell*, vol. 101, no. 2, pp. 173–185, 2000.

[192] P. Y. Lozach, "C-type Lectins L-SIGN and DC-SIGN Capture and Transmit Infectious Hepatitis C Virus Pseudotype Particles," *Journal of Biological Chemistry*, vol. 279, pp. 32035–32045, Apr. 2004.

List of Acronyms

Ago ..... Argonaute
AP2 ..... Adaptor protein 2
ASN ..... AllSstarsNegative
ATP2A2 (SERCA) ..... ATPase, Ca^2+ transporting, cardiac muscle, slow twitch 2
ATP6V1A1 ..... ATPase, H^+ transporting, lysosomal 70 kDa, V1 subunit A1
ATP6V1B2 ..... ATPase, H^+ transporting, lysosomal 56/58 kDa, V1 subunit B2
CCHFV ..... Crimean-Congo hemorrhagic fever
CCP ..... Clathrin-coated pits
CD209 (DC-SIGN) ..... Dendritic cell-specific ICAM-3-grabing non-integrin
CCV ..... Clathrin-coated vesicles
CLIC ..... Clathrin-independent carrier
CME ..... Clathrin-mediated endocytosis
CTxB ..... Cholera toxin subunit B
CV ..... Cross validation
DCs ..... Dendritic cells
dsRNA ..... Double stranded RNA
DC-SIGN (CD209) ..... Dendritic cell-specific ICAM-3-grabing non-integrin
DV ..... Dengue virus
EE(s) ..... Early endosome(s)
EHD2 ..... Eps-15 homology domain-containing protein 2
eIF ..... Eukaryotic initiation factor
ER ..... Endoplasmic reticulum
ESCRT ..... Endosomal sorting complex required for transport
EVs ..... Vaccinia virus extracellular virions
fdr ..... False-discovery-rate
ffu ..... foci forming units
HCC ..... Hepatocellular carcinoma cells
HSD3B7 .. Hydroxy-delta-5-steroid dehydrogenase, 3 beta- and steroid delta-isomerse 7
HTS ..... High throughput screening
HV ..... Hantaan virus
G_c ..... Glycoprotein C
G_n ..... Glycoprotein N
GAPs ..... GTPase-activating proteins
GDIs ..... GDP-dissociation inhibitors
GDP ..... Guanosine diphosphate
GDFs ..... GDI displacement factors
GEFs ..... Guanosine-nucleotide exchange factors
GPs ..... Glycoproteins

GPI ..... Glycosylphosphatidyl-inositol
GTP ..... Guanosine triphospate
IIF ..... Indirect immunofluorescence
IL2R ..... Interleukin-2 receptor
JEV ..... Japanese encephalitis virus
Kif11 ..... Kinesin family member 11
L ..... Large negative-sense, single-stranded RNA segment
LACV ..... La Crosse virus
LE(s) ..... Late endosome(s)
loess ..... Locally weighted scatterplot smoothing
LYS ..... Lysosomes
M ..... Medium negative-sense, single-stranded RNA segment
MAD ..... Median absolute deviation
miRs ..... Mimic-miRNAs
miRNA ..... MicroRNA
MHV ..... Mouse hepatitis virus
MVs ..... Vaccinia virus mature virions
moi ..... Multiplicity of infection
LHX1 ..... LIM homeobox 1
MTL5 ..... Metallothionein-like 5, testis-specific
N ..... Nucleoprotein
NY-1 ..... New York 1 virus
NS_s ..... Nonstructural protein S
NS_m ..... Nonstructural protein M
NTRs ..... Non-translated regions
OV ..... Oropouche virus
piRNA ..... PIWI-interacting RNAs
PKCε ..... Protein kinase C epsilon
PM ..... Plasma membrane
PLK1 ..... Polo-like kinase 1
PS ..... Phosphatidylserine
PtdIns ..... Phosphatidylinositol
PtdIns(4,5)P_2 ..... Phosphatidylinositol-4,5-bisphosphate
RISC ..... RNA-induced silencing complex
RNAi ..... RNA interference
RNP ..... Ribonucleoprotein
RdRp ..... RNA-dependent RNA polymerase
RSA ..... Redundant siRNA activity
RVFV ..... Rift Valley fever virus
S ..... Small negative-sense, single-stranded RNA segment
scr ..... scrambled
siRNA ..... Small interfering RNA
SFTSV ..... Huaiyangshan virus
SNARE ..... Soluble NSF attachement protein receptor
SNV ..... Sin Nombre virus
SSMD ..... Strictly standardized mean difference
SV40 ..... Simian virus 40
TeTx ..... Tetanus toxin
UUKV ..... Uukuniemi virus

UTR ..... Untranslated region
VAMP3 ..... Vesicle-associated membrane protein 3 (cellubrevin)

Acknowledgements

First of all, many thanks to you, Ari, for giving me the opportunity to do my PhD in your laboratory, for your support and advice, and giving me the freedom to pursue my ideas.

Thanks a lot to you, Pierre-Yves, for introducing me into the work with bunyaviruses, fruitful discussions, and your great supervision. I enjoyed working together with you.

I am very grateful to the members of my thesis committee, Michèle Bouloy, Hubert Hilbi, and Alexandra Trkola for the discussions and the constructive comments on my project. Thank you!

Many thanks to all the current and former members of the LMSC ETHZ for their support.
I particularly thank Peter Horvath, for the great collaboration, the fruitful discussions, and the exciting times.

I thank Christian von Mering and Andrea Franceschini for our collaboration on the seed analysis.

Many thanks to all the current and former members of the Helenius group for all the help, discussion, advice, and the pleasant atmosphere.
Miriam, thank you very much for your great support and help especially during the writing phase. I am very thankful about it!
Thomas, thanks a lot for good discussions and your great help and support whenever I needed help. Especially, many thanks to your great help during the writing phase.
Flo, many thanks for your PBMCs, your support and introducing me to the confocal microscopy!
Thank you, Roberta and Yassen, for your support and your helpfulness.

Many thanks to all the people who helped proofread my thesis: Ari, Pierre-Yves, Maggie, Thomas and Miriam.

I thank all my students who did their semester and/or master projects with me. I learned a lot from you!
Many thanks to you, Ben, for all your work on the CLCs and the DC-SIGN clones. It was great to work with you.
Thanks a lot to you, Marilou, for your work on the miR-142-3p!

Thank you, Sonia, for introducing me into the work with primary human dendritic cells. Thank you, Peter and Shuyang, for taking the blood samples.

Thank you, Amadou, for helping me with the quantitative RT-PCR.

Thank you, Vadim, for introducing me to the Alpha Innotech machine.

Thank you, Daniel, Klaus and Dr. Coppolino for sharing materials.

I thank the members of the Functional Genomics Center Zurich UZH / ETH Zurich and the Flow Cytometry Facility ETH Zurich for their technical assistance.

Thanks a lot to the consulting team of the Seminar for Statistics ETHZ.

Thanks to the IBC staff for their help!
I thank Nico and Roland for the great IT support.
Big thanks to Toni and Maria for all their help especially during the screening phases.

Many thanks go to my friends and family for always being there when needed and sharing great times together.

Karen, thanks a lot for your love, your believe in me and your great support.